

8-2023

## Using Computational Fluid Dynamics for Predicting Hydraulic Performance of Arced Labyrinth Weirs

Shelby J. Koldewyn  
*Utah State University*

Follow this and additional works at: <https://digitalcommons.usu.edu/etd>

 Part of the Civil and Environmental Engineering Commons

---

### Recommended Citation

Koldewyn, Shelby J., "Using Computational Fluid Dynamics for Predicting Hydraulic Performance of Arced Labyrinth Weirs" (2023). *All Graduate Theses and Dissertations, Spring 1920 to Summer 2023*. 8899.  
<https://digitalcommons.usu.edu/etd/8899>

This Thesis is brought to you for free and open access by  
the Graduate Studies at DigitalCommons@USU. It has  
been accepted for inclusion in All Graduate Theses and  
Dissertations, Spring 1920 to Summer 2023 by an  
authorized administrator of DigitalCommons@USU. For  
more information, please contact  
[digitalcommons@usu.edu](mailto:digitalcommons@usu.edu).



USING COMPUTATIONAL FLUID DYNAMICS FOR  
PREDICTING HYDRAULIC PERFORMANCE  
OF ARCED LABYRINTH WEIRS

by

Shelby J. Koldewyn

A thesis submitted in partial fulfillment  
of the requirements for the degree

of

MASTER OF SCIENCE

in

Civil and Environmental Engineering

Approved:

---

Blake P. Tullis, Ph.D.  
Major Professor

---

Zac Sharp, Ph.D.  
Co-Advisor

---

Som Dutta, Ph.D.  
Committee Member

---

D. Richard Cutler, Ph.D.  
Vice Provost for Graduate Studies

UTAH STATE UNIVERSITY  
Logan, Utah

2023

Copyright © Shelby Koldewyn 2023

All Rights Reserved

## ABSTRACT

Using Computational Fluid Dynamics for Predicting Hydraulic Performance of

Arced Labyrinth Weirs

by

Shelby J. Koldewyn, Master of Science

Utah State University, 2023

Major Professor: Dr. Blake P. Tullis and Dr. Zac Sharp

Department: Civil and Environmental Engineering

Our world is dynamic and as hydrologic research continues, the magnitude of flood estimates used in hydraulic design for reservoirs has increased. Consequently, many existing spillways are now undersized and unable to meet discharge requirements. These spillways often have a fixed footprint so nonlinear weirs (e.g., labyrinth weirs) are often a viable solution. Sometimes in reservoir applications, arcing labyrinth weirs in plan view can increase hydraulic efficiency because of better cycle orientation to the approaching flow from the reservoir.

This study supplements available physical arced labyrinth weir hydraulic data by observing flow characteristics of two numerical models ( $\alpha=16^\circ$ ;  $\theta=10^\circ$  and  $\alpha=20^\circ$ ;  $\theta=30^\circ$ ) and predicting hydraulic efficiency. Both numerical models were developed using two commercially available Computational Fluid Dynamics (CFD) solvers. The purpose of the CFD analysis was to assess the appropriateness of default settings compared to user-defined settings in a CFD model and to better understand CFD as a design tool for arced labyrinth weir rating curve development.

Rating curves were developed using numerical models and compared with existing rating curves developed from physical models. Five discharge rates for each model were completed

with variations in mesh size, turbulence model, and commercial solver. Concurrence between physical and numerical rating curves was found. Results determined that default settings are not always appropriate for developing a rating curve. The  $k$ - $\varepsilon$  standard turbulence model provided the best results and first-order momentum advection schemes can provide a faster result with reasonable accuracy. The numerical models accurately demonstrated nappe behavior when compared with the physical model independent of solver. For arced labyrinth weirs, CFD can be a useful tool for implementing site-specific conditions; however, CFD models should be calibrated to reliable laboratory or field data.

This study's data may be used, with sound engineering judgement, to aid in the design of arced labyrinth weirs.

(127 pages)

## PUBLIC ABSTRACT

### Using Computational Fluid Dynamics to Predict Hydraulic Performance of Arced Labyrinth Weirs

Shelby J. Koldewyn

Our world is dynamic and as hydrologic research continues, the magnitude of flood estimates used in hydraulic design for reservoirs has increased. Consequently, many existing spillways are now undersized and unable to meet discharge requirements. These spillways often have a fixed footprint, so nonlinear weirs (e.g., labyrinth weirs) are often a viable solution. For reservoir applications, arcing labyrinth weirs in plan view increases hydraulic efficiency because of better cycle orientation to the approaching flow from the reservoir. This study supplements available physical arced labyrinth weir hydraulic data by observing flow characteristics of two numerical models ( $\alpha=16^\circ$ ;  $\theta=10^\circ$  and  $\alpha=20^\circ$ ;  $\theta=30^\circ$ ). Both numerical models were developed using two commercially available CFD software. The purpose of the CFD analysis was to assess the appropriateness of default settings in a CFD model and to better understand CFD as a design tool for arced labyrinth weir rating curve development. Results determined that default settings are not always appropriate for a rating curve. For arced labyrinth weirs, CFD can be a useful tool for implementing site-specific conditions; however, CFD models should be calibrated to reliable laboratory or field data. This study's data may be used, with sound engineering judgement, to aid in the design of arced labyrinth weirs.

## ACKNOWLEDGMENTS

I would like to thank Dr. Blake Tullis for his confidence and trust in me to complete this research. I will forever be grateful to him for taking a chance on a young aspiring engineering student. I attribute my success in my coursework and research to his mentorship. I would also like to thank Ricky Anderson, who helped unlock my passion for fluid mechanics and opened doors for me at the water lab. Furthermore, I am grateful to Dr. Zac Sharp for his patience, mentorship, and willingness to go above and beyond. My other committee member, Dr. Som Dutta, deserves great thanks for his suggestions, input, and direction. I must thank Nate and Hope Young for their friendship, mentorship, and kindness through all the years of school and research.

Lastly, I would like to give special thanks to my husband, Conner Koldewyn; my family; and God. Conner has been a constant support, a true friend, and listening ear I have needed while completing a task of this scope. My family, especially my parents, have supported me in my educational goals and pushed me to achieve them. I will forever be thankful for their love and support. Finally, I must thank God for blessing me with the opportunity to further my education and for giving me the strength, motivation, and knowledge to accomplish a dream.

Shelby J. Koldewyn

## CONTENTS

	Page
ABSTRACT.....	iii
PUBLIC ABSTRACT .....	v
ACKNOWLEDGMENTS .....	vi
LIST OF TABLES.....	ix
LIST OF FIGURES .....	xi
NOMENCLATURE .....	xiii
DISCLAIMER .....	1
INTRODUCTION .....	1
LITERATURE REVIEW .....	5
Arced Labyrinth Weir Research .....	5
Numerical Modeling .....	10
Research Objectives.....	15
NUMERICAL MODEL SETUP .....	16
Numerical Models.....	16
Flow-3D® .....	17
Star CCM+® .....	19
Turbulence Models .....	20
Model Creation .....	23
Flow-3D® .....	24

Star CCM+® .....	27
Numerical Simulations.....	31
NUMERICAL MODEL RESULTS .....	32
Sensitivity Analysis .....	33
Grid Convergence Index.....	34
Comparison to Physical Data.....	36
Comparison to existing CFD data.....	41
Comparison of Turbulence Models .....	44
Comparison of Momentum Advection Order .....	47
Flow Structure and Nappe Aeration Behavior.....	49
CONCLUSION.....	51
REFERENCES .....	54
APPENDICES .....	58

## LIST OF TABLES

	Page
Table 1. Summary of runs completed using Flow-3D.....	25
Table 2. Summary of CFD mesh boundary conditions.....	26
Table 3. Summary of runs completed using Star CCM+.....	30
Table 4. Summary of CFD mesh boundary conditions.....	31
Table 5. Half-round crested arced labyrinth weir curve fit coefficients for Eq. [10] valid for $0.05 \leq H/P \leq 0.8$ (modified from Thompson, 2019). .....	35
Table 6. Calculated GCI for $\alpha=16^\circ$ : $\theta=10^\circ$ using results from Flow-3D and Star CCM+ models as per ASCE (2009). .....	35
Table 7. Calculated GCI for $\alpha=20^\circ$ : $\theta=30^\circ$ using results from Flow-3D and Star CCM+ models as per ASCE (2009). .....	35
Table 8. Different capabilities and setups of Star-CCM+ and Flow-3D. ....	41
Table 9. Model setup for this study and Thompson (2019).....	42
Table 10. Relative error ( $\varepsilon_{Cd}$ ) between numerical results of turbulence models at $H/P = 0.5$ and empirical (Eq. [10]) tabulated results for $\alpha=16^\circ$ : $\theta=10^\circ$ and $\alpha=20^\circ$ : $\theta=30^\circ$ weirs. ....	45
Table 11. Relative error ( $\varepsilon_{Cd}$ ) between numerical results of momentum advection scheme order at $H/P = 0.5$ and empirical (Eq. [10]) results for $\alpha=16^\circ$ : $\theta=10^\circ$ and $\alpha=20^\circ$ : $\theta=30^\circ$ . ....	49
Table C1. Tabulated time series data for $\alpha=16^\circ$ , $\theta=10^\circ$ arced labyrinth weir at $H/P = 0.3$ .....	68
Table C2. Tabulated time series data for $\alpha=16^\circ$ , $\theta=10^\circ$ arced labyrinth weir at $H/P = 0.4$ .....	70
Table C3. Tabulated time series data for $\alpha=16^\circ$ , $\theta=10^\circ$ arced labyrinth weir at $H/P = 0.5$ .....	73
Table C4. Tabulated time series data for $\alpha=16^\circ$ , $\theta=10^\circ$ arced labyrinth weir at $H/P = 0.5$ .....	75
Table C5. Tabulated time series data for $\alpha=16^\circ$ , $\theta=10^\circ$ arced labyrinth weir at $H/P = 0.5$ .....	78

Table C6. Tabulated time series data for $\alpha=16^\circ$ , $\theta=10^\circ$ arced labyrinth weir at H/P = 0.7 .....	80
Table C7. Tabulated time series data for $\alpha=16^\circ$ , $\theta=10^\circ$ arced labyrinth weir at H/P = 0.3 .....	83
Table C8. Tabulated time series data for $\alpha=16^\circ$ , $\theta=10^\circ$ arced labyrinth weir at H/P = 0.3 .....	86
Table C9. Tabulated time series data for $\alpha=16^\circ$ , $\theta=10^\circ$ arced labyrinth weir at H/P = 0.3 .....	89
Table C10. Tabulated time series data for $\alpha=20^\circ$ , $\theta=30^\circ$ arced labyrinth weir at H/P = 0.3 .....	92
Table C11. Tabulated time series data for $\alpha=20^\circ$ , $\theta=30^\circ$ arced labyrinth weir at H/P = 0.3 .....	94
Table C12. Tabulated time series data for $\alpha=20^\circ$ , $\theta=30^\circ$ arced labyrinth weir at H/P = 0.3 .....	97
Table C13. Tabulated time series data for $\alpha=20^\circ$ , $\theta=30^\circ$ arced labyrinth weir at H/P = 0.3 .....	100
Table C14. Tabulated time series data for $\alpha=20^\circ$ , $\theta=30^\circ$ arced labyrinth weir at H/P = 0.3 .....	103
Table C15. Tabulated time series data for $\alpha=20^\circ$ , $\theta=30^\circ$ arced labyrinth weir at H/P = 0.3 .....	105
Table C16. Tabulated time series data for $\alpha=20^\circ$ , $\theta=30^\circ$ arced labyrinth weir at H/P = 0.3 .....	108
Table C17. Tabulated time series data for $\alpha=20^\circ$ , $\theta=30^\circ$ arced labyrinth weir at H/P = 0.3 .....	110

## LIST OF FIGURES

	Page
Figure 1. Plan view of a (a) linear weir, (b) labyrinth weir, and (c) arced labyrinth weir specific to a reservoir-to-channel transition (Christensen, 2012).....	2
Figure 2. Isabella Dam in Bakersfield, California (Photo: US Army Corps of Engineers).....	3
Figure 3. Arced labyrinth weir nomenclature (Crookston, 2010).....	6
Figure 4. Discharge efficiency comparison between $\alpha=6^\circ$ labyrinth weirs of varying $\theta$ with reservoir approach flow (Crookston 2010).....	8
Figure 5. $C_d$ versus H/P showing nappe aeration conditions for arced labyrinth weirs of $\alpha = 20^\circ$ (Christensen, 2012).....	9
Figure 6. $C_d$ vs. H/P comparison between physical and numerical results for the $\alpha=16^\circ$ : $\theta=30^\circ$ weir (Modified from Thompson, 2019).....	13
Figure 7. $\alpha=16^\circ$ : $\theta=30^\circ$ H/P=0.4 comparison between numerical and physical nappe and tailwater aeration (Thompson, 2019). .....	13
Figure 8. Comparison of Flow-3D and Star CCM+ volume discretization and meshing methods.....	18
Figure 9. Flow-3D VOF method for tracking the free surface (Flow-3D, 2016). .....	18
Figure 10. CFD reservoir and weir model showing domain origin, mesh boundaries, boundary conditions, history probe, and initial fluid region.....	24
Figure 11. CFD reservoir and weir model showing mesh boundaries, boundary conditions, and isosurface location.....	29
Figure 12. Relative error ( $\varepsilon_{Cd}$ ) between numerical and empirical results of sensitivity analysis.....	33
Figure 13. Relative error ( $\varepsilon_{Cd}$ ) between numerical and empirical results for all mesh configurations for the $\alpha=16^\circ$ : $\theta=10^\circ$ weir using Flow-3D and Star CCM+. ....	36
Figure 14. Relative error ( $\varepsilon_{Cd}$ ) between numerical and empirical results for all mesh configurations for the $\alpha=20^\circ$ : $\theta=30^\circ$ weir using Flow-3D and Star CCM+. ....	37
Figure 15. $C_d$ vs. H/P comparison between physical results, empirical calculations (Eq. [10]), and fine mesh results using Flow-3D for the $\alpha=16^\circ$ : $\theta=10^\circ$ weir. ....	38
Figure 16. $C_d$ vs. H/P comparison between physical results, empirical calculations (Eq. [10]), and fine mesh results using Star CCM+ for the $\alpha=16^\circ$ : $\theta=10^\circ$ weir. ....	39

Figure 17. $C_d$ vs. H/P comparison between physical results, empirical calculations (Eq. [10]), and fine mesh results using Flow-3D for the $\alpha=20^\circ$ : $\theta=30^\circ$ weir. ....	39
Figure 18. $C_d$ vs. H/P comparison between physical results, empirical calculations (Eq. [10]), and fine mesh results using Star CCM+ for the $\alpha=20^\circ$ : $\theta=30^\circ$ weir. ....	40
Figure 19. Relative error ( $\varepsilon_{Cd}$ ) between numerical data collected by the author and data collected by Thompson (2019).....	43
Figure 20. Relative error ( $\varepsilon_{Cd}$ ) between numerical results of turbulence models at H/P = 0.5 and empirical (Eq. [10]) results for $\alpha=16^\circ$ : $\theta=10^\circ$ .....	46
Figure 21. Relative error ( $\varepsilon_{Cd}$ ) between numerical results of turbulence models at H/P = 0.5 (or 0.3) and empirical (Eq. [10]) results for $\alpha=20^\circ$ : $\theta=30^\circ$ .....	46
Figure 22. Relative error ( $\varepsilon_{Cd}$ ) between numerical results of momentum advection scheme order at H/P = 0.5 and empirical (Eq. [10]) results for $\alpha=16^\circ$ : $\theta=10^\circ$ and $\alpha=20^\circ$ : $\theta=30^\circ$ . ....	48
Figure 23. Nappe aeration behavior observed on the ‘distal half cycles’ at H/P = 0.5 for the $\alpha=16^\circ$ ; $\theta=10^\circ$ arced labyrinth weir using (a) Star CCM+ and (b) Flow-3D.....	50
Figure B1. Plan view of reservoir headbox with diffuser, baffle wall, stilling well tap, apron, and approach ramps labeled. Additionally, the numerical computational domain for the sectional model is labeled by the red box. (modified from Thompson, 2019).....	65
Figure B2. $\alpha=16^\circ$ , $\theta=10^\circ$ weir geometry. ....	66
Figure B3. $\alpha=20^\circ$ , $\theta=30^\circ$ weir geometry. ....	67

## NOMENCLATURE

A	Upstream interior apex length
$A_i$	Grid surface interface area
Cd	Discharge coefficient
$Cd_{-phys}$	Discharge coefficient calculated directly from physical data
$Cd_{-emp}$	Discharge coefficient calculated from empirical fit to physical data
$f_i$	CFD solution of interest
F	Froude Number
Fs	Factor of safety
GCI	Grid Convergence Index
g	Gravitational constant
h	Piezometric head
H	Total head
H/P	Headwater ratio
$l_c$	Centerline length of sidewall
$L_c$	Centerline length of weir, $L_c=L_c\text{-cycle} * N$
$L_{c\text{-cycle}}$	Centerline length of one complete cycle
N	Number of cycles
p	Fluid pressure
$p_c$	Order of convergence
P	Weir height
Q	Discharge or volumetric flow rate
$\rho$	Fluid density
r	Segment height from channel opening to center of imaginary arc circle
$r'$	Segment height from channel opening to perpendicular downstream apex
$r_g$	Grid refinement ratio, $r_g=\Delta 2/\Delta 1$
R	Arched radius, $R=(W^2/4 + r'^2)/2$
$R_{crest}$	Radius of crest shape
$t_w$	Wall thickness at crest
u	Local velocity in the y direction
v	Local velocity in the y direction

V	Depth averaged velocity
w	Local velocity in the z direction
w'	Cycle arc width, $w' = W'/N$
W	Downstream channel width
W'	Arced labyrinth weir arc width ( $R\Theta$ )
X	Horizontal Cartesian coordinate direction perpendicular to channel outlet
Y	Horizontal Cartesian coordinate direction parallel to channel outlet
$Y_c$	Critical depth
z	Vertical Cartesian coordinate direction
$\alpha$	Sidewall angle
$\alpha'$	Upstream sidewall angle, $\alpha' = \alpha + \theta/2$
$\varepsilon$	Relative error between CFD grid size
$\varepsilon$	Turbulent dissipation term in numerical turbulence model
$\varepsilon_{Cd}$	Relative error in $C_d$ between CFD and physical models
$\varepsilon'$	Cycle efficiency $\varepsilon' = C_d * L_{c-cycle} / w$
k	Turbulent kinetic energy in numerical turbulence model
$\omega_{xi}$	Sensitivity coefficient for each measured variable
$\theta$	Cycle arc angle, $\theta = \Theta/N$
$\Theta$	Central arc angle, $\Theta = W'/R$

## NOMENCLATURE

A	Upstream interior apex length
$A_i$	Grid surface interface area
Cd	Discharge coefficient
$Cd_{-phys}$	Discharge coefficient calculated directly from physical data
$Cd_{-emp}$	Discharge coefficient calculated from empirical fit to physical data
$f_i$	CFD solution of interest
F	Froude Number
Fs	Factor of safety
GCI	Grid Convergence Index
g	Gravitational constant
h	Piezometric head
H	Total head
H/P	Headwater ratio
$l_c$	Centerline length of sidewall
$L_c$	Centerline length of weir, $L_c=L_c\text{-cycle} * N$
$L_{c\text{-cycle}}$	Centerline length of one complete cycle
N	Number of cycles
p	Fluid pressure
$p_c$	Order of convergence
P	Weir height
Q	Discharge or volumetric flow rate
$\rho$	Fluid density
r	Segment height from channel opening to center of imaginary arc circle
$r'$	Segment height from channel opening to perpendicular downstream apex
$r_g$	Grid refinement ratio, $r_g=\Delta 2/\Delta 1$
R	Arched radius, $R=(W^2/4 + r'^2)/2$
$R_{crest}$	Radius of crest shape
$t_w$	Wall thickness at crest
u	Local velocity in the y direction
v	Local velocity in the y direction

V	Depth averaged velocity
w	Local velocity in the z direction
w'	Cycle arc width, $w' = W'/N$
W	Downstream channel width
W'	Arced labyrinth weir arc width ( $R\Theta$ )
X	Horizontal Cartesian coordinate direction perpendicular to channel outlet
Y	Horizontal Cartesian coordinate direction parallel to channel outlet
$Y_c$	Critical depth
z	Vertical Cartesian coordinate direction
$\alpha$	Sidewall angle
$\alpha'$	Upstream sidewall angle, $\alpha' = \alpha + \theta/2$
$\varepsilon$	Relative error between CFD grid size
$\varepsilon$	Turbulent dissipation term in numerical turbulence model
$\varepsilon_{Cd}$	Relative error in $C_d$ between CFD and physical models
$\varepsilon'$	Cycle efficiency $\varepsilon' = C_d * L_{c-cycle} / w$
k	Turbulent kinetic energy in numerical turbulence model
$\omega_{xi}$	Sensitivity coefficient for each measured variable
$\theta$	Cycle arc angle, $\theta = \Theta/N$
$\Theta$	Central arc angle, $\Theta = W'/R$

## DISCLAIMER

The purpose of this research is not to promote or discredit any commercially available Computational Fluid Dynamics (CFD) solvers. The results from this research are applicable only to the mesh, boundary conditions, other user-defined settings, and geometries tested. The scope of this research is small and does not encompass the full capabilities of either solver; however, this research does highlight the importance of user-defined settings independent of solver. It is also important to note that the full or optimized capabilities of each solver may not have been utilized and may affect results.

## INTRODUCTION

Successful water management and conveyance are critical for human safety and quality of life. Hydraulic structures are an important piece of this management process. Weirs are a common hydraulic structure used to divert, store, and measure the flow of water; weirs have been used in streams, canals, rivers, ponds, and reservoirs (Crookston, 2010). There are many types of weir geometries for a variety of water management applications. Many existing weirs need rehabilitation or replacement due to aging infrastructure, updated regulations, and undersized capacity to meet current hydrological predictions, changes in land development, and a changing climate. For many of these projects, modifying the existing spillway to a hydraulically more efficient design is the most efficient and economical solution (Tullis et al, 1995).

Weir discharge capacity is calculated based on the weir's crest length per a standard weir head-discharge equation (Eq. [1]) (Henderson, 1966). In Eq. [1], Q is the discharge over the weir's crest, L is the crest length, g is the acceleration due to gravity, H is the total head or depth of water over the weir crest, and  $C_d$  is an empirically determined discharge coefficient representing weir efficiency.

$$Q = \frac{2}{3} C_d L \sqrt{2gH^{\frac{3}{2}}} \quad [1]$$

The discharge capacity of a weir is governed by the crest length (L), crest geometry, and the approach flow conditions. Since the width of the channel or reservoir spillway is often restricted, folding the weir (in plan-view) into trapezoidal segments (cycles) is one way to increase the discharge capacity within a fixed channel width (see Figure 1). This is a labyrinth weir.

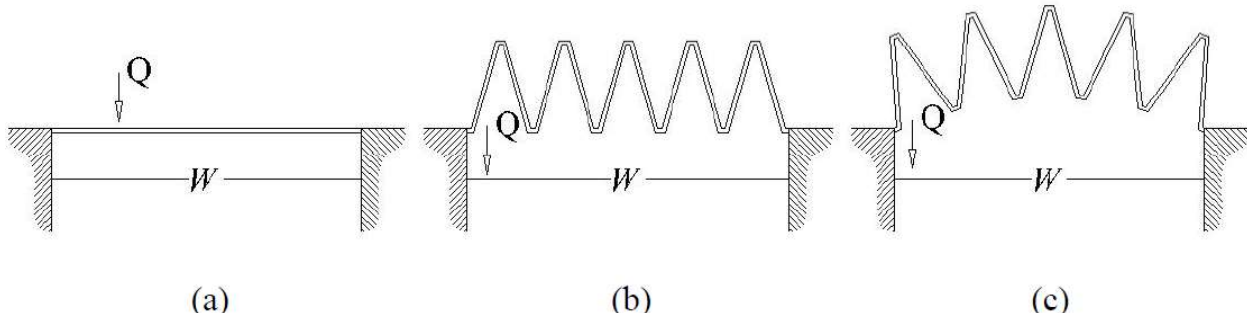


Figure 1. Plan view of a (a) linear weir, (b) labyrinth weir, and (c) arced labyrinth weir specific to a reservoir-to-channel transition (Christensen, 2012).

A labyrinth weir increases the effective weir length for a given channel or spillway width, which increases the discharge capacity of a spillway. Labyrinth weirs have been the topic of interest for researchers, engineers, and water managers over the last few decades. Labyrinth weirs are hydraulically more efficient, meaning they can pass the same discharge at a lower upstream water surface elevation, or upstream head. Typical labyrinth weirs are built with a linear centerline axis (see Figure 1b). Since the initial efforts of Bruno Gentilini in 1940, many studies have looked into the labyrinth weir design method: Taylor (1968), Hay and Taylor (1970), Darvas (1971), Hinchliff and Houston (1984), Lux and Hinchliff (1985), Magalhães and Lorena (1989), Tullis et al. (1995), Melo et al. (2002), Falvey (2003), Tullis et al. (2007), Lopes et al. (2006, 2008), and Crookston and Tullis (2013).

Arcing the labyrinth weir (Figure 1c) for reservoir applications increases the hydraulic efficiency by 5-11% (Crookston, 2011; Crookston and Tullis, 2013). When the spillway is engaged, the arced cycles are better oriented to efficiently handle converging reservoir approach flows and increase the inlet cycle's hydraulic capacity (Thompson, 2019). Figure 2 shows an example of an arced labyrinth weir, Isabella Dam under construction in Bakersfield, California.



Figure 2. Isabella Dam in Bakersfield, California (Photo: US Army Corps of Engineers).

Several laboratory studies have been completed for arced labyrinth weir design: Yildiz and Uzecek (1996), Copeland and Fletcher (2000), Crookston (2011), Christensen (2012), Crookston and Tullis (2012), and Thompson (2019).

Flow patterns over a labyrinth weir are three-dimensional in nature and often difficult to accurately describe mathematically; empirically determined discharge coefficients, obtained from physical modeling, are applied to the head-discharge equation (Eq [1]). Numerical modeling or computational fluid dynamics (CFD) has been successfully applied to predict traditional labyrinth weir hydraulic performance: Sangsefidi et al (2015), Savage et al (2016), and Crookston (2019).

While physical and numerical design guidance for traditional labyrinth weirs is plentiful, limited research has been performed for arced labyrinth weirs. Crookston (2010), Crookston and Tullis (2012), Christensen (2012), and Thompson (2019) researched the effects of cycle number, sidewall angle, and arc angle (see Figure 3) on discharge capacity and efficiency. This comprises the preliminary empirical data used to predict hydraulic performance of prototype arced labyrinth weirs. The proposed study will provide some insights related to best practices in CFD design for

predicting hydraulic performance of arced labyrinth weirs along with methods for estimating the level of uncertainty.

The purpose of this research is not to promote or discredit any commercially available Computational Fluid Dynamics (CFD) solvers. The results from this research are applicable only to the mesh, boundary conditions, other user-defined settings, and geometries tested. The scope of this research is small and does not encompass the full capabilities of either solver; however, this research does highlight the importance of user-defined settings independent of solver. It is also important to note that the full or optimized capabilities of each solver may not have been utilized and may affect results.

## LITERATURE REVIEW

Labyrinth weirs in channelized applications are oriented such that water approaches perpendicular to the weir centerline axis. Likewise, labyrinth weirs in reservoir applications can be modified to orient the cycles more optimally to the converging reservoir approach flow. The cycle layout follows the arc of a circle and is called an arced labyrinth weir. This literature review discusses prior research on arced labyrinth weirs and the use of CFD to numerically model non-linear weirs.

### **Arced Labyrinth Weir Research**

Previous studies have shown that non-linear approach flow conditions can decrease the discharge capacity of a traditional labyrinth weir. Since traditional labyrinth weirs are typically designed for channelized applications, it makes sense to orient the cycles of a labyrinth weir in a reservoir application along an arc, so approach flows better align with upstream inlets. Copeland and Fletcher (2000) stated that a labyrinth weir's discharge capacity is sensitive to the approach flow magnitude and direction. Yildiz and Uzeck (1996) claim an arced labyrinth weir can discharge twice as much as a traditional labyrinth weir because of better flow accommodation. However, Houston's (1983) data shows a 20% increase in discharge for a weir projecting into a reservoir as compared to an in-channel weir at a similar head ( $H$ ).

Falvey (2003) cited four model studies (Prado, Kizilcapinar, Sarioglan, and Avon spillways) which were impacted by non-ideal approach flow conditions and suggests that arcing the spillway alignment would have increased spillway efficiency. These non-ideal approach flow conditions resulted in decreased discharge capacity, turbulent flow at the crest, flow separation, and unstable nappe aeration. The Kizilcapinar and Avon spillways have since had geometry changes where an arced weir was installed to address these concerns.

Crookston (2010), used six laboratory-scale arced labyrinth weir geometries and two traditional labyrinth weir in a reservoir headbox to compare discharge efficiency. The nomenclature established by Crookston (2010) will be used throughout this study (see Figure 3).

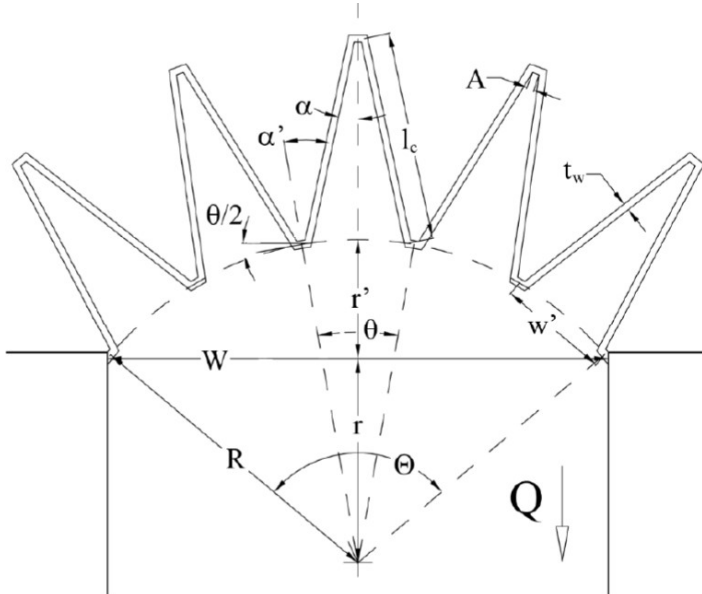


Figure 3. Arced labyrinth weir nomenclature (Crookston, 2010).

Arced labyrinth weir geometric parameters include:

A	Upstream interior apex length
$l_c$	Centerline length of the sidewall
$L_c\text{-cycle}$	Centerline length of one complete cycle
N	Number of cycles or trapezoidal folds
Q	Discharge or volumetric flow rate
r	Segment height from channel opening to center of imaginary arc circle
$r'$	Segment height from channel opening to perpendicular downstream apex
R	Arched radius, $R = (W^2/4 + r'^2)^{1/2}$

$t_w$	Wall thickness at crest
$w'$	Cycle arc width, $w' = W'/N$
$W$	Downstream channel width
$\alpha$	Sidewall angle
$\alpha'$	Upstream sidewall angle, $\alpha' = \alpha + \theta/2$
$\theta$	Cycle arc angle, $\theta = \Theta/N$
$\Theta$	Central arc angle, $\Theta = W'/R$

Crookston and Tullis (2012) tested 5-cycle arced labyrinth weirs with sidewall angles of  $\alpha = 6^\circ$  and  $12^\circ$  and cycle arc angles of  $\theta = 10^\circ, 20^\circ$ , and  $30^\circ$ . They found the arced labyrinth weir configurations had a higher discharge capacity compared to the traditional configuration. They also found this increased discharge capacity exceeds the outlet cycle free-flow capacity faster than a traditional configuration. In other words, the arced configuration increases the discharge per unit weir length; however, this causes local submergence on the weir at a lower upstream head ( $H$ ).

This is presented clearly in Figure 4, which shows data from Crookston and Tullis (2012) for arced and traditional labyrinth weirs with  $\alpha = 6^\circ$  and selected cycle arc angles ( $\theta$ ). The data show arced labyrinth weirs are more efficient than non-arced weirs in a reservoir under specific site conditions.

Crookston and Tullis (2012) conclude that site-specific flow conditions directly affect the efficiency of arced labyrinth weirs. A designer must consider existing conditions when selecting an arced vs traditional labyrinth weir; for example, Tacail et al. (1990) found that under certain site-specific conditions, arced and traditional labyrinth weirs produce approximately the same discharge at maximum head.

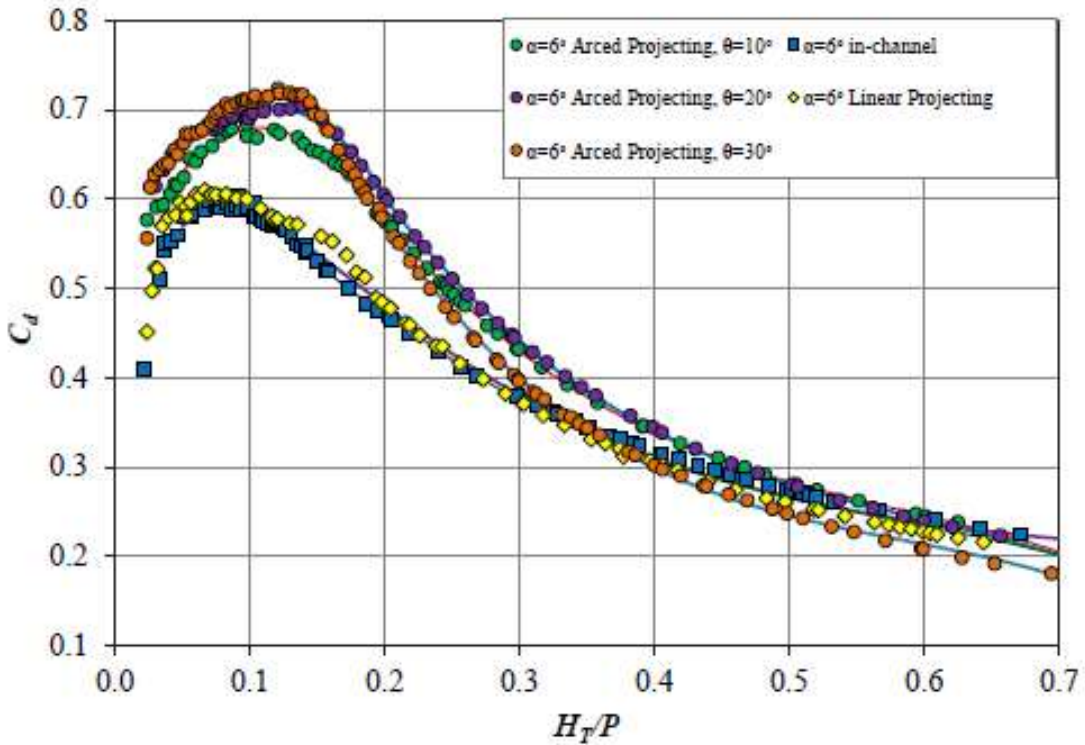


Figure 4. Discharge efficiency comparison between  $\alpha=6^\circ$  labyrinth weirs of varying  $\theta$  with reservoir approach flow (Crookston, 2010).

Christensen (2012) furthered the research performed by Crookston (2010) and Crookston and Tullis (2012) with physical models of arced labyrinth weirs with a sidewall angle of  $\alpha = 12^\circ$  and  $20^\circ$  and cycle arc angles of  $\theta = 10^\circ, 20^\circ$ , and  $30^\circ$ . He also evaluated the effect of cycle numbers ( $N = 5, 7$ , and  $10$ ). He observed that varying the cycle number resulted in little to no change in discharge efficiency ( $C_d$ ) for a given geometry, which suggests that the end effects associated with two distal cycles is relatively limited on discharge efficiency.

Christensen (2012) studied the effects of different sidewall angles on the behavior of the nappe and found that larger sidewall angles resulted in more unsteady nappe aeration conditions and spatial variability (Figure 5).

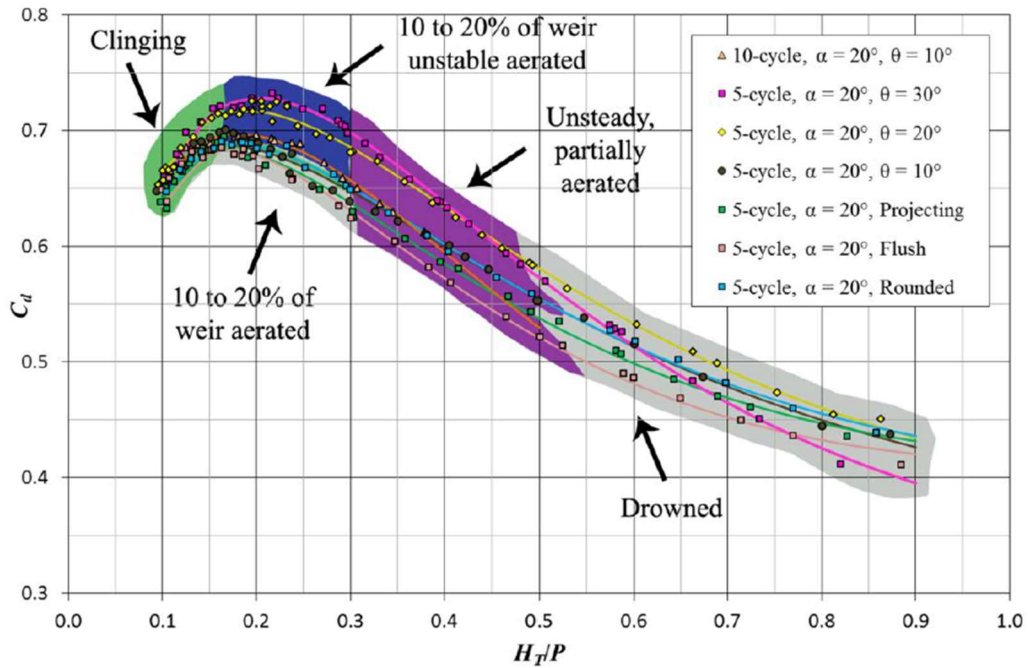


Figure 5.  $C_d$  versus  $H/P$  showing nappe aeration conditions for arced labyrinth weirs of  $\alpha = 20^\circ$  (Christensen, 2012).

To improve this nappe stability, Christensen (2012) installed triangular columns (nappe breakers) on the downstream apex of each cycle. The purpose of a nappe breaker is to provide a path for air to reach the underside of the nappe (i.e., vent the nappe) to eliminate negative pressures and improve nappe stability. Christensen (2012) found that nappe stability increased with nappe breakers installed, but discharge efficiency decreased.

Furthermore, Christensen (2012) compared traditional and arced labyrinth weirs of the similar geometries and found that both  $\alpha = 12^\circ$  and  $20^\circ$  resulted in a higher discharge efficiency when arced;  $\alpha = 12^\circ$  increased by as much as ~20% and  $\alpha = 20^\circ$  only increased by as much as ~8%. Christensen (2012) concluded the discharge efficiency advantage of an arced labyrinth weir versus a traditional labyrinth weir decreases with increasing  $\alpha$ .

Sangsefidi et al. (2015), validated the Crookston and Tullis (2012) data using CFD. With the validated model, Sangsefidi et al. (2015) also observed increased local submergence for

arced labyrinth weirs. They found by lowering the downstream apron of the labyrinth weir, by the same height as the weir's height, they were able to increase the free-flow capacity of the cycles. This design may be less practical as it would require more excavation and filling during construction; therefore, it may likely be more practical to utilize a taller weir instead.

Thompson (2019) built on the work of Christensen (2012) and Sangsefidi et al. (2015), by combining physical and numerical modeling to better understand the hydraulic behavior of arced labyrinth weirs in reservoir applications. He tested several arced labyrinth weirs with a sidewall angle of  $\alpha = 16^\circ$  and  $\theta = 10^\circ, 20^\circ$ , and  $30^\circ$ . Thompson (2019) found the  $\alpha = 16^\circ$  arced labyrinth weirs are more hydraulically efficient than would be predicted by interpolating between  $\alpha = 12^\circ$  and  $20^\circ$ . Thompson (2019) data also show the  $\theta=30^\circ$  geometry is the most efficient for  $H/P < 0.35$  and the least efficient for  $H/P > 0.4$ . He attributes this to better cycle alignment for low flows and increased flow momentum and local submergence at high flows.

## **Numerical Modeling**

The use of computational fluid dynamics (CFD) as a design tool is becoming more common for practicing engineers. CFD models are often validated using empirical data, however, a CFD model is likely to be a potential design option when applicable empirical data is not available. Models that fall under this latter category still need to be validated. The American Society of Civil Engineer's (ASCE) Task Committee on 3D Free-Surface Flow Model Verification and Validation have extensive resources for validation, verification, error estimation, and uncertainty of numerical models (ASCE, 2009). The committee specifically requires the use of the Grid Convergence Index (GCI) for numerical model verification as designed by Roache (1998).

The GCI provides a method of reporting grid convergence as shown in Eq. [2]. In Eq. [2],  $r_g$  is the grid refinement ratio ( $r_g = \Delta_2/\Delta_1$ ;  $\Delta$  = size of grid elements),  $p_c$  is the order of convergence,  $\varepsilon$  is the relative error between grid size solutions (residuals or  $|f_2-f_1|/f_1$ ), and  $F_s$  is an empirically calculated factor of safety

$$GCI = F_s \frac{|\varepsilon|}{r_g^{p_c-1}} \quad [2]$$

The recommended  $F_s$  is 1.25 for three mesh sizes and 3 for two mesh sizes. This corresponds with numerical 95% error bounds (ASCE, 2009). The GCI provides mesh convergence criteria but a direct comparison with physical laboratory data is ideal. The rest of this section will highlight previous nonlinear weir related research conducted using CFD.

In an effort to extend predictive head-discharge relationship to much greater upstream heads than previously reported in the literature, Savage et al. (2016) built on the laboratory data research of Crookston and Tullis (2012) for an  $\alpha = 15^\circ$ , in-channel, traditional labyrinth weir from heads of  $H/P = 1.0$  to 2.0 using physical and numerical modeling. They used two turbulence models, LES and RNG k- $\varepsilon$ , and found that different turbulence models had little effect on discharge estimation for traditional labyrinth weirs. They concluded that their numerical model trended toward over prediction of physical data (5-7%). Savage et al. (2016) used the ASCE (2009) GCI method to present model convergence and prove their solutions were independent of model mesh size. They concluded that grid refinement did result in increased relative error between numerical and physical results. This error is contributed to the use of the FAVOR algorithm to resolve solid geometries by volume of obstacle to volume-of-cell ratio and the ratio of obstacle area to cell face area. In other words, the solid obstacles (in this case the weir), are seen by the algorithm differently as the mesh changes.

Crookston et al. (2018) numerically modeled two piano key (PK) weir geometries that were previously physically modeled by Anderson and Tullis (2013). Some studies have shown that no turbulence models are required for head-discharge measurements (Lefebvre et al., 2014 and Pralong et al., 2011); Crookston et al. (2018) sought to determine the effects of different turbulence models on the output simulation results. Similarly to Savage et al. (2016), they used two separate turbulence models, LES and RNG k- $\epsilon$ , to determine solution dependence on turbulence for several hydraulic structures. Crookston et al. (2018) found that both turbulence models were suitable for estimating hydraulic conditions within 4% error. They concluded that CFD can be a higher order design tool than empirically obtained design methods because there is the ability to include site-specific conditions. Quantifying the uncertainty of these results is critical to project success; physical model data or observations and collected data from an event are needed for calibration and validation of numerical models used for design.

Thompson (2019) provided numerical model results with concurrence to physical model results (Figure 6). His data provided relative errors between -2.5% and 3.6% with his converged mesh model. Thompson (2019) used a GCI value of less than 2.2% to verify his numerical solutions independence from mesh.

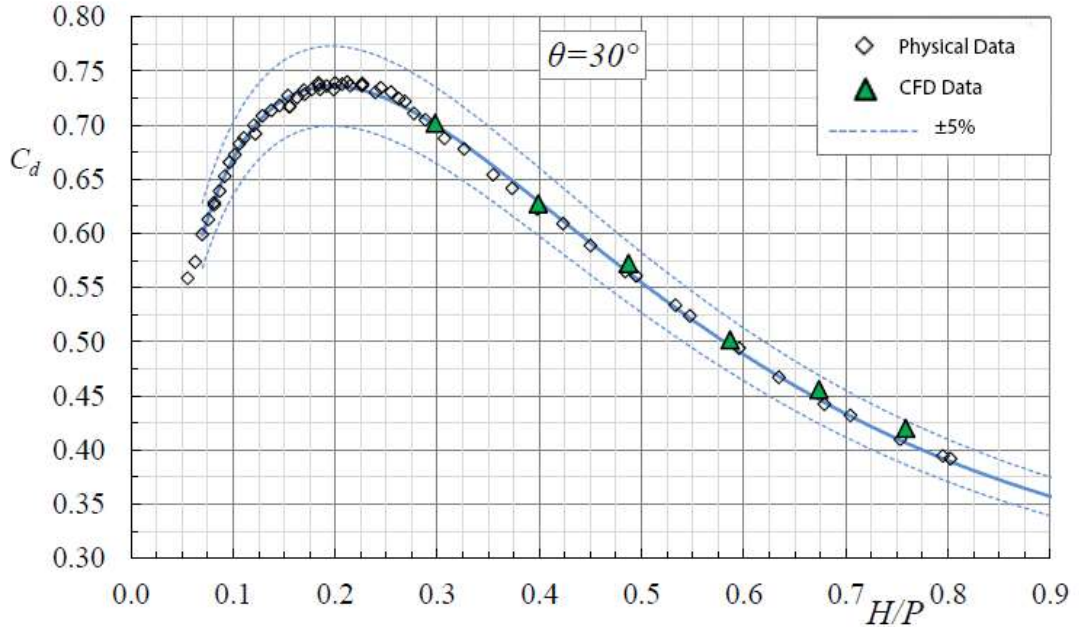


Figure 6.  $C_d$  vs. H/P comparison between physical and numerical results for the  $\alpha=16^\circ$ :  $\theta=30^\circ$  weir (Modified from Thompson, 2019).

Comparing the physical and numerical model results, Thompson (2019) found that the numerical model generally replicates the nappe and local submergence behaviors for larger cycle arc angles ( $\theta = 30^\circ$ ) (Figure 7).

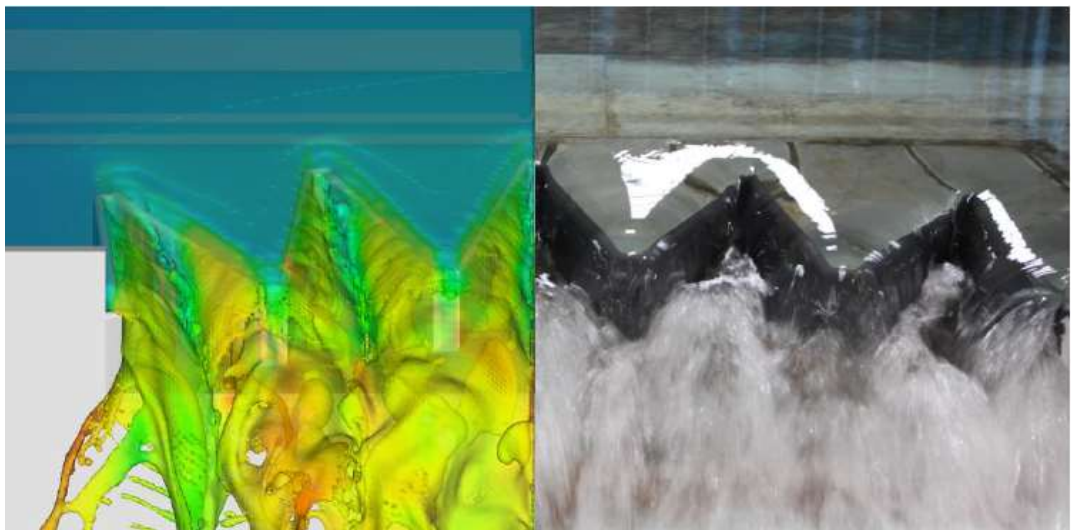


Figure 7.  $\alpha=16^\circ$ :  $\theta=30^\circ$  H/P=0.4 comparison between numerical and physical nappe and tailwater aeration (Thompson, 2019).

Thompson (2019) emphasized when using empirical data, designers need to consider site specific conditions that might affect discharge efficiency (i.e., local submergence, approach flow angles, and increased nappe instability). Thompson (2019) concluded “CFD can be a useful tool in the hydraulic design of arced labyrinth weirs.”

The current study uses two 5-cycle arced labyrinth weir geometries,  $\alpha=16^\circ$ :  $\theta=10^\circ$  and  $\alpha=20^\circ$ :  $\theta=30^\circ$  with numerical models built in two commercially available solvers, Flow 3D® and Star CCM+®. A sensitivity analysis was completed using the  $\alpha=20^\circ$ :  $\theta=30^\circ$  arced labyrinth weir model to determine which user-defined parameters affect the predicted hydraulic efficiency. Simulations were then completed in both solvers to outline a rating curve ( $H/P = 0.3, 0.4, 0.5, 0.7$ , and  $0.8$ ), along with a mesh convergence at two rating curve points ( $H/P = 0.3$  and  $0.7$ ). These simulations were completed using only default solver settings. The midpoint of the rating curve ( $H/P = 0.5$ ) was repeated with additional user-defined changes to the default settings including mesh configuration, momentum advection scheme order, and turbulence model. The results are compared quantitatively and qualitatively to existing physical data collected by Christensen (2012) and Thompson (2019) for their respective geometries, as well as to numerical data collected by Thompson (2019) for the  $\alpha=16^\circ$ :  $\theta=10^\circ$  arced labyrinth weir.

The results provide insight into the repeatability of numerical data, the ability for CFD to simulate hydraulic behavior, the sensitivity of numerical models to user-defined settings, the relative error associated with default solver settings, and the reduction or increase of relative error with user-defined changes to solver settings.

## Research Objectives

The following represent the key research objectives in this study:

- Explore the feasibility of using CFD as a design tool for designing arced labyrinth weirs by comparing existing physical and numerical hydraulic performance data for arced labyrinth weirs of  $\alpha = 16^\circ$ ,  $\theta = 10^\circ$  and  $\alpha = 20^\circ$ ,  $\theta = 30^\circ$  with new data from the current study. Quantitative and qualitative results will be compared to existing physical and numerical data to determine repeatability and expand knowledge of different weir geometries.
- Observe hydraulic behavior as simulated in CFD and anomalies on various arced labyrinth weir models that match or vary from physical model observations to provide advantages and disadvantages of the numerical modeling approach.
- Define parameters within CFD model setup that affect results through a sensitivity analysis.
- Compare different commercially available solvers and determine if there is an advantage to using one over the other when modeling arced labyrinth weirs.
- Add to existing design tools and expand knowledge of model creation and setup beyond using defaults within commercially available solvers.
- Provide insight into some CFD capabilities beyond what can be measured in a physical model (e.g., flow structure, unit discharge nonuniformity along weir crest, and weir pressures).

## NUMERICAL MODEL SETUP

The numerical modeling of the current study involves the  $\alpha=20^\circ$ :  $\theta=30^\circ$  and  $\alpha=16^\circ$ :  $\theta=10^\circ$  arced labyrinth weirs using two different commercially available CFD solvers, Flow-3D® and Star CCM+®. This section provides a description of the equations solved and algorithms used to render the solid and track the free water surface; additionally, an explanation of the numerical model setup for each solver package is given. Appendix A provides a glossary of terms used in CFD.

### Numerical Models

Both solver packages (Flow-3D and Star-CCM+) solve the Reynold's-Averaged Navier Stokes (RANS) equations which describe fluid motion by differentiating Newton's Second Law to relate the forces which are acting on the finite element or volume (Flow-3D, 2016). This includes gravitational, pressure, and viscous forces (Finnemore and Franzini, 2002). A common assumption for water in free surface applications is incompressible fluid and constant viscosity. With these assumptions applied to Cartesian coordinates (with z increasing vertically), the RANS equations in the x, y, and z directions are defined in Eq. [3].

$$x : -\frac{dp}{dx} + \mu \left( \frac{\partial^2 u}{\partial x^2} + \frac{\partial^2 u}{\partial y^2} + \frac{\partial^2 u}{\partial z^2} \right) = \rho \left( \frac{\partial u}{\partial t} + u \frac{\partial u}{\partial x} + v \frac{\partial u}{\partial y} + w \frac{\partial u}{\partial z} \right) \quad \text{Eq. [3a]}$$

$$y : -\frac{dp}{dy} + \mu \left( \frac{\partial^2 v}{\partial x^2} + \frac{\partial^2 v}{\partial y^2} + \frac{\partial^2 v}{\partial z^2} \right) = \rho \left( \frac{\partial v}{\partial t} + u \frac{\partial v}{\partial x} + v \frac{\partial v}{\partial y} + w \frac{\partial v}{\partial z} \right) \quad \text{Eq. [3b]}$$

$$z : -\rho g - \frac{dp}{dz} + \mu \left( \frac{\partial^2 w}{\partial x^2} + \frac{\partial^2 w}{\partial y^2} + \frac{\partial^2 w}{\partial z^2} \right) = \rho \left( \frac{\partial w}{\partial t} + u \frac{\partial w}{\partial x} + v \frac{\partial w}{\partial y} + w \frac{\partial w}{\partial z} \right) \quad \text{Eq. [3c]}$$

The force terms are on the left side of the equation, while the convection and local acceleration terms are on the right. In both solver packages, the computational mesh domain was comprised of hexahedral (cube) cells, which were refined in size (made smaller) close to the weir. Within each cell, the RANS equations (Eq. [3]) are used to calculate flow parameters such as average

pressure ( $p$ ) and velocity ( $u, v, w$ ). The mesh is also used to define the flow boundary solid surfaces (e.g., arced labyrinth weir, apron, and downstream wing walls).

### **Flow-3D®**

Flow 3D® numerically solves Eq. [3] using a or finite volume approximation. Each cell has associated local average values of all dependent variables. The calculated pressures represent the cell center value while the calculated velocities are resolved at all grid cell faces.

Flow-3D uses an algorithm called the fractional area/volume obstacle representation (FAVOR) method. The FAVOR method is used to numerically define the region of a cell that contains an “obstacle” (i.e., wall boundaries and other solid geometric features). This is done by computing the ratio of the obstacle area to cell face area and the obstacle volume to cell volume. If this ratio ( $F$ ) is one (i.e., the whole cell is an obstacle), the cell becomes a solid. A ratio equal to zero defines a cell in the fluid domain. A ratio between zero and one represents a partially filled cell (Flow-3D, 2016). This method defines each surface as a series of interconnected, flat planes, so a curved surface is approximated as flat surfaces in each cell using the first-order technique as demonstrated in Figure 8. The algorithm is run during preprocessing, rendering the weir and reservoir prior to the simulation. These obstacles or solids are held stationary throughout the simulation process. Savage et el. (2016) commented that the FAVOR renderings return very similar results to triangulated irregular network (TIN) commonly used in geospatial surveys for geographic information systems.

The free surface varies spatially and temporally, so it is tracked using an algorithm called modified volume-of-fluid (VOF) method (Hirt and Nichols, 1981). Similarly to the FAVOR method, the VOF method uses a ratio to calculate the fraction of a cell that is filled with fluid (Figure 9).

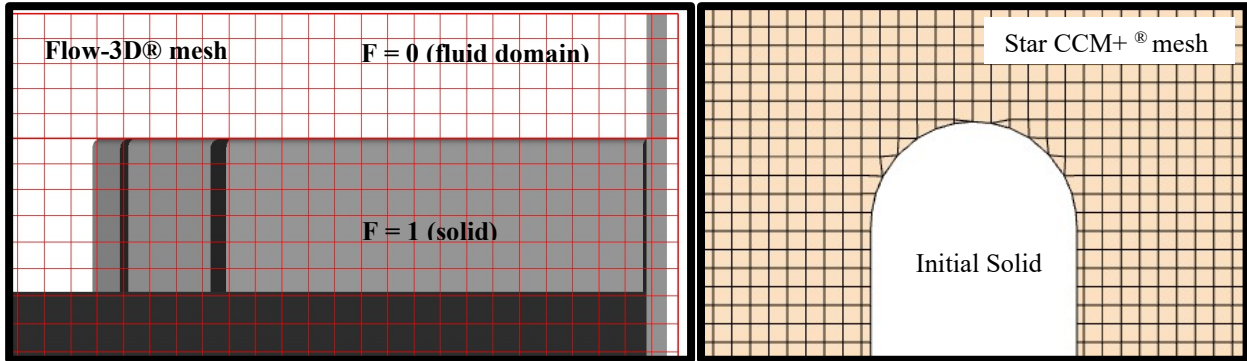


Figure 8. Comparison of Flow-3D and Star CCM+ volume discretization and meshing methods.

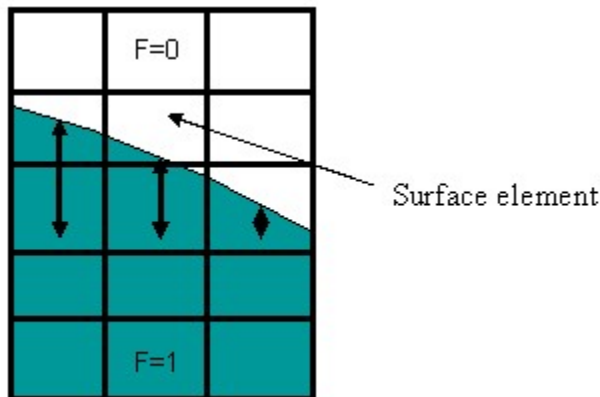


Figure 9. Flow-3D VOF method for tracking the free surface (Flow-3D, 2016).

Flow-3D is optimized for open channel water applications, where it is typically suitable to neglect the inertia of the air adjacent to the water surface. This is because water is much denser than air, so the impacts of the air are negligible. The volume of air is replaced with empty space, void of mass, resulting in a single fluid model. The empty space has a constant (atmospheric) pressure and temperature (Flow-3D, 2016). This assumption reduces the computational demand required to track the free surface. A standard VOF method results in a “misty region” within the cells located at the free surface. The modified VOF method (used by Flow-3D) allows for small volume corrections to the volume of these misty regions at the end of each time step to define the water surface more accurately than the standard VOF method (Savage et al, 2016). The sum of the corrections throughout a simulation are generally less than  $\pm 0.01\%$ , which is considered insignificant to the solution.

Flow-3D provides the user with six (6) turbulence closure schemes or turbulence models to choose from in each simulation: Prandtl mixing length, one-equation (turbulent energy model), Two-equation ( $k-\varepsilon$ ) model, Renormalized group (RNG  $k-\varepsilon$ ) model, Two-equation ( $k-\omega$ ) model, and the Large Eddy Simulation (LES) model. The RNG model is the set default for Flow-3D. Turbulence models will be discussed below.

### **Star CCM+®**

Star CCM+® solves Eq. [3] using a finite difference approximation. Each cell can have any number of faces if there are enough faces to create a closed cell volume. An algorithm called the surface remesher is used to numerically define the initial surface geometry (in this case imported from a STL or similar file). The mesh is formed around the solids, seamlessly joining them to the cells with potential for fluid flow (Figure 8). There are nine (9) mesher algorithms available in Star CCM+; however, for this study, an algorithm called the trimmed cell mesh was chosen to most closely match the mesh selection for Flow-3D. This model utilizes a template mesh constructed from hexahedral cells at a user defined target size. The mesh is trimmed to the user-defined surface size and shape (Star CCM+, 2021). Additionally, prism layer and volumetric control meshes can be added to ensure capture of boundary layers, better refinement of important elements, more or less dense meshes on different parts or locations in the extents, and self-adjusting mesh to refine the mesh near areas of high gradients. Accurate and detailed meshes provide more accurate turbulence modeling.

Star CCM+ uses a pressure-velocity coupling algorithm called SIMPLE, which uses the predictor-corrector approach to calculate velocity and pressure. The predictor-corrector approach is constructed from the continuity equation and the momentum equations such that the velocity field predicted fulfills the continuity equation by correcting the pressure (Star CCM+, 2021).

Multiphase flows, meaning multiple fluids flowing in the discretized domain, are common in many engineering applications. An arced labyrinth weir, for example, has two phases (i.e., water and air) forming a free surface between phases. Star-CCM+ uses user-defined phases, for example in this study Phase 1 (water) and Phase 2 (air). The VOF method is used to track the free surface. This free surface tracking resolves the position and shape of the interface between phases with a ratio to calculate the fraction of the cell that is filled with Phase 1 (Star CCM+). If this ratio is zero, the cell is completely filled with Phase 2 (air); a ratio equal to one defines a cell as filled with Phase 1 (water); and a ratio between zero and one indicates the presence of an interface between Phase 1 and Phase 2 (Star CCM+, 2021). In cells where both phases are present, the volume fraction transport is solved for only Phase 1. The volume fraction of Phase 2 is adjusted so the sum of the volume fractions equals 1 for each cell (Star CCM+, 2021).

Star CCM+ provides user with 21 turbulence closure schemes or turbulence models to choose from in each simulation: 16 RANS-based models, 2 LES models, and three DES models. The Realizable ( $k-\varepsilon$ ) two-layer model (a RANS-based model) is the default model for Star-CCM+. Turbulence models will be discussed below.

## **Turbulence Models**

Turbulence in fluid flow cannot be explicitly solved because of its random, unsteady, three-dimensional characteristics. Richard Feynman, an American theoretical physicist and winner of the Nobel Prize in Physics, said, “Turbulence is the most important unsolved problem of classical physics.” CFD utilizes turbulence closure schemes or turbulence models as a simplifying method to numerically approximate turbulence. Rigorous effort is required to produce accurate numerical approximations because turbulence is unsteady, irregular and changing in time and space, three-dimensional, dissipative, and diffusive at varying intensities

dependent on the level of turbulence (Solmaz, 2022). Turbulence closure schemes are a key issue in most CFD simulations and almost all engineering applications for CFD are turbulent and therefore require a turbulence model. There are over 35 different turbulence models or variations for specific applications: these models range from a Direct Numerical Solution (often impractical or impossible) to LES, and RANS-based turbulence models (CFD Online Wiki, 2011). RANS-based and LES models are the most common for open channel flow applications. Flow-3D has six (6) available turbulence models, five of which are RANS-based models. For this study, only RANS-based models were used so only RANS-based models are discussed in this section.

The default turbulence model for Flow-3D is the RNG ( $k-\varepsilon$ ) turbulence model and Realizable ( $k-\varepsilon$ ) two-layer model for Star-CCM+. Each of these models were used in the current study; additionally, a one-equation model (Prandtl mixing length or Spalart-Allmaras), and 2 two-equation models ( $k-\omega$  standard, and  $k-\varepsilon$  standard) were used in the current study.

Flow-3D and Star CCM+ have different available one-equation models, Prandtl and Spalart-Allmaras, respectively. One-equation models solve one turbulent transport equation, usually the turbulent kinetic energy ( $k$ ). Prandtl was the original one-equation model (Eq. [4]) where  $v$  is velocity,  $k$  is turbulent kinetic energy,  $\sigma$  is a constant of 2/3, and  $l$  is the turbulent length scale. This model is based on the concept that a fluid parcel will conserve its properties for a specified length (the mixing length) before it mixes with the surrounding fluid. The mixing length ( $l$ ) depends on the nature of the flow but is typically treated as a constant input to the simulation (7% of the smallest mesh size) (Flow-3D, 2016). Spalart-Allmaras can resolve the entire flow field down to the solid wall and is robust with moderate resolution requirements. It does not accurately compute fields that exhibit shear flow, separated flow, or decaying turbulence (CFD Online Wiki, 2011).

$$\frac{\partial k}{\partial t} + U_j \frac{\partial k}{\partial x_j} = \tau_{ij} \frac{\partial U_i}{\partial x_j} - C_D \frac{k^{\frac{3}{2}}}{l} + \frac{\partial}{\partial x_j} \left[ \left( \nu + \frac{\nu_T}{\sigma_k} \right) \frac{\partial k}{\partial x_j} \right] \quad \text{Eq. [4]}$$

The  $k$ - $\varepsilon$  (standard, realizable, and RNG) model utilizes two transport equations: one for turbulent kinetic energy ( $k$ ) and another for turbulent dissipation ( $\varepsilon$ ).  $k$  determines the energy of the turbulence while  $\varepsilon$  determines the scale. The model transport equation for  $k$  is derived from the exact equation (Eq. [5]), but the  $\varepsilon$  is obtained using physical reasoning and does not resemble the exact equation (Eq. [6]) where  $\mu$  is turbulent viscosity,  $P_k$  is the production of  $k$ ,  $P_b$  is the Prandtl number,  $S_\varepsilon$  is the modulus of the mean rate-of-strain tensor, and  $C$  is a range of known constants.

$$\frac{\partial}{\partial t}(\rho k) + \frac{\partial}{\partial x_i}(\rho k u_i) = \frac{\partial}{\partial x_j} \left[ \left( \mu + \frac{\mu_t}{\sigma_k} \right) \frac{\partial k}{\partial x_j} \right] + P_k + P_b - \rho \epsilon - Y_M + S_k \quad \text{Eq. [5]}$$

$$\frac{\partial}{\partial t}(\rho \epsilon) + \frac{\partial}{\partial x_i}(\rho \epsilon u_i) = \frac{\partial}{\partial x_j} \left[ \left( \mu + \frac{\mu_t}{\sigma_\epsilon} \right) \frac{\partial \epsilon}{\partial x_j} \right] + C_{1\epsilon} \frac{\epsilon}{k} (P_k + C_{3\epsilon} P_b) - C_{2\epsilon} \rho \frac{\epsilon^2}{k} + S_\epsilon \quad \text{Eq. [6]}$$

The standard and realizable  $k$ - $\varepsilon$  are dependent on a single turbulence length scale (Prandtl number,  $P_b$ ), while the RNG  $k$ - $\varepsilon$  model mathematically accounts for turbulent mixing at various scales of motion.

The standard  $k$ - $\varepsilon$  model works well with external flow interactions with complex geometry but is only applicable for fully turbulent flow. The RNG  $k$ - $\varepsilon$  model works well with free-surface flows and rotating turbulent patterns with small mean pressure gradients but shows no improvement over the standard  $k$ - $\varepsilon$  model for predicting vortex evolution (CFD Online Wiki). The realizable  $k$ - $\varepsilon$  model satisfies certain mathematical constraints on the Reynolds stress that neither the standard nor RNG models satisfy. This means the realizable  $k$ - $\varepsilon$  model more accurately predicts the spreading rate of jets, performance of flow involving rotation, and

boundary layers under strong pressure gradients, separation, and recirculation. The realizable  $k-\varepsilon$  model is limited in situations where the computational domain contains both rotational and stationary fluid zones.

The standard  $k-\omega$  model also utilizes two transport equations: one for turbulent kinetic energy ( $k$ ) and another for specific dissipation ( $\omega$ ).  $k$  determines the energy of the turbulence while  $\omega$  determines the scale (Eq. [7] and Eq. [8]). In Eq. [7] and [8], all terms not previously defined are known constants.

$$\frac{\partial k}{\partial t} + U_j \frac{\partial k}{\partial x_j} = P_k - \beta^* k \omega + \frac{\partial}{\partial x_j} \left[ (\nu + \sigma_k \nu_T) \frac{\partial k}{\partial x_j} \right] \quad \text{Eq. [7]}$$

$$\frac{\partial \omega}{\partial t} + U_j \frac{\partial \omega}{\partial x_j} = \alpha S^2 - \beta \omega^2 + \frac{\partial}{\partial x_j} \left[ (\nu + \sigma_\omega \nu_T) \frac{\partial \omega}{\partial x_j} \right] + 2(1 - F_1) \sigma_{\omega^2} \frac{1}{\omega} \frac{\partial k}{\partial x_i} \frac{\partial \omega}{\partial x_i} \quad \text{Eq. [8]}$$

The standard  $k-\omega$  model is useful for instances of internal flows, flows that exhibit strong curvature, separated flows, and jets. This model is more non-linear than the others and more dependent on initial conditions for convergence.

## Model Creation

In modeling the two geometries of arced labyrinth weirs ( $\alpha=20^\circ$ :  $\theta=30^\circ$  and  $\alpha=16^\circ$ :  $\theta=10^\circ$ ), three-dimensional (3D) stereolithography (stl) and initial graphics exchange specification (igs) files of the two weirs and headbox were exported from 3D drawing files drafted in AutoCAD™. A sectional model was used for all final runs which consisted of half the physical model setup (Figure 10 and Figure 11). Drawings of the physical model setup and complete drawing details of each weir are included in Appendix B. Methods for model creation are solver specific and detailed in the sections below.

### Flow-3D®

Flow-3D® uses .stl files to define the computational domain. The FAVOR algorithm requires a whole number of cells to accurately render wing walls in the computational domain. Imported .stl files were modified as Thompson (2019) suggested and translated 0.05 ft in the y-direction and the headbox (outflow for downstream boundary) was extended 1.00 feet downstream (see Figure 10).

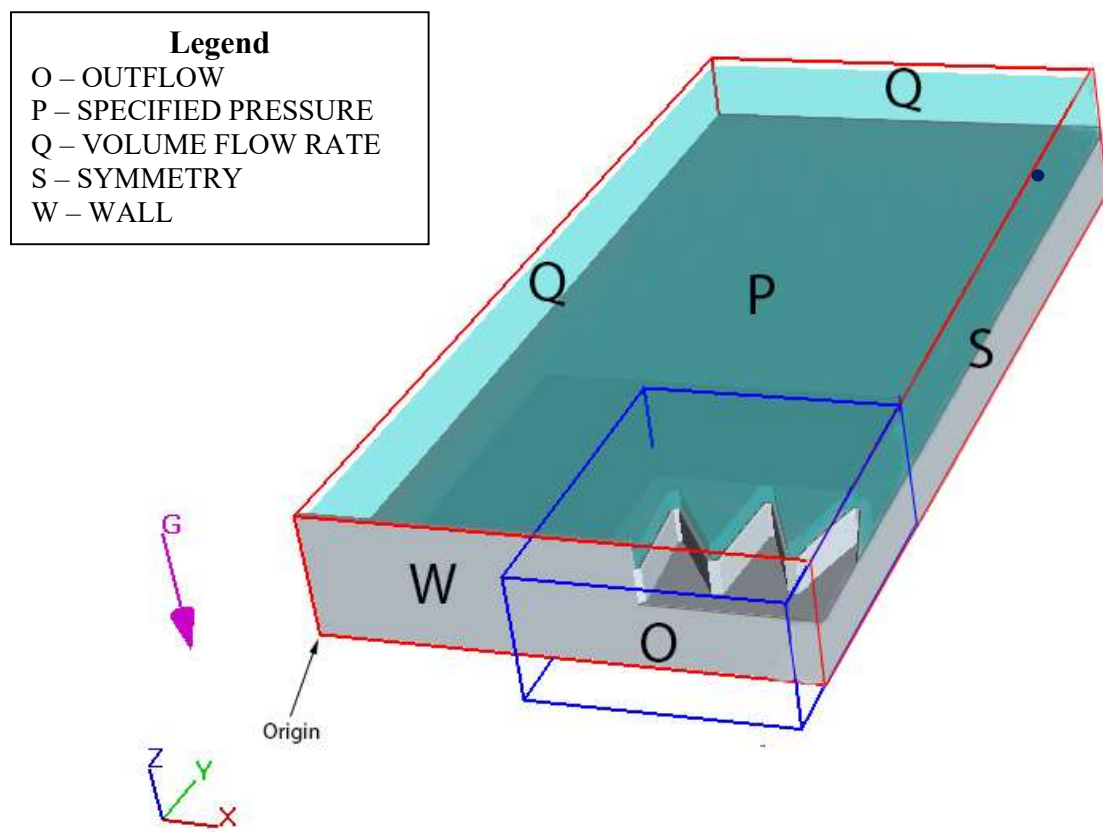


Figure 10. CFD reservoir and weir model showing domain origin, mesh boundaries, boundary conditions, history probe, and initial fluid region.

The domain was split into two sections, the reservoir mesh area (shown in red in Figure 10) and the weir mesh area (shown in blue in Figure 10). The reservoir mesh size was set at 0.12 ft. and three weir mesh sizes of 0.12 ft. (coarse), 0.06 ft. (medium), and 0.03 ft. (fine) were tested for specific discharges on the rating curve for a GCI. The results of the GCI indicated that a fine mesh produced the most accurate and mesh independent results, so the rest of the simulations

were completed using the fine mesh or 0.03 ft. weir mesh size. Several other runs were completed with the fine mesh and other user defined settings changed, (i.e., turbulence model). Additionally, it is important to note that Flow-3D was the only solver which had a variance in momentum advection scheme order. This is because the second-order simulations were too unstable to converge or run to completion. A summary of these runs is detailed in Table 1.

Table 1. Summary of runs completed using Flow-3D.

	H/P	Mesh Size	Order	Turbulence Model
$\alpha=20^\circ; \theta=30^\circ$	0.30	coarse	2 <sup>nd</sup>	RNG
	0.30	medium		
	0.30	fine		
	0.40	fine		
	0.50	fine		
	0.70	coarse		
	0.70	medium		
	0.70	fine		
	0.80	fine		
0.50		fine	1 <sup>st</sup>	
		fine	2 <sup>nd</sup>	k-epsilon Standard
		fine		k-omega Standard
		fine		1 Equation (Prandtl)
$\alpha=16^\circ; \theta=10^\circ$	0.30	coarse	1 <sup>st</sup>	RNG
	0.30	medium		
	0.30	fine		
	0.40	fine		
	0.50	coarse		
	0.50	medium		
	0.50	fine		
	0.70	coarse		
	0.70	medium		
	0.70	fine	2 <sup>nd</sup>	k-epsilon Standard
	0.80	fine		
	0.50	fine		
	0.50	fine		
	0.50	fine	1 <sup>st</sup>	k-omega Standard
	0.50	fine		
	0.50	fine		

For the current study  $\alpha = 16^\circ$  arced labyrinth weir simulations, the same weir geometry, reservoir geometry, and boundary conditions as Thompson (2019) were used. To capture the converging flow field in the headbox, Q was specified as a constant at the minimum x (x-min) and maximum y (y-max) boundaries (see Q in Figure 10) (Thompson, 2019). Discharge was chosen based on corresponding values of H/P from physical model results (Thompson, 2019 and Christensen, 2012). Increments of 0.1 between 0.3 and 0.8 H/P were evaluated in the model (Table 1).

Symmetry or free-slip (S) boundaries were placed between the nested mesh boundaries and at the x-max plane (see S in Figure 10). The symmetry boundaries create a free-slip interaction between the meshes, meaning there is no flow across the boundary and no scalar flux across the boundary, but on both sides of the boundary, the same processes exist (Flow-3D, 2016). Outflow boundaries (O) were placed at the free discharge boundary (y-min), downstream of the weir to create a free outfall condition. Specified pressure (P) boundaries were applied at the z-max plane (see P in Figure 10) with a specified VOF fluid fraction of zero. A summary of each boundary condition for all mesh conditions and discharges is given in Table 2, and the locations of each boundary are displayed in Figure 10.

Table 2. Summary of CFD mesh boundary conditions.

<b>Boundary</b>	<b>Reservoir Mesh</b>	<b>Weir Mesh</b>
<b>x-min</b>	constant Q	symmetry
<b>x-max</b>	symmetry	symmetry
<b>y-min</b>	symmetry	outflow
<b>y-max</b>	constant Q	symmetry
<b>z-min</b>	outflow	outflow
<b>z-max</b>	constant P	constant P

The total head (H) was computed using a history probe located in the exact location of the piezometer tap in the physical models (dark blue circle in Figure 10). Flow-3D uses history

probes to report hydraulic variables at a specific location in the x-y plane). A flux surface was also placed across the crest of the weir to measure unit discharge. A flux surface has a fixed porosity equal to one and is used to measure the flow of quantities through it, for this study it was unit discharge.

The primary goal of the CFD modeling was to compare rating curve data ( $C_d$  data) between the physical models specified in the current study and a range of numerical model configurations, starting with default parameters. Savage et al. (2016) and Crookston et al. (2018) found that turbulence model section has little effect on  $C_d$  relative to non-linear weirs in Flow-3D. However, Thompson (2019) completed numerical modeling on arced labyrinth weirs using only the default turbulence model. Therefore, four (4) turbulence models were chosen for this study. The model utilized the split-Lagrangian VOF advection to track the free surface coupled with a first or second-order approximation for the momentum advection scheme (Table 1). Pressures in each cell were solved using the generalized minimal residual (GMRES) method algorithm (Saad and Schultz, 1986). The fluid flow solved the full momentum and continuity equations.

### **Star CCM+®**

Star CCM+® can import a variety of shapefiles including .stl; however, for ease of setting boundary conditions, an .igs file was used for this study. The imported file was split into parts based on boundary conditions and mesh flexibility (Figure 11). Once the geometry was split into parts and assigned a region, the meshing continua was created. The base size was set to 0.12 ft, with 2 prism layers, and a “very slow” boundary growth rate. Within the region the weir boundary condition was modified with no prism layers, a very slow boundary growth rate, and a custom mesh size of 0.12 ft. (coarse), 0.06 ft. (medium), and 0.03 ft. (fine) for specific

discharges on the rating curve (Table 1). A volumetric control was created for each model at the approximate water surface elevation with a custom mesh size of 0.029 ft and 5 prism layers.

It is important to note that all boundary conditions were matched to the Flow-3D setup as closely as possible. To capture the converging flow field in the headbox, Q was specified as a constant at the minimum x (x-min) and maximum y (y-max) boundaries (shown in yellow (Q) in Figure 11) (Thompson, 2019). Discharge was chosen based on corresponding values of H/P from physical model results (Thompson, 2019 and Christensen, 2012). Increments of 0.1 between 0.3 and 0.8 H/P were selected (Table 3).

A symmetry or free-slip (S) boundary was placed in the x-max plane (shown in blue in Figure 11). The symmetry boundaries create a free-slip interaction between the meshes meaning there is no flow across the boundary and no scalar flux across the boundary, but on both sides of the boundary, the same processes exist. Pressure Outlet (O) boundaries (shown in orange in Figure 11) were placed at the free discharge boundary, downstream of the weir and at the floor of the downstream of the weir, to create a free outfall condition. This boundary condition specifies an outlet pressure, in this case atmospheric.

A Stagnation Inlet (P) boundary was set on the z-max plane to allow for mixing of Fluid 1 and Fluid 2 (shown in pink in Figure 11). This works by having a set pressure outside of the domain, again atmospheric for the current study, allowing a gradient for flow to enter the system (in this case Fluid 2 or air). Wall or no-slip (W) boundaries were placed on the remaining surfaces (shown in grey in Figure 11). A summary of each boundary condition for all mesh conditions and discharges is given in Table 4, and the locations of each boundary condition are displayed in Figure 11.

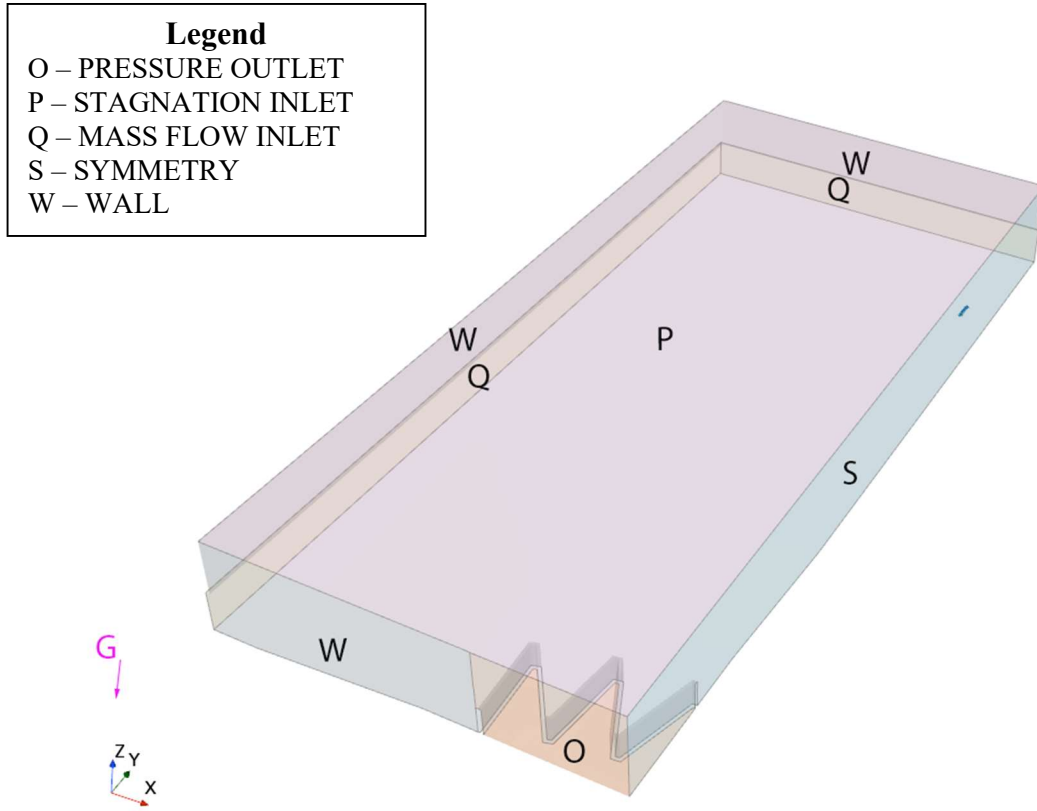


Figure 11. CFD reservoir and weir model showing mesh boundaries, boundary conditions, and iso-surface location.

The total head ( $H$ ) was computed using an iso-surface located in the exact location of the piezometer tap in the physical models (blue square in Figure 11). For the purpose of this study, an iso-surface was set to track the water surface elevation in the location of the physical model's piezometer tap. A report, monitor, and plot were created to measure these specified hydraulic variables and create data for export and analysis. The same approach was used to track other scalars like minimum weir pressure, looking specifically along the downstream side of the weir.

Thompson (2019) completed numerical modeling on arced labyrinth weirs using only the default turbulence model. Therefore, like with the simulations completed in Flow-3D, four (4) turbulence models were chosen for the Star CCM+ evaluations. The model utilized the Eulerian

VOF advection to track the free surface coupled with a first or second-order approximation for the momentum advection scheme (Table 3). The fluid flow solver solved the multiphase equations of state.

Table 3. Summary of runs completed using Star CCM+

	H/P	Mesh Size	Turbulence Model
$\alpha=20^\circ; \theta=30^\circ$	0.30	coarse	Realizable
	0.30	medium	
	0.30	fine	
	0.40	fine	
	0.50	fine	
	0.70	coarse	
	0.70	medium	
	0.70	fine	
	0.80	fine	
	0.50	fine	
		fine	k-epsilon Standard
		fine	k-omega Standard
		fine	1 Equation (Spalart-Allmaras)
$\alpha=16^\circ; \theta=10^\circ$	0.30	coarse	Realizable
	0.30	medium	
	0.30	fine	
	0.40	fine	
	0.50	fine	
	0.70	coarse	
	0.70	medium	
	0.70	fine	
	0.80	fine	
	0.50	fine	
		fine	k-epsilon Standard
		fine	k-omega Standard
		fine	1 Equation (Spalart-Allmaras)

Table 4. Summary of CFD mesh boundary conditions.

Boundary	Mesh
yellow	mass flow inlet
pink	stagnation inlet
blue	symmetry
grey	wall
orange	pressure outlet

### Numerical Simulations

A total of 50 simulations were completed using Flow-3D and Star-CCM+. That includes  $H/P = 0.3, 0.4, 0.5, 0.7$  and  $0.8$  for several mesh, turbulence, and momentum advection schemes (see Tables 1 and 3). Momentum advection schemes were only changed for models in Flow-3D because the second-order schemes were unstable and would not converge. It is important to note that an additional 20 simulations were completed in the sensitivity analysis using Star-CCM+. Each simulation was modeled for 60 seconds or until the results reached steady state. Data were extracted via text files into Microsoft Excel. After the model reached steady-state, 15-second averages of  $H$  were used to compute time-averaged  $C_d$  values and corresponding relative errors ( $\varepsilon$ ) between the a) physical and numerical results and b) different numerical simulation configurations. Model views and post processing figures were created using Flow-3D POST or within Star CCM+ (for each respective model).

## NUMERICAL MODEL RESULTS

The numerical models of the 5-cycle arced labyrinth weir geometries used in this study,  $\alpha=16^\circ$ :  $\theta=10^\circ$  and  $\alpha=20^\circ$ :  $\theta=30^\circ$ , were built in two commercially available CFD solvers, Flow 3D® and Star CCM+®. A sensitivity analysis was completed using the  $\alpha=20^\circ$ :  $\theta=30^\circ$  arced labyrinth weir model to determine which user-defined parameters affect the predicted hydraulic efficiency. Simulations were then completed in both solvers to outline a rating curve ( $H/P = 0.3, 0.4, 0.5, 0.7$ , and  $0.8$ ), along with a grid (mesh) convergence at two rating curve points ( $H/P = 0.3$  and  $0.7$ ). These simulations were completed using only default solver settings. The midpoint of the rating curve ( $H/P = 0.5$ ) was repeated with additional user-defined changes to the default settings including mesh configuration, momentum advection scheme order, and turbulence model. The results are compared quantitatively and qualitatively to existing physical data collected by Christensen (2012) and Thompson (2019) for their respective geometries, as well as to numerical data collected by Thompson (2019) for the  $\alpha=16^\circ$ :  $\theta=10^\circ$  arced labyrinth weir.

The results, which are discussed below, provide insight into the repeatability of numerical data, the ability for CFD to simulate hydraulic behavior, the sensitivity of numerical models to user-defined settings, the relative error associated with default solver settings, and the reduction or increase of relative error with user-defined changes to solver settings. Measurements and analysis for this study were completed upstream of the weir (i.e., subcritical flow); no measurements were recorded in the downstream section of the weir where the fluid is highly turbulent.

These findings are specific to the geometries, solvers, user defined setting associated with each solver, and the discharges tested in this study; however, engineering judgement may be used in application of these findings. The results presented in this section are time-averaged over

15 seconds. Time series data and plots, with specified Q and time averaged H values are found in Appendix C.

### Sensitivity Analysis

A sensitivity analysis was completed using Star CCM+ and a sectional model of the center weir cycle. Mesh size, time step, and turbulence models were adjusted, and simulations run for  $H/P = 0.3$ . Two variations of  $k-\varepsilon$  (Realizable and Standard) were the turbulence models used in the sensitivity analysis. Because there were variations in the numerically calculated H, the numerical results were compared to the physical data using Equation [10] at the same H; the results of this sensitivity analysis are presented in Figure 12. A table quantifying these results is shown in Appendix C.

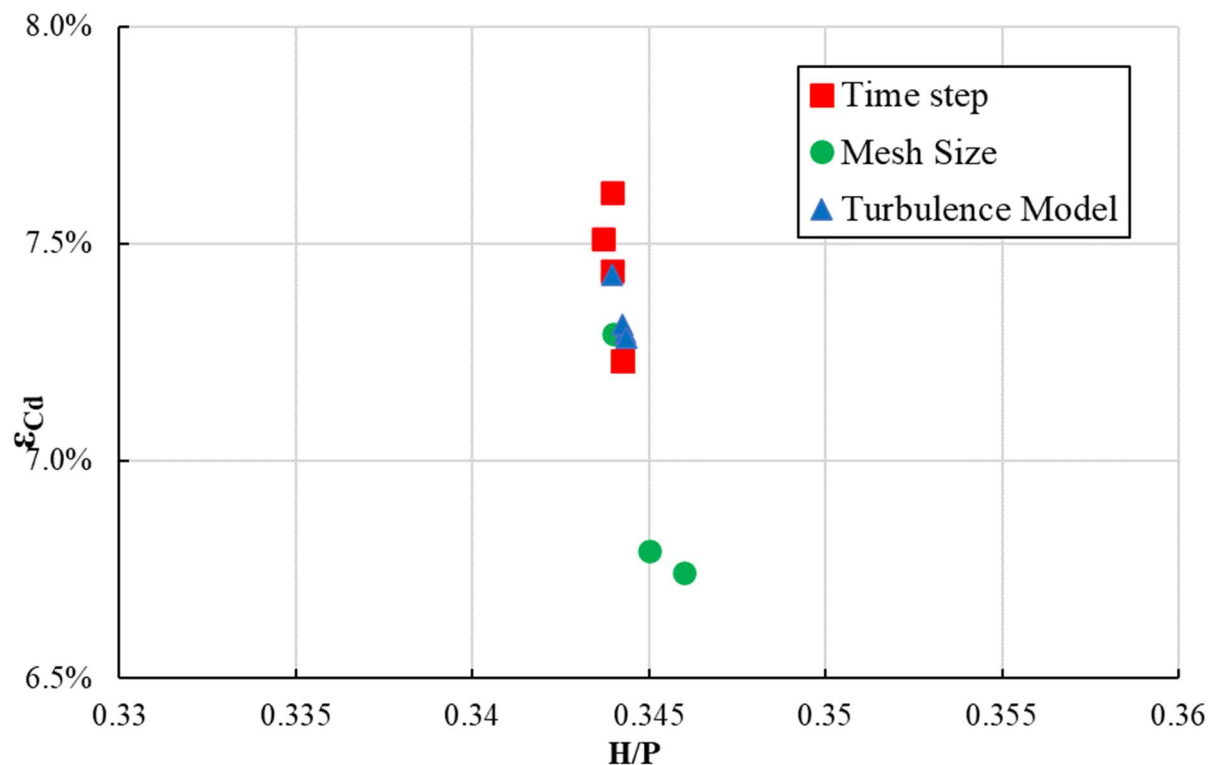


Figure 12. Relative error ( $\varepsilon_{Cd}$ ) between numerical and empirical results of sensitivity analysis.

The mesh size had the most significant effect on the model, while turbulence and time step had smaller impacts. The author concluded that mesh convergence would be the more important factor in matching physical data, as well as further investigation into other turbulence models. The following sections discuss the authors findings and recommendations for the mesh convergence and turbulence scheme to create a model to accurately predict the hydraulic efficiency of an arced labyrinth weir.

### **Grid Convergence Index**

Using the mesh configurations in Tables 1 and 3, a grid convergence index (GCI) was calculated using Eq. [2] with  $p_c = 2$ ,  $r = 2$ , and  $F_s = 1.25$  as per ASCE (2009). This value was calculated for  $H/P = 0.3$  and  $0.7$  for coarse, medium, and fine mesh resolutions around the weir. The GCI was computed with the relative error ( $\varepsilon_{Cd}$ ) for  $C_d$  values of the numerical models using Eq. [9] and  $C_d$  values calculated from the empirical equation for the physical models (Eq. [10] and Table 5, Thompson, 2019 and Christensen, 2012). These values produced GCI values of less than 1% for nearly all discharges with a fine mesh (Tables 6 and 7).

However, at  $H/P = 0.3$  for the  $\alpha=16^\circ: \theta=10^\circ$  weir while using Flow-3D the solution diverged at the finest mesh to a GCI of approximately 4.7%. It is the author's opinion that this is due to the medium mesh resolution results being about 13% larger than either the coarse or fine mesh resolution results. It is also interesting to note that when using Star CCM+, the coarse mesh has a lower computed relative error and the finer mesh configurations deviate from the physical data, which is discussed in the following section.

$$C_d = \frac{3}{2} \frac{Q}{L_c \sqrt{2gH^2}} \quad \text{Eq. [9]}$$

$$C_d = \frac{1}{\alpha(\frac{H}{P} + b)^2} + d \ln(\frac{H}{P}) \quad \text{Eq. [10]}$$

Table 5. Half-round crested arced labyrinth weir curve fit coefficients for Eq. [10] valid for  $0.05 \leq H/P \leq 0.8$  (modified from Thompson, 2019).

Geometry		Empirical Coefficients			Correlation Coefficient	
$\theta$ [°]	$\alpha$ [°]	$a$	$b$	$c$	$d$	$R^2$
<b>10</b>	12	1.6633	0.2532	0.4867	0.3342	0.998
	16	1.2573	0.2784	0.4420	0.4128	0.995
	20	0.8774	0.5045	0.4539	0.2735	0.984
<b>20</b>	12	2.1060	0.1227	0.5972	0.3214	0.999
	16	1.43872	0.1636	0.6310	0.3100	0.996
	20	1.0847	0.3008	0.5319	0.3276	0.995
<b>30</b>	12	2.7769	0.0482	0.6341	0.3244	0.992
	16	2.1022	0.0410	0.7260	0.2751	0.998
	20	1.6654	0.1040	0.6576	0.3142	0.996

Table 6. Calculated GCI for  $\alpha=16^\circ$ :  $\theta=10^\circ$  using results from Flow-3D and Star CCM+ models as per ASCE (2009).

$\alpha=16^\circ: \theta=10^\circ$			Flow-3D			Star CCM+			
	Mesh (ft)	$C_d$	$C_{d-emp}$	$\epsilon_{Cd}$	GCI (%)	$C_d$	$C_{d-emp}$	$\epsilon_{Cd}$	GCI (%)
<b>H/P = 0.3</b>	0.12	0.61	0.641	-0.048	-	-	-	-	-
	0.06	0.740	0.673	0.099	<b>8.7%</b>	-	-	-	-
	0.03	0.655	0.666	-0.017	<b>4.7%</b>	0.723	0.659	0.096	-
	0.12	1.045	0.599	0.745	-	0.468	0.459	0.020	-
	0.06	0.488	0.471	0.036	<b>22.2%</b>	0.501	0.473	0.059	<b>6.4%</b>
	0.03	0.484	0.471	0.028	<b>0.3%</b>	0.549	0.481	0.141	<b>0.7%</b>

Table 7. Calculated GCI for  $\alpha=20^\circ$ :  $\theta=30^\circ$  using results from Flow-3D and Star CCM+ models as per ASCE (2009).

$\alpha=20^\circ: \theta=30^\circ$			Flow-3D			Star CCM+			
	Mesh	$C_d$	$C_{d-emp}$	$\epsilon_{Cd}$	GCI (%)	$C_d$	$C_{d-emp}$	$\epsilon_{Cd}$	GCI (%)
<b>H/P = 0.3</b>	0.12	3.51	0.657	4.343	-	0.715	0.671	0.066	-
	0.06	0.740	0.702	0.054	<b>158.2%</b>	0.720	0.672	0.071	<b>0.3%</b>
	0.03	0.720	0.700	0.029	<b>1.1%</b>	0.725	0.673	0.077	<b>0.3%</b>
	0.12	0.881	0.605	0.456	-	-	-	-	-
	0.06	0.534	0.498	0.072	<b>16.4%</b>	-	-	-	-
	0.03	0.524	0.494	0.061	<b>0.8%</b>	0.699	0.622	0.124	-

## Comparison to Physical Data

Strong agreement was found when comparing the numerical results to the physical model data collected by Thompson (2019) and Christensen (2012) for the  $\alpha=16^\circ$ :  $\theta=10^\circ$  and  $\alpha=20^\circ$ :  $\theta=30^\circ$  weirs (respectively). This agreement was found for the results of both Flow-3D and Star CCM+. Because there were variations in the numerically calculated H, the numerical results were compared to the physical data using Equation [10] at the same H; these comparisons, along with physical data points are shown in Figures 13 and 14 for the  $\alpha=16^\circ$ :  $\theta=10^\circ$  and  $\alpha=20^\circ$ :  $\theta=30^\circ$  weirs, respectively. The results from both solvers are presented together.

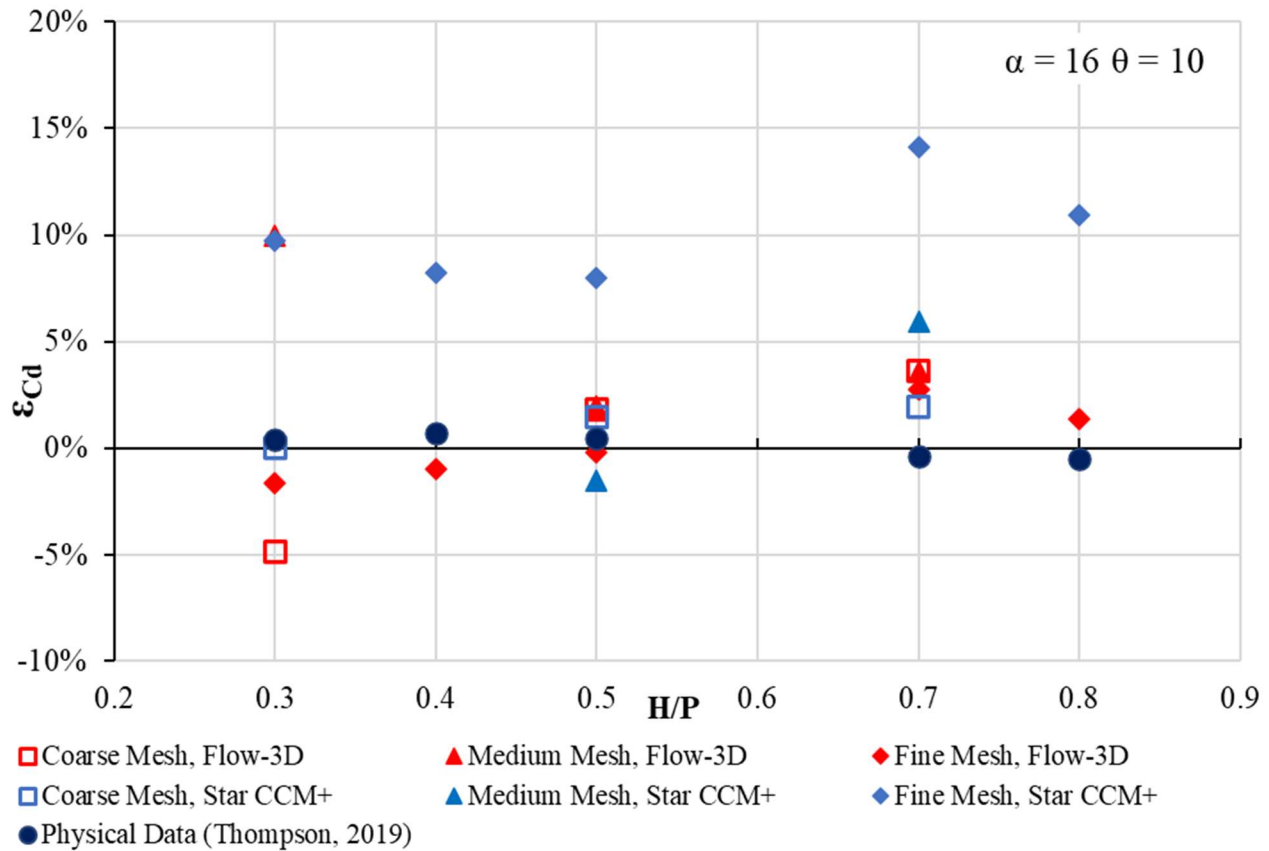


Figure 13. Relative error ( $e_{Cd}$ ) between numerical and empirical results for all mesh configurations for the  $\alpha=16^\circ$ :  $\theta=10^\circ$  weir using Flow-3D and Star CCM+.

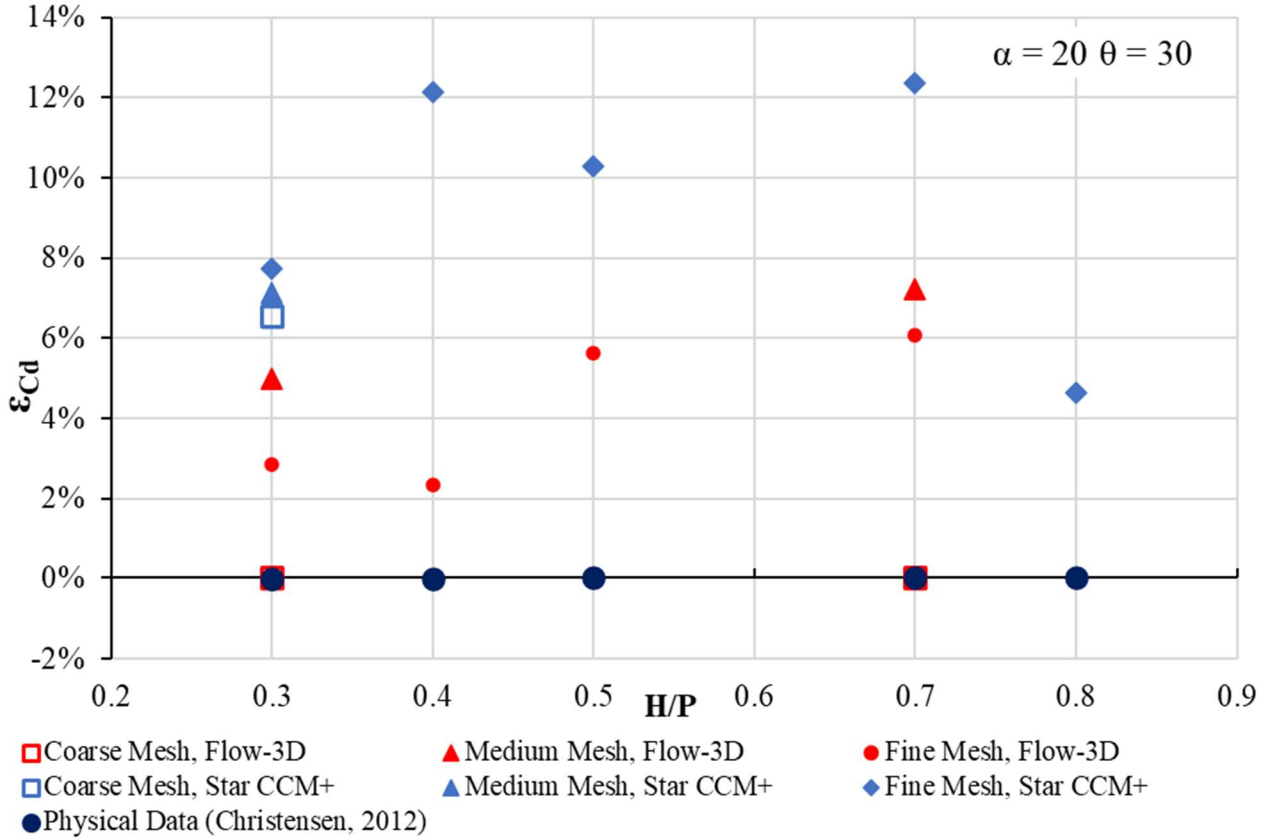


Figure 14. Relative error ( $\epsilon_{Cd}$ ) between numerical and empirical results for all mesh configurations for the  $\alpha=20^\circ$ :  $\theta=30^\circ$  weir using Flow-3D and Star CCM+.

The fine mesh provided the best results when using Flow-3D; however, the coarse mesh provided the best results when using Star CCM+. When using the fine mesh in Flow-3D, the relative errors of  $C_d$  were between -1.7% and 2.9% for the  $\alpha=16^\circ$ :  $\theta=10^\circ$  weir and less than between 2.3% and 6% for the  $\alpha=20^\circ$ :  $\theta=30^\circ$  weir. The  $\alpha=20^\circ$ :  $\theta=30^\circ$  weir has an outlier at  $H/P = 0.8$  where the relative error is 12.85%. This is potentially associated with specific user-defined modeling parameters, which may have resulted in not fully optimizing the capabilities of each solver.

When using the coarse mesh in Star CCM+, the relative errors in  $C_d$  were between 1.5% and 2% for the  $\alpha=16^\circ$ :  $\theta=10^\circ$  weir and between 6% and 7% for the  $\alpha=20^\circ$ :  $\theta=30^\circ$  weir. However, the rendered solid using the coarse mesh in Star CCM+ does not accurately represent the

physical system and cannot be used as a final simulation run. The inaccurate solid rendered does introduce more loss to the system and results in a less efficient  $C_d$  value. Comparatively, the fine mesh in Star CCM+ resulted in a relative error in  $C_d$  of between 8% and 14.2% for the  $\alpha=16^\circ$ :  $\theta=10^\circ$  weir and between 5% and 12.4% for the  $\alpha=16^\circ$ :  $\theta=10^\circ$  weir.

The  $C_d$  values of the physical, empirical (Eq. [10]), and numerical data are shown in Figures 15 through 18. Figures 15 and 17 present results from Flow-3D for  $\alpha=16^\circ$ :  $\theta=10^\circ$  and  $\alpha=20^\circ$ :  $\theta=30^\circ$ , respectively. Figures 16 and 18 present results from Star CCM+ for  $\alpha=16^\circ$ :  $\theta=10^\circ$  and  $\alpha=20^\circ$ :  $\theta=30^\circ$ , respectively.

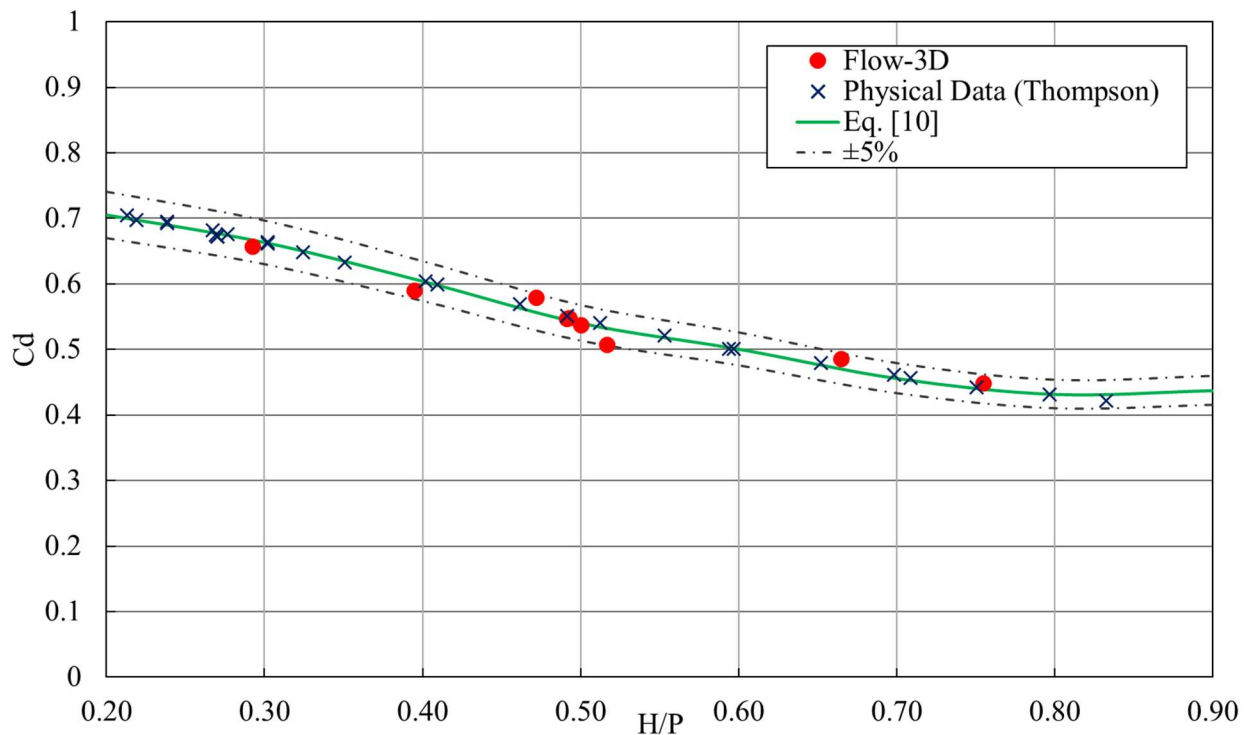


Figure 15.  $C_d$  vs.  $H/P$  comparison between physical results, empirical calculations (Eq. [10]), and fine mesh results using Flow-3D for the  $\alpha=16^\circ$ :  $\theta=10^\circ$  weir.

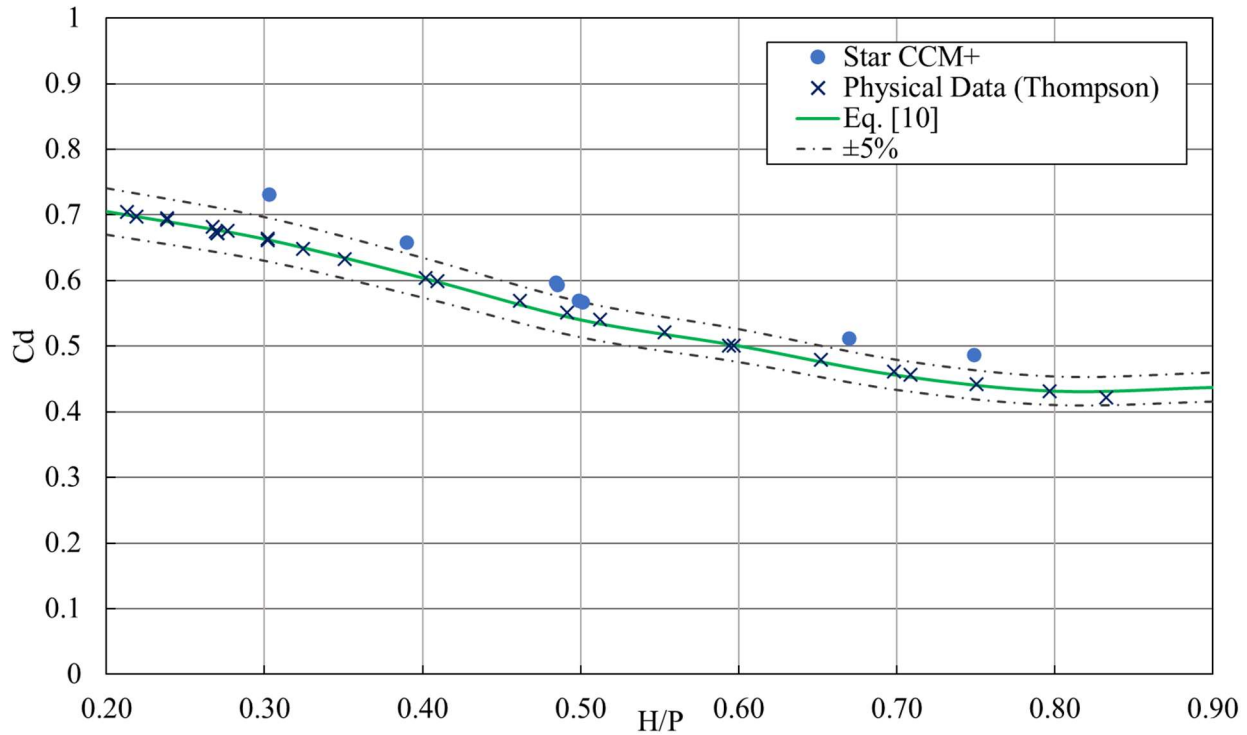


Figure 16.  $C_d$  vs. H/P comparison between physical results, empirical calculations (Eq. [10]), and fine mesh results using Star CCM+ for the  $\alpha=16^\circ$ :  $\theta=10^\circ$  weir.

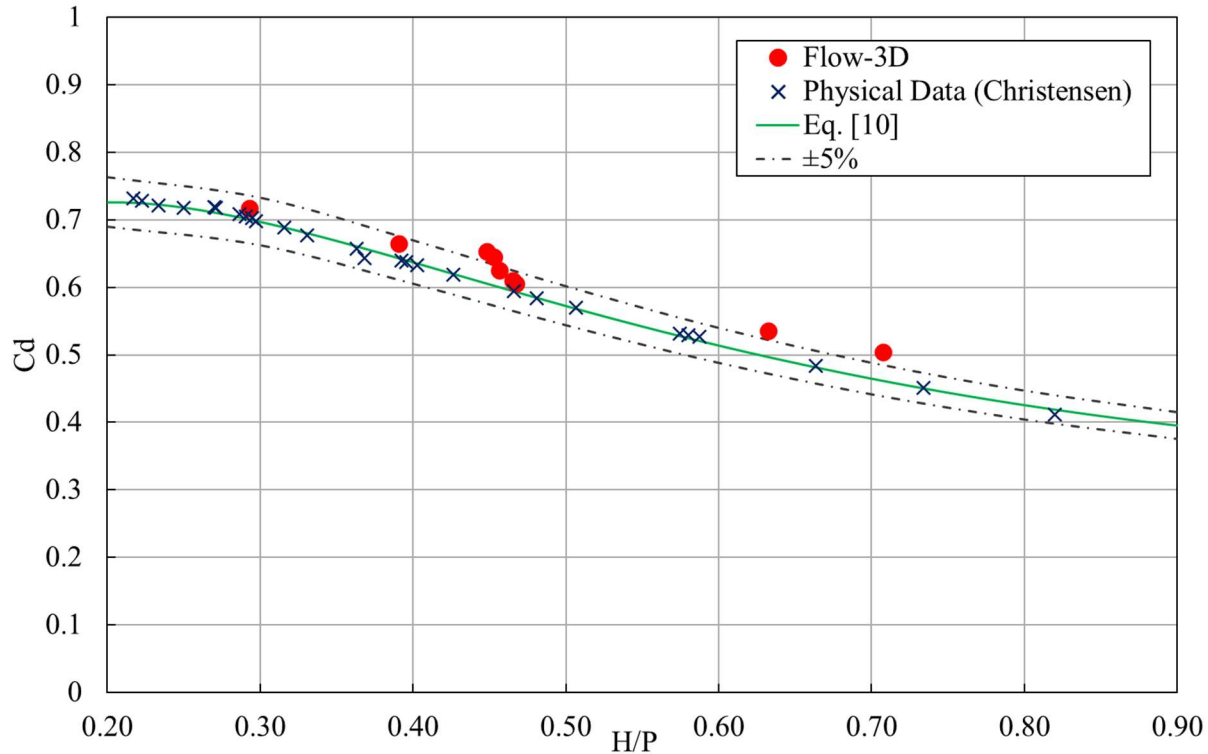


Figure 17.  $C_d$  vs. H/P comparison between physical results, empirical calculations (Eq. [10]), and fine mesh results using Flow-3D for the  $\alpha=20^\circ$ :  $\theta=30^\circ$  weir.

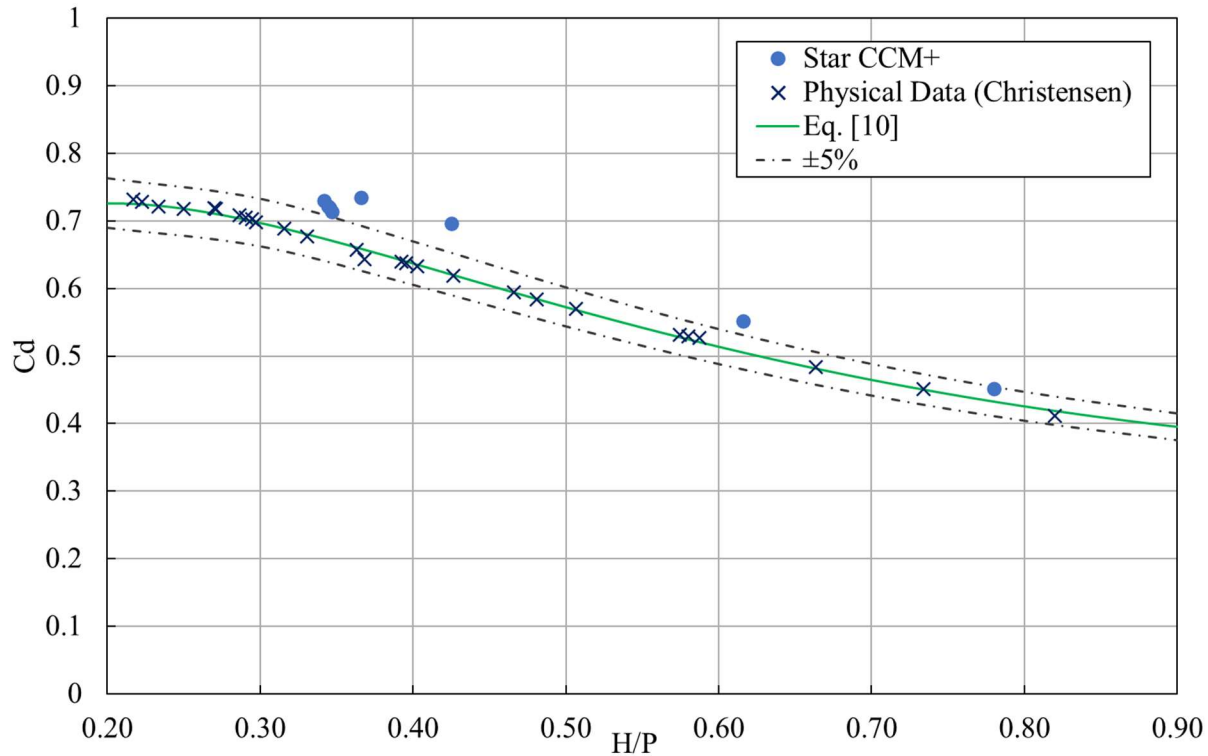


Figure 18.  $C_d$  vs.  $H/P$  comparison between physical results, empirical calculations (Eq. [10]), and fine mesh results using Star CCM+ for the  $\alpha=20^\circ$ ;  $\theta=30^\circ$  weir.

Star CCM+ tends to over predict the  $C_d$  values compared to observed physical data. The author believes this is because Star CCM+ uses a higher order momentum advection scheme for all simulations. The higher order terms are less dissipative and tend to bounce around between iterations which may result in high 15 second averages and simulate higher efficiency results (Star CCM+, 2021). The momentum advection scheme order was only changed in Flow-3D to aid in simulation convergence and stability.

The strong agreement and behavior of the CFD models suggest that both the numerical and physical models are representative of reality and accurately represent the hydraulic behavior of the arced labyrinth weir geometry tested. Additionally, the agreement of the models created independently in different solvers (Flow-3D and Star CCM+) contribute to this conclusion. These results suggest that CFD is a potential tool for predicting hydraulic performance for other

geometric variations of arced labyrinth weir. CFD can also provide additional data that is often difficult to collect in a physical model, like actual unit discharge and negative pressures along the weir crest, these will be discussed further in sections below. The author recommends that the results of CFD models be validated through empirical data or a physical model.

### **Comparison to existing CFD data**

Existing CFD data by Thompson (2019) was collected in Flow-3D. This study collected data in Star-CCM+ and Flow-3D. The two commercial solvers have very different user-defined settings and processes for model setup (as shown above in the Model Creation section). Table 8 shows the biggest differences between the two solvers' capabilities and highlights a need for different model setup procedures, which was outside of the scope for this study.

Table 8. Different capabilities and setups of Star-CCM+ and Flow-3D.

	<b>Star CCM+</b>	<b>Flow-3D</b>
Mesh Size	User-initialized	User-defined
Mesh Types	9 mesher algorithms, prism layers, volumetric controls, parts-based meshing, Adaptive mesh, polyhedral, trimmer, cylinder extrusion.	Trimmer (hexahedral)
Time Step	User-defined	User-initialized
Number of Flow Phases	Multiphase	Max of Two
Default Turbulence Model	Varies	RNG k- $\epsilon$
Available Turbulence Schemes	21	6
Method for Tracking the Free Surface	VOF method	Modified VOF method
Solid/obstacle representation	Mesh formed around solids	FAVOR Method
Discretization	Finite Difference (Finite Volume) Approximation	Finite Difference (Finite Volume) Approximation

Because the existing data was collected in Flow-3D and Thompson (2019) model setup was mimicked in both solvers for this study, it was anticipated that Flow-3D results would match the existing results best. Table 9 shows the model setup of each solver for this study and Thompson (2019) and highlights the important differences between the model setup that might affect the results.

The author has concluded that the best practices of model setup in Flow-3D (used in this study) are not the best practices for model setup in Star-CCM+. The results from the Star-CCM+ model are not a representation of the solver's full capabilities and further studies should be conducted in this area. Therefore, any analysis from this point on is not a direct comparison of the two solvers but a presentation of results based on this model setup. The results presented here show the importance of understanding user-defined settings and that these settings are essential to getting good model results. The results also highlight that different solvers use different setups to achieve optimal results.

Table 9. Model setup for this study and Thompson (2019).

<b>Solver</b>	<b>Star CCM+ (Koldewyn)</b>	<b>Flow-3D (Koldewyn)</b>	<b>Flow-3d (Thompson)</b>
Mesh Size	User-initialized	User-defined	User-defined
Mesh Type	Trimmer (Hexahedral)	Hexahedral	Hexahedral
Time Step	User-defined	User-initialized	User-initialized
Number of Flow Phases	Multiphase (2)	Single	Single
Default Turbulence Model	Realizable k- $\epsilon$	RNG k- $\epsilon$	RNG k- $\epsilon$
Momentum advection scheme order	2 <sup>nd</sup>	1 <sup>st</sup> and 2 <sup>nd</sup>	2 <sup>nd</sup>
Additional Mesh Features Used	Prism layers and volumetric controls along with different mesh sizes for each part.	N/A	N/A

The numerically calculated  $C_d$  of this study and the numerically calculated  $C_d$  by Thompson (2019) were compared directly with physical data of the same H using Eq. [10]; these comparisons are shown in Figure 19. Good agreement (less than or equal to 3%) was found for low heads and slightly less good agreement (between 3 and 5%) was found at higher heads between the numerical results of Flow-3D presented in this study and the numerical results presented by Thompson (2019) for an arced labyrinth weir of  $\alpha=16^\circ$ :  $\theta=10^\circ$ . However, the results in Flow-3D were not identical even though the model setup was. The results from Star-CCM+ show a similar shape but highlight the need for a different user-defined setup to optimize this solver.

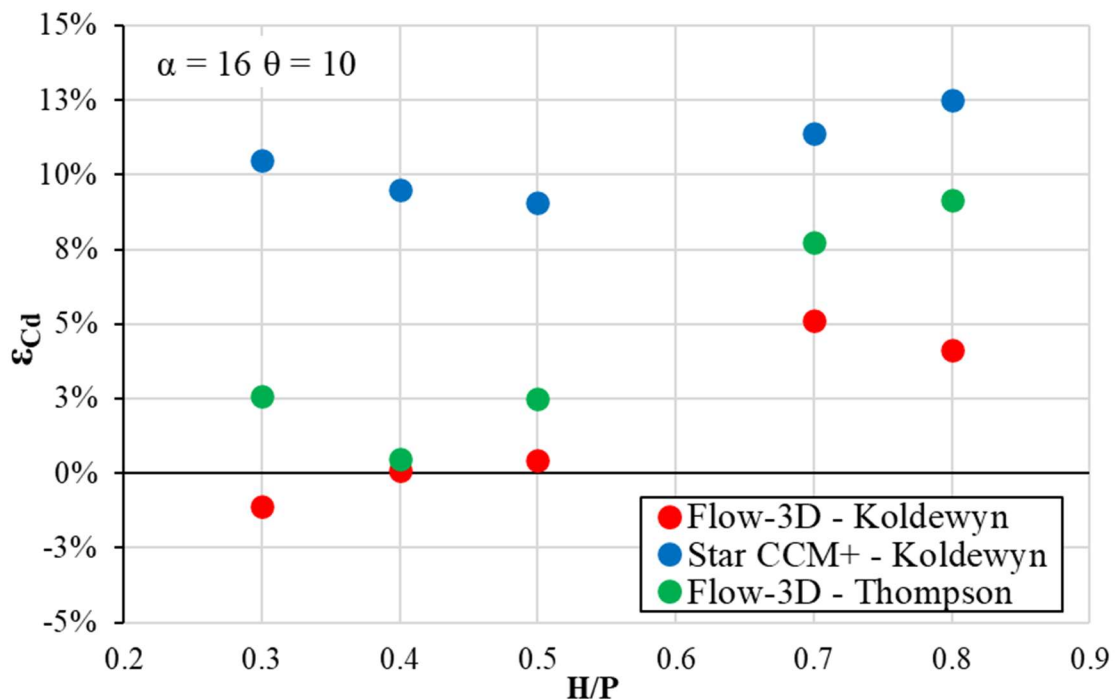


Figure 19. Relative error ( $\varepsilon_{Cd}$ ) between numerical data collected by the author and data collected by Thompson (2019).

In a poster presented by Flow-3D in 2017, the results of CFD prediction for hydraulic efficiency of piano key weirs found that CFD models over predicted the physical data within a range of about 5% (Flow-3D, 2017). Additionally, modeling only a section of the weir resulted

in another 2% difference between the sectional model and the full model. It is the author's opinion that this provides evidence that the current study is an accurate representation of hydraulic behavior even though there is a slight over-prediction of the physical model data.

Additionally, the repeatability of numerical models for arced labyrinth weirs is highlighted. Even with an identical setup, the author was not able to perfectly replicate the results of Thompson (2019); however, there remains a visible trend in the data with solver accuracy decreasing as H/P increases. The author believes this is because the accuracy of the numerical model diminishes in CFD as turbulence increases, especially when the selected turbulence model does not accurately describe the turbulence (Solmaz, 2022).

### **Comparison of Turbulence Models**

Four (4) turbulence models were selected and tested during this study as mentioned above in the model creation section. Concurrence was found when comparing the different turbulence models numerical results to the physical model data. As with the results above, the numerical results were compared with the physical data via Eq. [10] at the same H; these comparisons are shown in Figure 20 and 21 for the  $\alpha=16^\circ: \theta=10^\circ$  and  $\alpha=20^\circ: \theta=30^\circ$  weirs, respectively. The data are also summarized in Table 10. For both the  $\alpha=16^\circ: \theta=10^\circ$  and the  $\alpha=20^\circ: \theta=30^\circ$  weir, the  $k-\varepsilon$  standard turbulence model consistently provided results closest to the physical model data independent of solver. In Flow-3D, the turbulence model relative error in  $C_d$  had a range of -0.36% to 5% for the RANS 2-equation model.

Table 10. Relative error ( $\epsilon_{Cd}$ ) between numerical results of turbulence models at H/P = 0.5 and empirical (Eq. [10]) tabulated results for  $\alpha=16^\circ$ :  $\theta=10^\circ$  and  $\alpha=20^\circ$ :  $\theta=30^\circ$  weirs.

<b>Geometry</b>	<b>Model</b>	<b>Flow-3D</b>			<b>Star CCM+</b>		
		<b>C<sub>d</sub></b>	<b>C<sub>d-emp</sub></b>	<b>ε<sub>Cd</sub></b>	<b>C<sub>d</sub></b>	<b>C<sub>d-emp</sub></b>	<b>ε<sub>Cd</sub></b>
$\alpha = 16^\circ \theta = 10^\circ$	Default	0.547	0.548	-0.18%	0.632	0.564	12.06%
	1 Eq.*	0.494	0.532	-7.14%	0.571	0.545	4.77%
	k-ε standard	0.548	0.548	0.00%	0.561	0.542	3.51%
	k-ω standard	0.547	0.549	-0.36%	0.590	0.551	7.08%
$\alpha = 20^\circ \theta = 30^\circ$	Default	0.638	0.604	5.63%	0.725	0.673	7.73%
	1 Eq.*	0.595	0.59	0.85%	0.731	0.674	8.46%
	k-ε standard	0.62	0.599	3.51%	0.715	0.671	6.56%
	k-ω standard	0.628	0.601	4.49%	0.723	0.673	7.43%

\*1-Equation models differ between solvers, see Table 1 and Table 3 for more details

The one-equation model results were scattered between the models and show no clear pattern. Star CCM+ was more sensitive to turbulence model selection; the relative error in  $C_d$  ranged from 3% to 12% with the default model providing the poorest results. The one-equation model results using Star CCM+ were also scattered with no clear pattern. This was expected as one-equation models are built to solve problems where the fluid flow is more 2D than 3D, like an air foil, or airplane wing. As you move up and down the wing the problem is nearly the same. As we move up and down an arced labyrinth weir, this is not the case, as it is a highly dynamic and changing problem. This random behavior of the one-equation models for both commercial solvers suggests that it is not an appropriate turbulence model for arced labyrinth weirs.

The relatively consistent behavior of the CFD models regardless of turbulence model suggests the hydraulic efficiency of a weir may not be sensitive to turbulence model selection. However, when other results must be provided from the numerical model (like unit discharge and negative weir pressure) the CFD model results are much more sensitive.

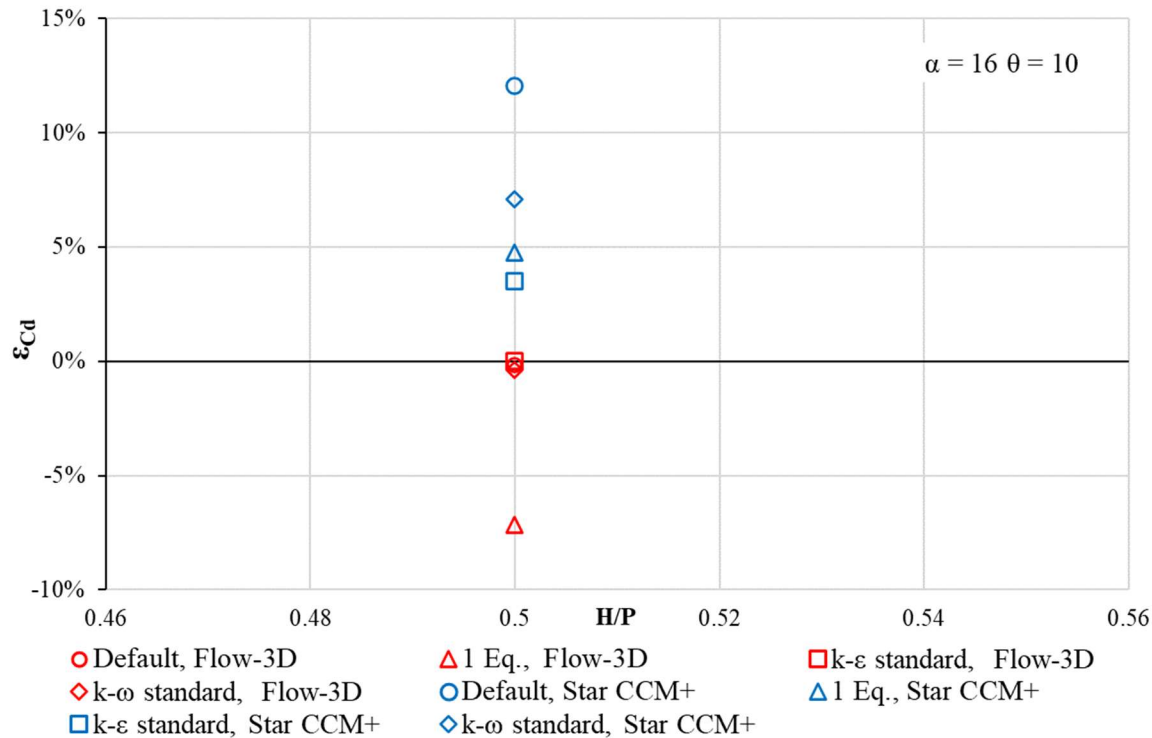


Figure 20. Relative error ( $\varepsilon_{Cd}$ ) between numerical results of turbulence models at  $H/P = 0.5$  and empirical (Eq. [10]) results for  $\alpha=16^\circ$ ;  $\theta=10^\circ$ .

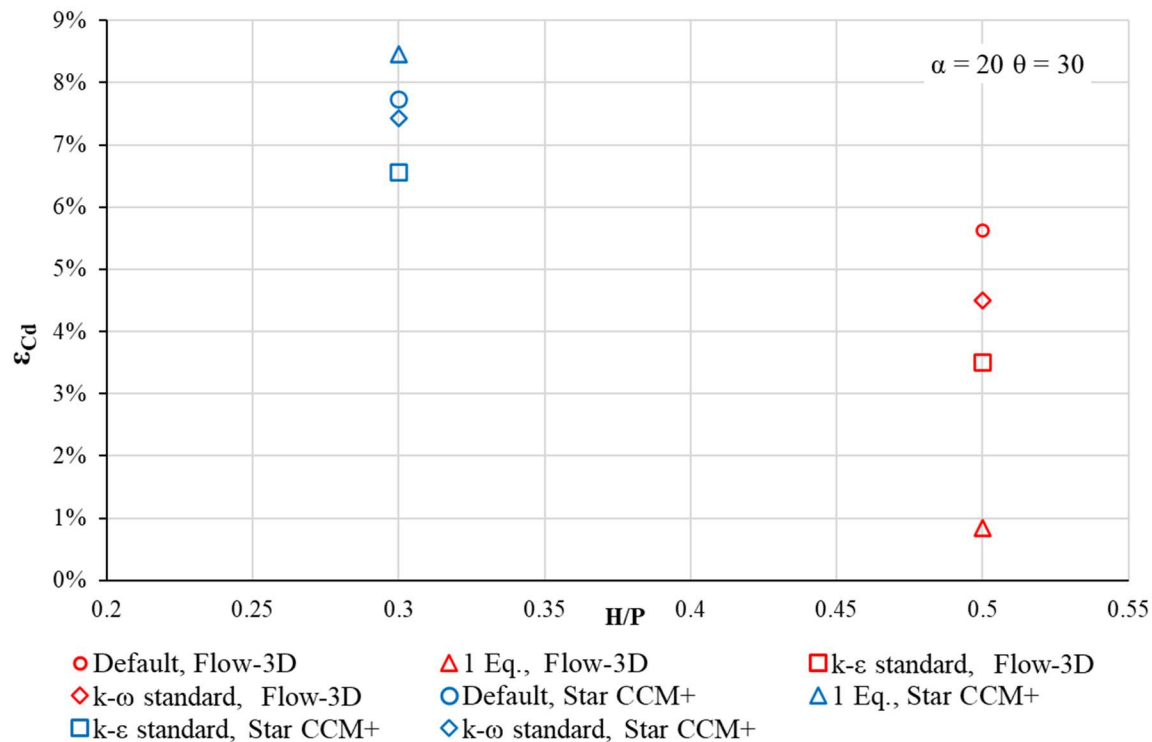


Figure 21. Relative error ( $\varepsilon_{Cd}$ ) between numerical results of turbulence models at  $H/P = 0.5$  (or 0.3) and empirical (Eq. [10]) results for  $\alpha=20^\circ$ ;  $\theta=30^\circ$ .

## Comparison of Momentum Advection Order

Simulations were originally conducted using a second-order momentum advection scheme to improve accuracy, which was successful on Star-CCM+. However, for several of the runs using Flow-3D, the simulations were unsteady and would not converge because time timestep would become infinitely small. The numeric settings were adjusted in Flow-3D between a first-order and second-order momentum advection schemes to accommodate this challenge and produce results (Flow-3D, 2016).

Concurrence was generally found between the difference momentum advection order models when comparing the numerical results to the physical model data. As with the comparisons above, the numerical data is compared directly with physical data via Eq. [10] at the same H. This comparison is shown in Figure 22 and the results are summarized in Table 9. It is important to note that Star-CCM+ was not included in this analysis because all the default second-order simulations were stable and converged.

For values of  $H/P < 0.5$ , both the first-order and second-order schemes resulted in a relative error of between -2% and 3%. At values of  $H/P > 0.5$  the first-order scheme resulted in a relative error of > 3% and the second-order scheme was between 5% and 13%. The second-order momentum advection scheme is second-order accurate in both space in time; however, in some free surface flows this approximation may not be stable (Flow-3D, 2016). All simulations using the second-order scheme had higher fluctuations between iterations and more instability.

The author believes the 15 second averages, which included more spikes or high values because of the instability caused the second-order calculations to overpredict physical data. For free surface flows on an arc labyrinth weir using Flow-3D, the hydraulic properties for the geometries in this study were better approximated using the first-order scheme. First-order

methods tend to converge better because they are more dissipative and produce a less efficient  $C_d$  value that is closer to the observed physical data (CFD Online Wiki, 2011).

Additionally, a first-order scheme is the simplest and fastest method as shown by the simulations times in Table 9. In some cases, when using Flow-3D, the added accuracy of a second-order scheme may not be worth the additional computational time and cost, especially when the second-order method in Flow-3D cannot converge.

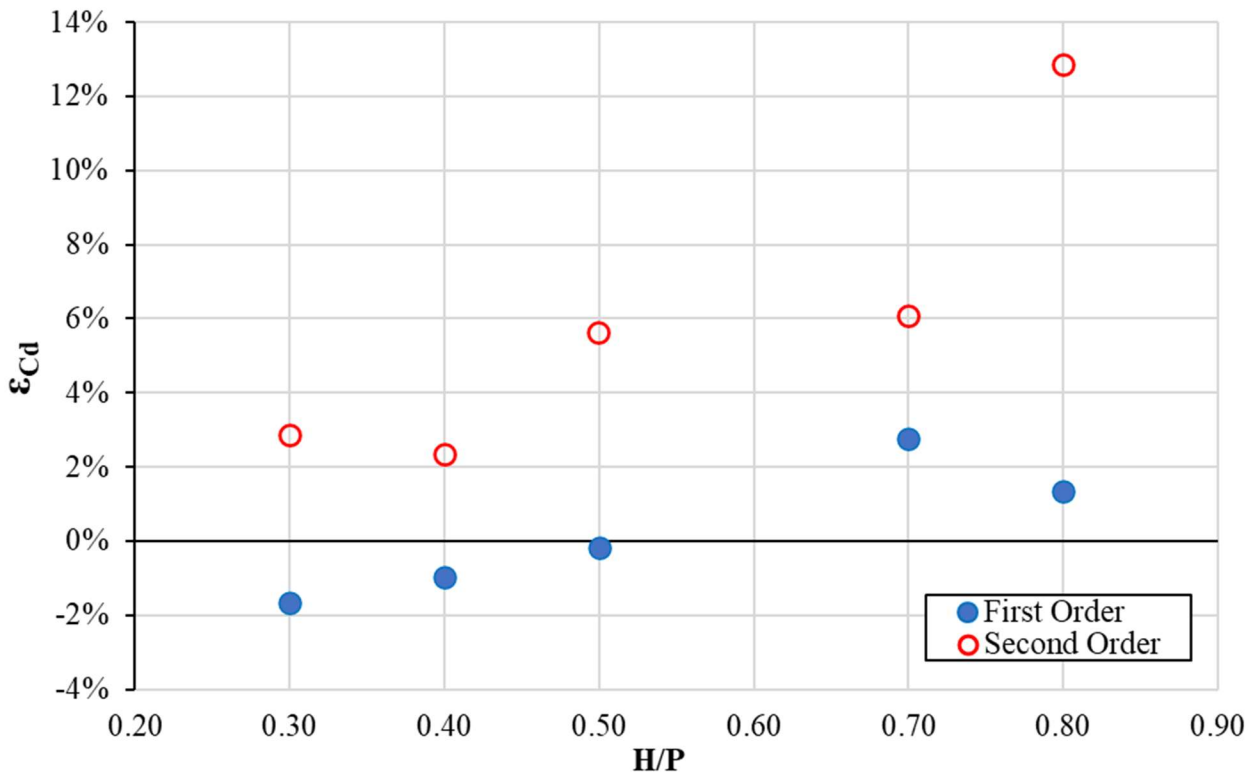


Figure 22. Relative error ( $\varepsilon_{Cd}$ ) between numerical results of momentum advection scheme order at  $H/P = 0.5$  and empirical (Eq. [10]) results for  $\alpha=16^\circ: \theta=10^\circ$  and  $\alpha=20^\circ: \theta=30^\circ$ .

Table 11. Relative error ( $\varepsilon_{Cd}$ ) between numerical results of momentum advection scheme order at H/P = 0.5 and empirical (Eq. [10]) results for  $\alpha=16^\circ$ :  $\theta=10^\circ$  and  $\alpha=20^\circ$ :  $\theta=30^\circ$ .

	H/P	Order	$C_d$	$C_{d-emp}$	$\varepsilon_{Cd}$	Simulation time	CPU Hours
$\alpha=16^\circ$ : $\theta=10^\circ$	0.30	1st	0.655	0.666	-1.65%	27 hours, 21 min, 6 sec	437.63
	0.40		0.602	0.608	-0.99%	24 hours, 25 min, 54 sec	390.91
	0.50		0.547	0.548	-0.18%	26 hours, 29 min, 11 sec	423.78
	0.70		0.484	0.471	2.76%	27 hours, 8 min, 1 sec	434.14
	0.80		0.451	0.445	1.35%	28 hours, 51 min, 39 sec	461.77
$\alpha=20^\circ$ : $\theta=30^\circ$	0.30	2nd	0.720	0.700	2.86%	28 hours, 3 min, 44 sec	4489.00
	0.40		0.657	0.642	2.34%	32 hours, 34 min, 48 sec	521.28
	0.50		0.638	0.604	5.63%	39 hours, 13 min, 40 sec	627.64
	0.70		0.524	0.494	6.07%	46 hours, 33 min, 45 sec	745.00
	0.80		0.518	0.459	12.85%	49 hours, 23 min, 28 sec	790.26

\*The simulation times are included as a relative reference for the machine used in this study but note that simulation times are subject to number of cores, rams, and specific computer configurations.

\*\* all Flow-3D runs were completed using a 16-core machine

### Flow Structure and Nappe Aeration Behavior

For both weir geometries modeled in this study, the nappes behavior rendered in CFD was very similar to what was observed in the physical model studies performed by Thompson (2019) and Christensen (2012). Thompson (2019) focused on the aeration of the ‘distal half cycles’ for all  $\alpha=16^\circ$  geometries. The numerical model produced this same aeration on the first and last half cycles for the  $\alpha=16^\circ$ ;  $\theta=10^\circ$  weir; however, Thompson (2019) observed this aeration only until  $H/P < 0.4$  while the CFD models continued to be aerated on the first and last half cycles until  $H/P > 0.5$ . This was true for both Flow-3D and Star CCM+ (Figure 23).

This study also highlighted a few of the additional capabilities of CFD beyond what can be reasonably captured or measured in a physical model including flow depths, pressures, and velocity fields. Specifically, unit discharges and weir crest pressures were calculated in both solvers.

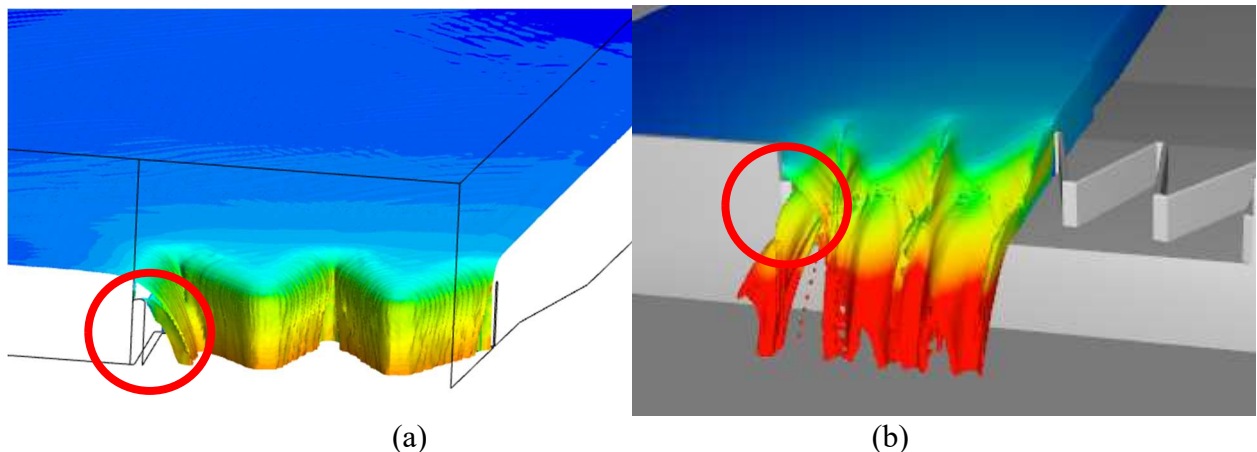


Figure 23. Nappe aeration behavior observed on the 'distal half cycles' at  $H/P = 0.5$  for the  $\alpha=16^\circ; \theta=10^\circ$  arced labyrinth weir using (a) Star CCM+ and (b) Flow-3D.

## CONCLUSION

The objective of this study was to further understand the process of capturing hydraulic efficiency and other hydraulic behaviors of arced labyrinth weirs using computational fluid dynamics in reservoir applications. The numerical models of the 5-cycle arced labyrinth weir geometries used in this study,  $\alpha=16^\circ$ :  $\theta=10^\circ$  and  $\alpha=20^\circ$ :  $\theta=30^\circ$ , were built in two commercially available solvers, Flow 3D® and Star CCM+. Simulations were completed in both solvers to outline a rating curve ( $H/P = 0.3, 0.4, 0.5, 0.7$ , and  $0.8$ ), along with a grid (mesh) convergence at two rating curve points ( $H/P = 0.3$  and  $0.7$ ). These simulations were completed using only default solver settings. The midpoint of the rating curve ( $H/P = 0.5$ ) was repeated with additional user-defined changes that mimic the study completed by to the default settings including mesh configuration, momentum advection scheme order, and turbulence model (see Table 1 and Table 3). The results are compared quantitatively and qualitatively to existing physical data collected by Christensen (2012) and Thompson (2019) for their respective geometries, as well as to numerical data collected by Thompson (2019) for the  $\alpha=16^\circ$ :  $\theta=10^\circ$  arced labyrinth weir.

These findings are specific to the geometries, solvers, and discharges in this study; however, engineering judgement may be used in application of these findings. The results of this study conclude:

- The numerical results of arced labyrinth weirs are dependent on user-defined settings for the geometries tested in this study and may be different depending on the solver. In this study, regardless of solver, the default CFD settings were not the most accurate way to capture hydraulic efficiency and other hydraulic behaviors of arced labyrinth weirs. Care should be taken in selecting applicable user-defined settings for the CFD problem to be solved.

- Best practices of model setup in Flow-3D (used in this study) are not the best practices for model setup in Star-CCM+. The results from the Star-CCM+ model may not represent the solver's full capabilities and further studies could be conducted in this area.
- CFD has the potential to be used as a design tool for arced labyrinth weirs when the designer has determined that the solution is mesh independent. Mesh size remains the most sensitive user-defined setting in CFD models.
- For the  $\alpha=16^\circ$ :  $\theta=10^\circ$  arced labyrinth weir, numerical model repeatability was good when using the same solver. The results of this study using Flow-3D were within 5% of all CFD results reported by Thompson (2019). Using a different solver, Star CCM+, but the same user-defined setup, produced results within 9% of all CFD results reported by Thompson (2019) and as close as 3%. This highlights the difference of setup required by unique solvers.
- Turbulence model selection increased the concurrence to physical data for the head discharge relationships of arced labyrinth weirs, but the  $k-\varepsilon$  standard model performed best in this study, independent of solver. The  $k-\varepsilon$  standard model resulted in relative error between 0 and 5% for both commercial solvers. Additionally, the one-equation model in both solvers had a scattered and unreliable result, suggesting that it is not an appropriate turbulence model for arced labyrinth weirs.
- From the experience in this study, the author concludes that reducing the momentum advection scheme order of accuracy to first-order in Flow-3D when you know it will converge may be appropriate depending on application. For the geometries tested in this study, accuracy decreased by between 3% and 8% when using second-order compared to first-order due to high fluctuations in the 15 second averages used for  $C_d$  calculations.

Additionally, many of the second-order momentum advection scheme simulations failed to converge due to instability which is common in some free surface applications. For second-order simulations in Flow-3D that were stable enough to converge, the computational time was between 25% and 46% longer than the first-order. Additional computational time may not be warranted in all applications. However, it is important to note that this result could be specific to this study and the specifics of the model setup and may not reflect a general outcome.

- CFD can be used to observe hydraulic behavior and anomalies on various arced labyrinth weir models that closely represent physical model observations. Additionally, CFD can provide insight beyond what can be measured in a physical model including important information about flow structure and depth, velocity fields, discharge nonuniformity along the weir crest, and pressures fields.
- Based on the author's experience and in the author's opinion, there are pros and cons to learning each of the commercially available CFD solvers discussed in this study. Flow-3D was much simpler and easy to understand. Model creation was intuitive, and the author was able to self-teach most of the model setup processes; however, due to the optimized and simplified nature of the solver, there was less control and fewer options to tweak the simulations as needed. Star-CCM+ proved to be more difficult to learn and operate but has many more tools and options to be able to customize simulations based on needs and technical understanding.

## REFERENCES

- ASCE. (2009). "CHAPTER 2 TERMINOLOGY AND BASIC METHODOLOGY." *Verification and Validation of 3D Free-Surface Flow Models*, 19–44.
- Christensen, N. A. (2012). "Flow Characteristics of Arced Labyrinth Weirs." M.S. thesis, Utah State University, Logan, Utah, USA.
- Crookston, B. M. (2010). "Labyrinth weirs." Ph.D. dissertation, Utah State University, Logan, Utah, USA.
- Crookston, B. M., Anderson, R. M., and Tullis, B. P. (2018). "Free-flow discharge estimation method for Piano Key weir geometries." *Journal of Hydro-Environment Research*, Elsevier, 19(4), 160–167.
- Crookston, B. M., and Tullis, B. P. (2012). "Arced Labyrinth Weirs." *Journal of Hydraulic Engineering*, 138(6), 555–562.
- Crookston, B. M., and Tullis, B. P. (2013). "Hydraulic Design and Analysis of Labyrinth Weirs. I: Discharge Relationships." *Journal of Irrigation and Drainage Engineering*, 139(5), 363–370.
- Darvas, L. (1971). "Discussion of performance and design of labyrinth weirs, by Hay and Taylor." *Journal of Hydraulic Engineering*, 97(8), 1246–1251.
- de Souza, Althea (2005) "How to Understand CFD Jargon" - NAFEMS.  
[https://www.nafems.org/downloads/edocs/how\\_to\\_understand\\_cfd\\_jargon-nafems.pdf](https://www.nafems.org/downloads/edocs/how_to_understand_cfd_jargon-nafems.pdf).
- Falvey, H. T. (2003). *Hydraulic Design of Labyrinth Weirs*. ASCE Press, ASCE, Reston, VA.
- Gentilini, B. (1940). "Stramazzi con cresta a planta obliqua e a zig-zag." *Memorie e Studi dell'Instituto di Idraulica e Costruzioni Idrauliche del Regio Politecnico di Milano*, No. 48.(in Italian).

- Hay, N., and Taylor, G. (1970). "Performance and design of labyrinth weirs." *Journal of Hydraulic Engineering*, 96(11), 2337–2357.
- Hinchliff, D., and Houston, K. (1984). "Hydraulic design and application of labyrinth spillways." *Proc. of 4th Annual USCOLD Lecture*, Washington, DC, USA.
- Hirt, C., and Nichols, B. (1981). "Volume of fluid (VOF) method for the dynamics of free boundaries." *Journal of Computational Physics*, Academic Press, 39(1), 201–225.
- "k-epsilon models." (2011). <[https://www.cfd-online.com/Wiki/K-epsilon\\_models](https://www.cfd-online.com/Wiki/K-epsilon_models)> (Feb. 5, 2023).
- "k-omega models." (2011). <[https://www.cfd-online.com/Wiki/K-omega\\_models](https://www.cfd-online.com/Wiki/K-omega_models)> (Feb. 5, 2023).
- Lopes, R., Matos, J., and Melo, J. (2006). "Discharge capacity and residual energy of labyrinth weirs." *Proc. of the Int. Junior Researcher and Engineer Workshop on Hydraulic Structures (IJREWHS '06)*, Montemor-o-Novo, Hydraulic Model Report No. CH61/06, Div. of Civil Engineering, the University of Queensland, Brisbane, Australia, 47–55.
- Lopes, R., Matos, J., and Melo, J. (2008). "Characteristic depths and energy dissipation downstream of a labyrinth weir." *Proc. of the Int. Junior Researcher and Engineer Workshop on Hydraulic Structures (IJREWHS '08)*, Pisa, Italy.
- Lux, F., and Hinchliff, D. (1985). "Design and construction of labyrinth spillways." *15th Congress ICOLD, Vol. IV, Q59-R15*, Lausanne, Switzerland, 249–274.
- Magalhães, A., and Lorena, M. (1989). "Hydraulic design of labyrinth weirs." *Report No. 736*, National Laboratory of Civil Engineering, Lisbon, Portugal.
- "One equation models." (2011). <[https://www.cfd-online.com/Wiki/One\\_equation\\_turbulence\\_models](https://www.cfd-online.com/Wiki/One_equation_turbulence_models)> (Feb. 5, 2023).
- Pralong, J., Montarros, B., Blancher, B., and Laugier, F. (2011). "A sensitivity analysis of Piano Key Weirs geometrical parameters based on 3D numerical modeling." *Labyrinth and*

- Piano Key Weirs - PKW 2011 - Erpicum et al. (eds)*, Taylor & Francis Group, London, England, 133–139.
- Roache, P. J. (1998). *Fundamentals of Computational Fluid Dynamics*. Hermosa Publishers, Albuquerque, NM.
- Saad, Y., and Schults, M. H. (1986). “GMRES: A Generalized Minimal Residual Algorithm for Solving Nonsymmetric Linear Systems.” *SIAM Journal on Scientific and Statistical Computing*, 7(3), 856–869.
- Sangsefidi, Y., Mehraein, M., and Ghodsian, M. (2015). “Numerical simulation of flow over labyrinth spillways.” 22(5), 1779–1787.
- Savage, B. M., Crookston, B. M., and Paxson, G. S. (2016). “Physical and Numerical Modeling of Large Headwater Ratios for a 15° Labyrinth Spillway.” *Journal of Hydraulic Engineering*, 142(11), 04016046.
- Taylor, G. (1968). “The performance of labyrinth weirs.” Ph.D. thesis, University of Nottingham, Nottingham, England
- Thompson, E. A., Cox, N. C., Ebner, L. L., and Tullis, B. (2016). “The Hydraulic Design of an Arced Labyrinth Weir at Isabella Dam.” *6th International Symposium on Hydraulic Structures: Hydraulic Structures and Water System Management, ISHS 2016*, Portland, OR.
- Thomson, S. D., (2019). “Reservoir Applications of Arced Labyrinth Weirs.” M.S. Thesis, Utah State University, Logan, Utah.
- Tullis, B. P., Young, J. C., and Chandler, M. A. (2007). “Head-Discharge Relationships for Submerged Labyrinth Weirs.” *Journal of Hydraulic Engineering*, 133(3), 248–254.

Tullis, J. P., Amanian, N., and Waldron, D. (1995). "Design of Labyrinth Spillways." *Journal of Hydraulic Engineering*, 121(3), 247–255.

Willmore, C. M. (2004). "Hydraulic characteristics of labyrinth weirs." Utah State University.

## APPENDICES

## Appendix A – CFD Glossary

All definitions were modified from de Souza (2005).

**Analytical solution** - a solution that is obtained directly using analytical methods as opposed to using computational or iterative methods.

**Boundary condition** - spatial or temporal specification of variable values or behavior necessary to produce a unique solution.

**Cell** - discrete area or volume over which governing equations are integrated. The complete group of cells should define the domain under consideration.

**Control volume** - the volume over which the partial differential equations describing fluid flow are integrated to obtain discretized (algebraic) equations.

**Direct Numerical Simulation (DNS)** -a method in which the turbulent flow is directly numerically simulated without any form of time or length averaging, i.e. both the mean flow and all turbulent fluctuations (eddies) are simulated. Since turbulent eddies are both three-dimensional and unsteady (time-variant), simulations using this method must also be both three-dimensional and unsteady and, since the length and time scales of turbulent eddies cover a large range, both the grid size and the time-step size must be very small to account for the smallest fluctuations. This makes this method very computationally expensive and even with current state-of-the-art computer hardware, only practical for simple flows at low Reynolds numbers.

**Discretization** - process by which the governing partial differential equations are converted into algebraic equations associated with discrete elements.

**Domain** - the geometrical region over which a simulation is performed. Sometimes referred to as the analytical domain or computational domain.

**External flows** - flows over the external surface of an object (e.g. an airfoil).

**Finite difference method (FDM)** - a method for approximating gradients as part of the procedure for numerical solution of differential equations, by estimating a derivative by the ratio of two finite differences.

**First order** - an approximation to an equation, or system of equations, where only the first terms in the Taylor expansions for functions are evaluated.

**Grid / mesh** - the outcome of splitting up the computational domain (discretization) into a number of elements or cells defining the discrete points at which the numerical solution is computed. The points are normally the cell centers or cell vertices.

**Grid refinement** - the act of refining a grid such that the distance between adjacent grid points is reduced enabling a more accurate calculation and representation of the solution.

**Hexahedral elements** - finite elements with six faces, i.e. cuboid or brick elements.

**Internal flows** - a fluid flow domain that is contained by and passes through a solid structure.

All boundaries of the domain can be defined as walls, periodic boundaries, inlets or outlets.

Compare with external flows.

**k- $\varepsilon$  turbulence model** - a two-equation turbulence model, formulated by the use of the eddy-viscosity hypothesis, where the effect of turbulence is captured by the fluid turbulent kinetic energy ( $k$ ) and energy dissipation rate ( $\varepsilon$ ).

**k- $\omega$  turbulence model** - a two-equation turbulence model, formulated by the use of the eddy-viscosity hypothesis, where the effect of turbulence is captured by the fluid turbulent kinetic energy ( $k$ ) and specific dissipation ( $\omega$ ).

**Large eddy simulation (LES) turbulence modeling** - this may be considered a compromise between direct numerical simulation (DNS) and the use of turbulence models (RANS). The unsteady flow equations are solved for the mean flow and larger eddies and a ‘sub-grid scale’ model is used to simulate the effects of the smaller eddies. Since it is the largest eddies which contain the most energy and interact most strongly with the mean flow, the LES approach results in a good model of the main effects of the turbulence. Since the grid size no longer has to be small enough to allow for the smallest turbulent eddies, this method is much less computationally expensive than DNS and may be applied to a wider range of flows. However, time dependent simulations using relatively fine meshes are still necessary, so the computational requirement is still high.

**Mesh** - see grid.

**Multiphase flow** - flow consisting of two or more phases (gas, liquid, solid), e.g. gas bubbles rising through a liquid.

**No slip condition** - where velocity components at a solid wall are set equal to the velocity of the walls, i.e. the fluid does not slip over the wall but exhibits a velocity gradient from stationary flow at the wall to the free stream velocity.

**Numerical Accuracy** - a measure of the accuracy of the numerical treatment (i.e. discretization and convergence) and one of the measures by which a solution is verified.

**Numerical diffusion** - a type of numerical error that smears simulated flow gradients giving the same effect as flow diffusion. It is due to truncation errors that arise as a result of representing the fluid flow equations in discrete form. It is inversely related to the grid resolution. Numerical diffusion may also be reduced by the use of higher order discretization schemes and alignment of the grid lines with the streamlines. It is also known as false diffusion and it results in a diffusive error.

**Numerical dispersion** - a numerical effect on the solution in Fourier space in which waves are spread in space, but not changed in amplitude.

**Numerical dissipation** - a numerical effect on the solution in Fourier space in which the variation of the coefficients (or amplitude) is reduced.

**Numerical instability** - an increasing oscillation of an iterative solution or the growth of errors due to round-off or truncation in a numerical scheme.

**Order of accuracy** - the number of terms retained in the series expansion used to approximate the equations in their discretized form.

**RANS (Reynolds averaged Navier Stokes)** - a form of the Navier Stokes equations in which additional terms (known as Reynolds stresses) are included to account for the time averaged effects of turbulence. See Turbulence Models.

**RNG k- $\epsilon$  turbulence model** - a variant of the standard k- $\epsilon$  turbulence model where the model constants are derived from Renormalization Group theory and are based on statistical techniques as opposed to empirical techniques as used in the standard k- $\epsilon$  model.

**Second order scheme** - a scheme which is second-order accurate in terms of a Taylor series.

**SIMPLE algorithm** - (Semi-Implicit Method for Pressure-Linked Equations) an algorithm which is used to compensate for the lack of an explicit pressure equation in the Navier Stokes equations using an iterative procedure consisting of a predictor and a corrector step.

**Stability** - the property of a numerical method that progresses towards a solution without wild oscillations or divergence.

**Symmetry boundary condition** - boundary condition where the normal velocity is zero and the normal gradients of all other variables are also zero.

**Time step** - the incremental change in time for which a flow is being solved.

**Turbulence** - a chaotic state of fluid motion where the velocity and pressure change continuously with time.

**Turbulence characteristic length** - a typical dimension of a turbulent eddy.

**Turbulence models** - sets of equations that determine the turbulent transport terms (Reynolds stresses) in the mean flow equations. They are based on hypotheses about turbulent processes and generally require significant empirical input in the form of constants or functions. These time averaged models do not simulate the details of the turbulent motion (the turbulent eddies), only the effect of turbulence on the mean flow behavior. Thus, with a particular set of empirical constants, they are valid only for a certain flow or at most a range of flows. This is also known as a RANS approach (Reynolds Averaged Navier-Stokes).

**Turbulent dissipation** - the reduction in turbulent kinetic energy caused by the work done by the smallest eddies converting turbulent kinetic energy to thermal internal energy.

**Two-equation model** - a turbulence model that uses two transport equations to model the effects of turbulence in the RANS equations.

**Volume-of-fluid method** - a multiphase (multi-fluid) technique in which a single set of momentum equations is shared by the fluids and the volume fraction in each cell is tracked through the domain. This method is generally used where the interface between the fluids is of interest.

**Zero gradient boundary condition** - a boundary condition where a variable is defined as constant across the boundary.

For more information about solver specific jargon see the respective user manual.

## Appendix B – Physical Model Setup with Numerical Computational Domain and Weir Geometries.

Sectional Model Domain

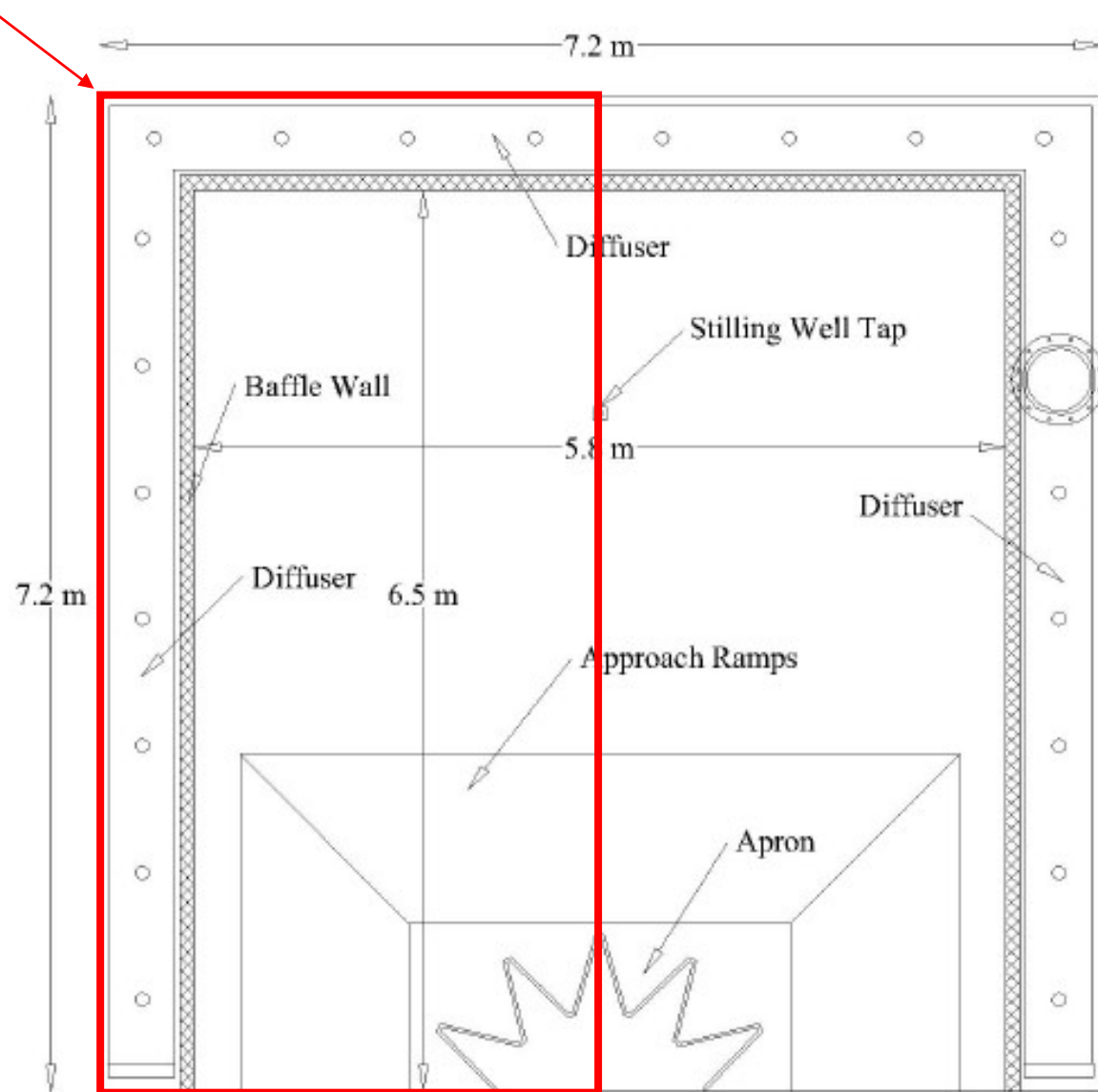
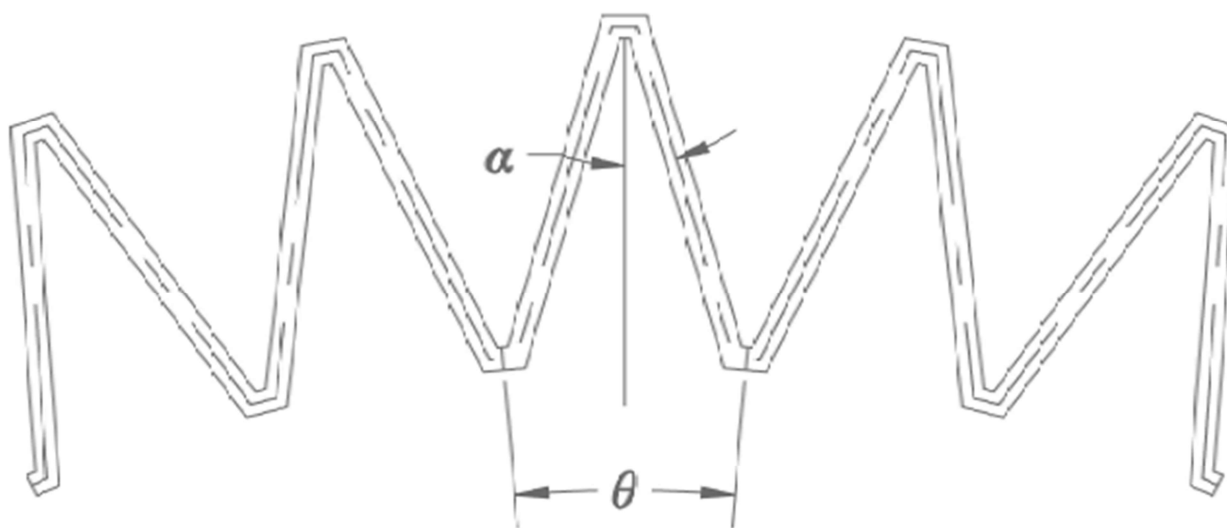


Figure B1. Plan view of reservoir headbox with diffuser, baffle wall, stilling well tap, apron, and approach ramps labeled. Additionally, the numerical computational domain for the sectional model is labeled by the red box. (modified from Thompson, 2019).



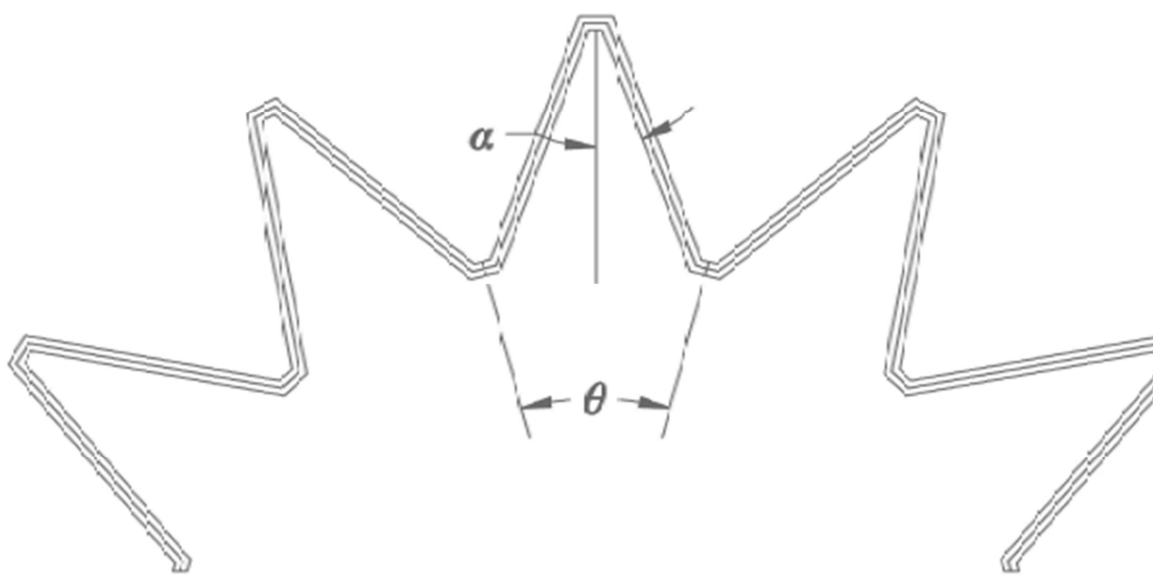
$$L_c = 20.492 \text{ ft} \quad W = 6.526 \text{ ft}$$

$$L_{c-cycle} = 4.091 \text{ ft} \quad w = 1.339 \text{ ft}$$

$$l_c = 1.899 \text{ ft} \quad B = 1.885 \text{ ft}$$

$$\alpha = 16^\circ; \theta = 10^\circ$$

Figure B2.  $\alpha=16^\circ$ ,  $\theta=10^\circ$  weir geometry.



$$L_c = 16.893 \text{ ft}$$

$$W = 4.904 \text{ ft}$$

$$L_{c-cycle} = 3.383 \text{ ft}$$

$$w = 1.339 \text{ ft}$$

$$l_c = 1.550 \text{ ft}$$

$$B = 1.469 \text{ ft}$$

$$\alpha = 20^\circ; \theta = 30^\circ$$

Figure B3.  $\alpha=20^\circ, \theta=30^\circ$  weir geometry.

## Appendix C – Numerical Model Time Series Data

Table C1. Tabulated time series data for  $\alpha = 16^\circ$ ;  $\theta = 10^\circ$  arced labyrinth weir at H/P = 0.3

STAR CCM+ (fine mesh)		
Cell count:	2,765,099	
P	8.00	in
$\alpha$	16.00	deg
$\theta$	10.00	deg
L	122.95	in
L	10.25	ft
tw	1.00	in
g	32.19	ft/s <sup>2</sup>
Q	3.63	cfs
h	2.16	
H	0.20	ft
H/P	0.30	-
Cd	0.750	-
Cd <sub>emp</sub>	0.664	-
$\varepsilon_{Cd-emp}$	13.007%	-

FLOW-3D (coarse mesh)		
Cell count:	346,668	
P	8.00	in
$\alpha$	16.00	deg
$\theta$	10.00	deg
L	122.95	in
L	10.25	ft
tw	1.00	in
g	32.19	ft/s <sup>2</sup>
Q	3.53	cfs
h	0.89	
H	0.22	ft
H/P	0.34	-
Cd	0.610	-
Cd <sub>emp</sub>	0.641	-
$\varepsilon_{Cd-emp}$	-4.845%	-

FLOW-3D (medium mesh)		
Cell count:	680,064	
P	8.00	in
$\alpha$	16.00	deg
$\theta$	10.00	deg
L	122.95	in
L	10.25	ft
tw	1.00	in
g	32.19	ft/s <sup>2</sup>
Q	3.28	cfs
h	1.14	
H	0.19	ft
H/P	0.28	-
Cd	0.738	-
Cd <sub>emp</sub>	0.673	-
$\varepsilon_{Cd-emp}$	9.687%	-

FLOW-3D (fine mesh)		
Cell count:	3,306,877	
P	8.00	in
$\alpha$	16.00	deg
$\theta$	10.00	deg
L	122.95	in
L	10.25	ft
tw	1.00	in
g	32.19	ft/s <sup>2</sup>
Q	3.10	cfs
h	1.15	
H	0.20	ft
H/P	0.29	-
Cd	0.655	-
Cd <sub>emp</sub>	0.666	-
$\varepsilon_{Cd-emp}$	-1.657%	-

time	h	H
45.00	2.154	0.20
45.15	2.154	0.20
45.3	2.154	0.20
45.45	2.154	0.20
45.6	2.154	0.20
45.75	2.154	0.20
45.9	2.154	0.20
46.05	2.154	0.20
46.2	2.154	0.20
46.35	2.154	0.20
46.5	2.154	0.20
46.65	2.154	0.20
46.8	2.154	0.20
46.95	2.154	0.20
47.1	2.154	0.20
47.25	2.154	0.20
47.4	2.154	0.20
47.55	2.154	0.20
47.7	2.154	0.20
47.85	2.154	0.20
48	2.154	0.20
48.15	2.154	0.20
48.3	2.154	0.20
48.45	2.154	0.20
48.6	2.154	0.20
48.75	2.154	0.20
48.9	2.154	0.20
49.05	2.154	0.20
49.2	2.154	0.20
49.35	2.154	0.20
49.5	2.155	0.20
49.65	2.155	0.20
49.8	2.155	0.20
49.95	2.155	0.20
50.1	2.155	0.20
50.25	2.155	0.20
50.4	2.155	0.20
50.55	2.155	0.20
50.7	2.155	0.20
50.85	2.155	0.20
51	2.155	0.20
51.15	2.155	0.20
51.3	2.155	0.20
51.45	2.155	0.20
51.6	2.155	0.20
51.75	2.155	0.20
51.9	2.155	0.20
52.05	2.155	0.20
52.2	2.155	0.20
52.35	2.155	0.20

time	h	H
0.00	1.16	0.202
0.60	1.16	0.204
1.20	1.19	0.235
1.80	1.18	0.228
2.40	1.19	0.233
3.00	1.16	0.201
3.60	1.11	0.155
4.20	1.10	0.148
4.80	1.09	0.130
5.40	1.05	0.093
6.00	1.06	0.102
6.60	1.08	0.127
7.20	1.05	0.096
7.80	1.07	0.114
8.40	1.08	0.120
9.00	1.04	0.086
9.60	1.11	0.155
10.20	1.05	0.090
10.80	1.08	0.120
11.40	1.05	0.094
12.00	1.00	0.042
12.60	1.09	0.133
13.20	1.01	0.056
13.80	1.05	0.096
14.40	0.95	-0.010
15.00	1.04	0.083
15.60	1.01	0.052
16.20	0.99	0.035
16.80	1.03	0.071
17.40	1.01	0.054
18.00	0.98	0.020
18.60	1.00	0.046
19.20	0.99	0.036
19.80	0.99	0.031
20.40	0.93	-0.028
21.00	1.05	0.093
21.60	0.95	-0.010
22.20	0.94	-0.017
22.80	0.97	0.016
23.40	1.00	0.043
24.00	0.97	0.016
24.60	0.97	0.012
25.20	0.93	-0.025
25.80	1.00	0.048
26.40	0.94	-0.018
27.00	0.96	0.002
27.60	0.97	0.012
28.20	0.90	-0.057
28.80	1.00	0.048
29.40	0.84	-0.116

time	h	H
0.00	1.29	0.335
0.60	1.29	0.337
1.20	1.31	0.354
1.80	1.33	0.370
2.40	1.33	0.370
3.00	1.28	0.328
3.60	1.27	0.317
4.20	1.26	0.303
4.80	1.20	0.245
5.40	1.23	0.271
6.00	1.22	0.263
6.60	1.22	0.268
7.20	1.24	0.285
7.80	1.22	0.259
8.40	1.24	0.279
9.00	1.26	0.302
9.60	1.23	0.275
10.20	1.20	0.239
10.80	1.18	0.228
11.40	1.18	0.226
12.00	1.21	0.251
12.60	1.19	0.229
13.20	1.18	0.218
13.80	1.19	0.228
14.40	1.19	0.233
15.00	1.20	0.239
15.60	1.22	0.268
16.20	1.18	0.218
16.80	1.18	0.219
17.40	1.18	0.221
18.00	1.18	0.218
18.60	1.18	0.221
19.20	1.16	0.205
19.80	1.15	0.191
20.40	1.18	0.219
21.00	1.18	0.221
21.60	1.18	0.227
22.20	1.18	0.219
22.80	1.15	0.196
23.40	1.17	0.218
24.00	1.16	0.207
24.60	1.16	0.206
25.20	1.16	0.200
25.80	1.15	0.189
26.40	1.15	0.189
27.00	1.16	0.204
27.60	1.16	0.204
28.20	1.16	0.204
28.80	1.15	0.197
29.40	1.15	0.196

time	h	H
0.002	1.158	0.202
0.600	1.160	0.203
1.200	1.177	0.220
1.800	1.193	0.236
2.400	1.207	0.251
3.000	1.176	0.219
3.600	1.172	0.215
4.200	1.168	0.211
4.800	1.132	0.175
5.400	1.154	0.197
6.000	1.155	0.198
6.600	1.143	0.186
7.200	1.172	0.200
7.800	1.156	0.199
8.400	1.161	0.204
9.000	1.183	0.226
9.600	1.184	0.228
10.200	1.154	0.197
10.800	1.152	0.195
11.400	1.146	0.190
12.000	1.159	0.202
12.600	1.159	0.203
13.200	1.144	0.187
13.800	1.153	0.197
14.400	1.159	0.202
15.000	1.157	0.200
15.600	1.183	0.227
16.200	1.157	0.200
16.800	1.152	0.195
17.400	1.159	0.202
18.000	1.153	0.196
18.600	1.159	0.202
19.200	1.158	0.201
19.800	1.142	0.185
20.400	1.145	0.188
21.000	1.161	0.204
21.600	1.167	0.210
22.200	1.160	0.204
22.800	1.150	0.194
23.400	1.151	0.195
24.000	1.156	0.199
24.600	1.161	0.204
25.200	1.154	0.197
25.800	1.149	0.192
26.400	1.146	0.189
27.000	1.152	0.196
27.600	1.157	0.200
28.200	1.157	0.200
28.800	1.152	0.196
29.400	1.157	0.200

52.5	2.155	0.20
52.65	2.155	0.20
52.8	2.155	0.20
52.95	2.155	0.20
53.1	2.155	0.20
53.25	2.155	0.20
53.4	2.155	0.20
53.55	2.155	0.20
53.7	2.155	0.20
53.85	2.155	0.20
54	2.155	0.20
54.15	2.155	0.20
54.3	2.155	0.20
54.45	2.155	0.20
54.6	2.155	0.20
54.75	2.155	0.20
54.9	2.155	0.20
55.05	2.155	0.20
55.2	2.156	0.20
55.35	2.156	0.20
55.5	2.156	0.20
55.65	2.156	0.20
55.8	2.156	0.20
55.95	2.156	0.20
56.1	2.156	0.20
56.25	2.156	0.20
56.4	2.156	0.20
56.55	2.156	0.20
56.7	2.156	0.20
56.85	2.156	0.20
57	2.156	0.20
57.15	2.156	0.20
57.3	2.156	0.20
57.45	2.156	0.20
57.6	2.156	0.20
57.75	2.156	0.20
57.9	2.156	0.20
58.05	2.156	0.20
58.2	2.156	0.20
58.35	2.156	0.20
58.5	2.156	0.20
58.65	2.156	0.20
58.8	2.156	0.20
58.95	2.156	0.20
59.1	2.156	0.20
59.25	2.156	0.20
59.4	2.156	0.20
59.55	2.156	0.20
59.7	2.156	0.20
59.85	2.156	0.20
60	2.156	0.20

30.00	1.02	0.059
30.60	0.93	-0.023
31.20	0.91	-0.048
31.80	0.98	0.027
32.40	0.89	-0.066
33.00	0.96	0.002
33.60	0.93	-0.027
34.20	0.90	-0.055
34.80	0.96	0.005
35.40	0.89	-0.064
36.00	0.91	-0.049
36.60	0.95	-0.005
37.20	0.90	-0.056
37.80	0.91	-0.046
38.40	0.92	-0.035
39.00	0.90	-0.055
39.60	0.88	-0.080
40.20	0.95	-0.009
40.80	0.89	-0.066
41.40	0.87	-0.083
42.00	0.88	-0.072
42.60	0.94	-0.016
43.20	0.87	-0.089
43.80	0.92	-0.035
44.40	0.92	-0.032
45.00	0.89	-0.065
45.60	0.87	-0.089
46.20	0.97	0.012
46.80	0.87	-0.088
47.40	0.84	-0.116
48.00	1.00	0.045
48.60	0.83	-0.122
49.20	0.87	-0.083
49.80	0.98	0.024
50.40	0.83	-0.131
51.00	0.90	-0.052
51.60	0.96	0.007
52.20	0.83	-0.122
52.80	0.87	-0.091
53.40	0.92	-0.035
54.00	0.92	-0.039
54.60	0.83	-0.130
55.20	0.91	-0.048
55.80	0.90	-0.059
56.40	0.85	-0.108
57.00	0.92	-0.041
57.60	0.93	-0.025
58.20	0.80	-0.161
58.80	0.93	-0.027
59.40	0.92	-0.039
60.00	0.81	-0.143

30.00	1.15	0.192
30.60	1.16	0.206
31.20	1.15	0.198
31.80	1.14	0.188
32.40	1.14	0.187
33.00	1.15	0.191
33.60	1.15	0.193
34.20	1.16	0.201
34.80	1.15	0.191
35.40	1.15	0.191
36.00	1.14	0.188
36.60	1.16	0.199
37.20	1.15	0.195
37.80	1.15	0.192
38.40	1.14	0.184
39.00	1.15	0.190
39.60	1.14	0.187
40.20	1.15	0.194
40.80	1.15	0.190
41.40	1.15	0.189
42.00	1.14	0.182
42.60	1.15	0.194
43.20	1.15	0.191
43.80	1.15	0.192
44.40	1.15	0.188
45.00	1.14	0.184
45.60	1.14	0.185
46.20	1.15	0.194
46.80	1.14	0.188
47.40	1.15	0.188
48.00	1.14	0.184
48.60	1.14	0.185
49.20	1.15	0.191
49.80	1.15	0.190
50.40	1.14	0.188
51.00	1.14	0.186
51.60	1.14	0.184
52.20	1.14	0.188
52.80	1.15	0.190
53.40	1.14	0.187
54.00	1.14	0.184
54.60	1.14	0.185
55.20	1.14	0.186
55.80	1.15	0.189
56.40	1.15	0.190
57.00	1.14	0.183
57.60	1.14	0.187
58.20	1.14	0.186
58.80	1.14	0.188
59.40	1.14	0.188
60.00	1.14	0.186

30.000	1.147	0.190
30.600	1.156	0.199
31.200	1.160	0.203
31.800	1.151	0.195
32.400	1.147	0.191
33.000	1.152	0.195
33.600	1.150	0.193
34.200	1.158	0.202
34.800	1.155	0.198
35.400	1.150	0.193
36.000	1.150	0.193
36.600	1.157	0.200
37.200	1.154	0.197
37.800	1.156	0.199
38.400	1.148	0.191
39.000	1.151	0.194
39.600	1.151	0.195
40.200	1.154	0.197
40.800	1.154	0.197
41.400	1.154	0.198
42.000	1.146	0.189
42.600	1.153	0.196
43.200	1.155	0.198
43.800	1.154	0.197
44.400	1.153	0.196
45.000	1.151	0.194
45.600	1.147	0.190
46.200	1.155	0.199
46.800	1.153	0.196
47.400	1.152	0.195
48.000	1.151	0.194
48.600	1.150	0.194
49.200	1.152	0.195
49.800	1.154	0.198
50.400	1.151	0.194
51.000	1.152	0.196
51.600	1.149	0.193
52.200	1.150	0.194
52.800	1.154	0.197
53.400	1.153	0.197
54.000	1.150	0.193
54.600	1.151	0.194
55.200	1.149	0.192
55.800	1.152	0.196
56.400	1.155	0.199
57.000	1.150	0.193
57.600	1.149	0.192
58.200	1.151	0.195
58.800	1.151	0.195
59.400	1.153	0.196
60.000	1.153	0.196

Table C2 Tabulated time series data for  $\alpha = 16^\circ$ ;  $\theta = 10^\circ$  arced labyrinth weir at H/P = 0.4

STAR CCM+ (fine mesh)		
Cell count:	2,756,778	
<b>P</b>	8.00	in
<b><math>\alpha</math></b>	16.00	deg
<b><math>\theta</math></b>	10.00	deg
<b>L</b>	122.95	in
<b>L</b>	10.25	ft
<b>tw</b>	1.00	in
<b>g</b>	32.19	ft/s <sup>2</sup>
<b>Q</b>	4.78	cfs
<b>h</b>	2.22	
<b>H</b>	0.26	ft
<b>H/P</b>	0.39	-
<b>Cd</b>	0.658	-
<b>Cd<sub>emp</sub></b>	0.608	-
<b><math>\epsilon_{Cd-emp}</math></b>	<b>8.29%</b>	-

FLOW-3D (fine mesh)		
Cell count:	3,306,877	
<b>P</b>	8.00	in
<b><math>\alpha</math></b>	16.00	deg
<b><math>\theta</math></b>	10.00	deg
<b>L</b>	122.95	in
<b>L</b>	10.25	ft
<b>tw</b>	1.00	in
<b>g</b>	32.19	ft/s <sup>2</sup>
<b>Q</b>	4.37	cfs
<b>h</b>	1.22	
<b>H</b>	0.26	ft
<b>H/P</b>	0.39	-
<b>Cd</b>	0.602	-
<b>Cd<sub>emp</sub></b>	0.608	-
<b><math>\epsilon_{Cd-emp}</math></b>	<b>-0.97%</b>	-

time	h	H
45.00	2.217	0.217
45.15	2.217	0.217
45.3	2.217	0.217
45.45	2.217	0.217
45.6	2.217	0.217
45.75	2.217	0.217
45.9	2.217	0.217
46.05	2.217	0.217
46.2	2.217	0.217
46.35	2.217	0.217
46.5	2.217	0.217
46.65	2.217	0.217
46.8	2.217	0.217
46.95	2.217	0.217
47.1	2.217	0.217
47.25	2.217	0.217
47.4	2.217	0.217
47.55	2.217	0.217
47.7	2.217	0.217
47.85	2.217	0.217
48	2.217	0.217
48.15	2.217	0.217
48.3	2.217	0.217
48.45	2.217	0.217

time	h	H
0.002	1.238	0.281
0.600	1.237	0.280
1.200	1.235	0.279
1.800	1.233	0.276
2.400	1.227	0.271
3.000	1.232	0.276
3.600	1.231	0.275
4.200	1.230	0.274
4.800	1.228	0.272
5.400	1.225	0.269
6.000	1.226	0.269
6.600	1.231	0.274
7.200	1.226	0.269
7.800	1.225	0.268
8.400	1.224	0.267
9.000	1.224	0.268
9.600	1.225	0.269
10.200	1.226	0.269
10.800	1.220	0.264
11.400	1.223	0.266
12.000	1.221	0.264
12.600	1.223	0.266
13.200	1.223	0.267
13.800	1.222	0.265

48.6	2.217	0.217
48.75	2.217	0.217
48.9	2.217	0.217
49.05	2.217	0.217
49.2	2.217	0.217
49.35	2.217	0.217
49.5	2.217	0.217
49.65	2.217	0.217
49.8	2.217	0.217
49.95	2.217	0.217
50.1	2.217	0.217
50.25	2.217	0.217
50.4	2.217	0.217
50.55	2.217	0.217
50.7	2.217	0.217
50.85	2.217	0.217
51	2.217	0.217
51.15	2.217	0.217
51.3	2.217	0.217
51.45	2.217	0.217
51.6	2.217	0.217
51.75	2.217	0.217
51.9	2.217	0.217
52.05	2.217	0.217
52.2	2.217	0.217
52.35	2.217	0.217
52.5	2.217	0.217
52.65	2.217	0.217
52.8	2.217	0.217
52.95	2.217	0.217
53.1	2.217	0.217
53.25	2.217	0.217
53.4	2.217	0.217
53.55	2.217	0.217
53.7	2.217	0.217
53.85	2.217	0.217
54	2.217	0.217
54.15	2.217	0.217
54.3	2.217	0.217
54.45	2.217	0.217
54.6	2.217	0.217
54.75	2.217	0.217
54.9	2.217	0.217
55.05	2.217	0.217

14.400	1.219	0.262
15.000	1.222	0.265
15.600	1.220	0.263
16.200	1.223	0.266
16.800	1.220	0.263
17.400	1.218	0.261
18.000	1.219	0.262
18.600	1.222	0.265
19.200	1.219	0.262
19.800	1.220	0.264
20.400	1.217	0.261
21.000	1.218	0.262
21.600	1.220	0.263
22.200	1.220	0.263
22.800	1.218	0.261
23.400	1.219	0.262
24.000	1.217	0.260
24.600	1.219	0.262
25.200	1.219	0.263
25.800	1.217	0.261
26.400	1.218	0.261
27.000	1.217	0.260
27.600	1.217	0.261
28.200	1.219	0.263
28.800	1.218	0.261
29.400	1.216	0.259
30.000	1.218	0.261
30.600	1.217	0.260
31.200	1.218	0.261
31.800	1.218	0.261
32.400	1.216	0.260
33.000	1.216	0.260
33.600	1.218	0.261
34.200	1.216	0.260
34.800	1.218	0.262
35.400	1.217	0.260
36.000	1.216	0.260
36.600	1.217	0.260
37.200	1.217	0.261
37.800	1.217	0.260
38.400	1.218	0.261
39.000	1.215	0.259
39.600	1.217	0.260
40.200	1.217	0.261

55.2	2.217	0.217
55.35	2.217	0.217
55.5	2.217	0.217
55.65	2.217	0.217
55.8	2.217	0.217
55.95	2.216	0.216
56.1	2.216	0.216
56.25	2.216	0.216
56.4	2.216	0.216
56.55	2.216	0.216
56.7	2.216	0.216
56.85	2.216	0.216
57	2.216	0.216
57.15	2.216	0.216
57.3	2.216	0.216
57.45	2.216	0.216
57.6	2.216	0.216
57.75	2.216	0.216
57.9	2.216	0.216
58.05	2.216	0.216
58.2	2.216	0.216
58.35	2.216	0.216
58.5	2.216	0.216
58.65	2.216	0.216
58.8	2.216	0.216
58.95	2.216	0.216
59.1	2.216	0.216
59.25	2.216	0.216
59.4	2.216	0.216
59.55	2.216	0.216
59.7	2.216	0.216
59.85	2.216	0.216
60	2.216	0.216

40.800	1.217	0.260
41.400	1.217	0.260
42.000	1.217	0.260
42.600	1.215	0.259
43.200	1.218	0.261
43.800	1.217	0.260
44.400	1.216	0.260
45.000	1.217	0.260
45.600	1.217	0.260
46.200	1.216	0.260
46.800	1.218	0.261
47.400	1.216	0.259
48.000	1.217	0.260
48.600	1.217	0.260
49.200	1.216	0.260
49.800	1.217	0.260
50.400	1.217	0.260
51.000	1.216	0.259
51.600	1.217	0.260
52.200	1.217	0.260
52.800	1.216	0.260
53.400	1.217	0.261
54.000	1.216	0.259
54.600	1.216	0.260
55.200	1.217	0.260
55.800	1.217	0.260
56.400	1.216	0.260
57.000	1.217	0.260
57.600	1.216	0.259
58.200	1.217	0.260
58.800	1.217	0.260
59.400	1.217	0.260
60.000	1.217	0.260

Table C3 Tabulated time series data for  $\alpha = 16^\circ$ ;  $\theta = 10^\circ$  arced labyrinth weir at H/P = 0.5

STAR CCM+ (coarse mesh)			STAR CCM+ (medium mesh)			STAR CCM+ (fine mesh)			STAR CCM+ (fine mesh, 1 Eq.)		
Cell count:	44,066		Cell count:	579,964		Cell count:	2,745,413		Cell count:	2,754,623	
<b>P</b>	8.00	in	<b>P</b>	8.00	in	<b>P</b>	8.00	in	<b>P</b>	8.00	in
<b>a</b>	16.00	deg	<b>a</b>	16.00	deg	<b>a</b>	16.00	deg	<b>a</b>	16.00	deg
<b>θ</b>	10.00	deg	<b>θ</b>	10.00	deg	<b>θ</b>	10.00	deg	<b>θ</b>	10.00	deg
<b>L</b>	122.95	in	<b>L</b>	122.95	in	<b>L</b>	122.95	in	<b>L</b>	122.95	in
<b>L</b>	10.25	ft	<b>L</b>	10.25	ft	<b>L</b>	10.25	ft	<b>L</b>	10.25	ft
<b>tw</b>	1.00	in	<b>tw</b>	1.00	in	<b>tw</b>	1.00	in	<b>tw</b>	1.00	in
<b>g</b>	32.19	ft/s <sup>2</sup>	<b>g</b>	32.19	ft/s <sup>2</sup>	<b>g</b>	32.19	ft/s <sup>2</sup>	<b>g</b>	32.19	ft/s <sup>2</sup>
<b>Q</b>	5.99	cfs	<b>Q</b>	5.99	cfs	<b>Q</b>	5.99	cfs	<b>Q</b>	6.00	cfs
<b>h</b>	2.30		<b>h</b>	2.31		<b>h</b>	2.27		<b>h</b>	2.29	
<b>H</b>	0.34	ft	<b>H</b>	0.35	ft	<b>H</b>	0.31	ft	<b>H</b>	0.33	ft
<b>H/P</b>	0.51	-	<b>H/P</b>	0.53	-	<b>H/P</b>	0.46	-	<b>H/P</b>	0.50	-
<b>Cd</b>	0.545	-	<b>Cd</b>	0.521	-	<b>Cd</b>	0.635	-	<b>Cd</b>	0.571	-
<b>Cd<sub>emp</sub></b>	0.537	-	<b>Cd<sub>emp</sub></b>	0.529	-	<b>Cd<sub>emp</sub></b>	0.564	-	<b>Cd<sub>emp</sub></b>	0.545	-
<b>ε<sub>Cd-emp</sub></b>	1.49%	-	<b>ε<sub>Cd-emp</sub></b>	-1.62%	-	<b>ε<sub>Cd-emp</sub></b>	12.54%	-	<b>ε<sub>Cd-emp</sub></b>	4.71%	-
time	h	H	time	h	H	time	h	H	time	h	H
45.00	2.30	0.34	45.00	2.31	0.35	45.00	2.26	0.31	45.00	2.29	0.33
45.15	2.30	0.34	45.15	2.31	0.35	45.15	2.26	0.31	45.15	2.29	0.33
45.30	2.30	0.34	45.30	2.31	0.35	45.30	2.26	0.31	45.30	2.29	0.33
45.45	2.30	0.34	45.45	2.31	0.35	45.45	2.26	0.31	45.45	2.29	0.33
45.60	2.30	0.34	45.60	2.31	0.35	45.60	2.26	0.31	45.60	2.29	0.33
45.75	2.30	0.34	45.75	2.31	0.35	45.75	2.26	0.31	45.75	2.29	0.33
45.90	2.30	0.34	45.90	2.31	0.35	45.90	2.26	0.31	45.90	2.29	0.33
46.05	2.30	0.34	46.05	2.31	0.35	46.05	2.26	0.31	46.05	2.29	0.33
46.20	2.30	0.34	46.20	2.31	0.35	46.20	2.26	0.31	46.20	2.29	0.33
46.35	2.30	0.34	46.35	2.31	0.35	46.35	2.26	0.31	46.35	2.29	0.33
46.50	2.30	0.34	46.50	2.31	0.35	46.50	2.26	0.31	46.50	2.29	0.33
46.65	2.30	0.34	46.65	2.31	0.35	46.65	2.26	0.31	46.65	2.29	0.33
46.80	2.30	0.34	46.80	2.31	0.35	46.80	2.26	0.31	46.80	2.29	0.33
46.95	2.30	0.34	46.95	2.31	0.35	46.95	2.27	0.31	46.95	2.29	0.33
47.10	2.30	0.34	47.10	2.31	0.35	47.10	2.27	0.31	47.10	2.29	0.33
47.25	2.30	0.34	47.25	2.31	0.35	47.25	2.27	0.31	47.25	2.29	0.33
47.40	2.30	0.34	47.40	2.31	0.35	47.40	2.27	0.31	47.40	2.29	0.33
47.55	2.30	0.34	47.55	2.31	0.35	47.55	2.27	0.31	47.55	2.29	0.33
47.70	2.30	0.34	47.70	2.31	0.35	47.70	2.27	0.31	47.70	2.29	0.33
47.85	2.30	0.34	47.85	2.31	0.35	47.85	2.27	0.31	47.85	2.29	0.33
48.00	2.30	0.34	48.00	2.31	0.35	48.00	2.27	0.31	48.00	2.29	0.33
48.15	2.30	0.34	48.15	2.31	0.35	48.15	2.27	0.31	48.15	2.29	0.33
48.30	2.30	0.34	48.30	2.31	0.35	48.30	2.27	0.31	48.30	2.29	0.33
48.45	2.30	0.34	48.45	2.31	0.35	48.45	2.27	0.31	48.45	2.29	0.33
48.60	2.30	0.34	48.60	2.31	0.35	48.60	2.27	0.31	48.60	2.29	0.33
48.75	2.30	0.34	48.75	2.31	0.35	48.75	2.27	0.31	48.75	2.29	0.33
48.90	2.30	0.34	48.90	2.31	0.35	48.90	2.27	0.31	48.90	2.29	0.33
49.05	2.30	0.34	49.05	2.31	0.35	49.05	2.27	0.31	49.05	2.29	0.33
49.20	2.30	0.34	49.20	2.31	0.35	49.20	2.27	0.31	49.20	2.29	0.33
49.35	2.30	0.34	49.35	2.31	0.35	49.35	2.27	0.31	49.35	2.29	0.33
49.50	2.30	0.34	49.50	2.31	0.35	49.50	2.27	0.31	49.50	2.29	0.33
49.65	2.30	0.34	49.65	2.31	0.35	49.65	2.27	0.31	49.65	2.29	0.33
49.80	2.30	0.34	49.80	2.31	0.35	49.80	2.27	0.31	49.80	2.29	0.33
49.95	2.30	0.34	49.95	2.31	0.35	49.95	2.27	0.31	49.95	2.29	0.33
50.10	2.30	0.34	50.10	2.31	0.35	50.10	2.27	0.31	50.10	2.29	0.33
50.25	2.30	0.34	50.25	2.31	0.35	50.25	2.27	0.31	50.25	2.29	0.33
50.40	2.30	0.34	50.40	2.31	0.35	50.40	2.27	0.31	50.40	2.29	0.33
50.55	2.30	0.34	50.55	2.31	0.35	50.55	2.27	0.31	50.55	2.29	0.33
50.70	2.30	0.34	50.70	2.31	0.35	50.70	2.27	0.31	50.70	2.29	0.33
50.85	2.30	0.34	50.85	2.31	0.35	50.85	2.27	0.31	50.85	2.29	0.33
51.00	2.30	0.34	51.00	2.31	0.35	51.00	2.27	0.31	51.00	2.29	0.33
51.15	2.30	0.34	51.15	2.31	0.35	51.15	2.27	0.31	51.15	2.29	0.33
51.30	2.30	0.34	51.30	2.31	0.35	51.30	2.27	0.31	51.30	2.29	0.33
51.45	2.30	0.34	51.45	2.31	0.35	51.45	2.27	0.31	51.45	2.29	0.33
51.60	2.30	0.34	51.60	2.31	0.35	51.60	2.27	0.31	51.60	2.29	0.33
51.75	2.30	0.34	51.75	2.31	0.35	51.75	2.27	0.31	51.75	2.29	0.33



Table C4 Tabulated time series data for  $\alpha = 16^\circ$ ;  $\theta = 10^\circ$  arced labyrinth weir at H/P = 0.5

STAR CCM+ (fine mesh, $k-\varepsilon$ )		
Cell count:		2,754,245
<b>P</b>	8.00	in
<b><math>\alpha</math></b>	16.00	deg
<b><math>\theta</math></b>	10.00	deg
<b>L</b>	122.95	in
<b>L</b>	10.25	ft
<b>tw</b>	1.00	in
<b>g</b>	32.19	ft/s <sup>2</sup>
<b>Q</b>	5.99	cfs
<b>h</b>	2.29	
<b>H</b>	0.34	ft
<b>H/P</b>	0.50	-
<b>Cd</b>	0.561	-
<b>Cd<sub>emp</sub></b>	0.542	-
<b><math>\epsilon_{Cd-emp}</math></b>	<b>3.48%</b>	-

STAR CCM+ (fine mesh, $k-\omega$ )		
Cell count:		2,754,245
<b>P</b>	8.00	in
<b><math>\alpha</math></b>	16.00	deg
<b><math>\theta</math></b>	10.00	deg
<b>L</b>	122.95	in
<b>L</b>	10.25	ft
<b>tw</b>	1.00	in
<b>g</b>	32.19	ft/s <sup>2</sup>
<b>Q</b>	6.01	cfs
<b>h</b>	2.28	
<b>H</b>	0.33	ft
<b>H/P</b>	0.49	-
<b>Cd</b>	0.590	-
<b>Cd<sub>emp</sub></b>	0.551	-
<b><math>\epsilon_{Cd-emp}</math></b>	<b>7.08%</b>	-

time	h	H
45.00	2.29	0.34
45.15	2.29	0.34
45.30	2.29	0.34
45.45	2.29	0.34
45.60	2.29	0.34
45.75	2.29	0.34
45.90	2.29	0.34
46.05	2.29	0.34
46.20	2.29	0.34
46.35	2.29	0.34
46.50	2.29	0.34
46.65	2.29	0.34
46.80	2.29	0.34
46.95	2.29	0.34
47.10	2.29	0.34
47.25	2.29	0.34
47.40	2.29	0.34
47.55	2.29	0.34
47.70	2.29	0.34
47.85	2.29	0.34
48.00	2.29	0.34
48.15	2.29	0.34
48.30	2.29	0.34
48.45	2.29	0.34

time	h	H
45.00	2.28	0.33
45.15	2.28	0.33
45.30	2.28	0.33
45.45	2.28	0.33
45.60	2.28	0.33
45.75	2.28	0.33
45.90	2.28	0.33
46.05	2.28	0.33
46.20	2.28	0.33
46.35	2.28	0.33
46.50	2.28	0.33
46.65	2.28	0.33
46.80	2.28	0.33
46.95	2.28	0.33
47.10	2.28	0.33
47.25	2.28	0.33
47.40	2.28	0.33
47.55	2.28	0.33
47.70	2.28	0.33
47.85	2.28	0.33
48.00	2.28	0.33
48.15	2.28	0.33
48.30	2.28	0.33
48.45	2.28	0.33

48.60	2.29	0.34
48.75	2.29	0.34
48.90	2.29	0.34
49.05	2.29	0.34
49.20	2.29	0.34
49.35	2.29	0.34
49.50	2.29	0.34
49.65	2.29	0.34
49.80	2.29	0.34
49.95	2.29	0.34
50.10	2.29	0.34
50.25	2.29	0.34
50.40	2.29	0.34
50.55	2.29	0.34
50.70	2.29	0.34
50.85	2.29	0.34
51.00	2.29	0.34
51.15	2.29	0.34
51.30	2.29	0.34
51.45	2.29	0.34
51.60	2.29	0.34
51.75	2.29	0.34
51.90	2.29	0.34
52.05	2.29	0.34
52.20	2.29	0.34
52.35	2.29	0.34
52.50	2.29	0.34
52.65	2.29	0.34
52.80	2.29	0.34
52.95	2.29	0.34
53.10	2.29	0.34
53.25	2.29	0.34
53.40	2.29	0.34
53.55	2.29	0.34
53.70	2.29	0.34
53.85	2.29	0.34
54.00	2.29	0.34
54.15	2.29	0.34
54.30	2.29	0.34
54.45	2.29	0.34
54.60	2.29	0.34
54.75	2.29	0.34
54.90	2.29	0.34
55.05	2.29	0.34

48.60	2.28	0.33
48.75	2.28	0.33
48.90	2.28	0.33
49.05	2.28	0.33
49.20	2.28	0.33
49.35	2.28	0.33
49.50	2.28	0.33
49.65	2.28	0.33
49.80	2.28	0.33
49.95	2.28	0.33
50.10	2.28	0.33
50.25	2.28	0.33
50.40	2.28	0.33
50.55	2.28	0.33
50.70	2.28	0.33
50.85	2.28	0.33
51.00	2.28	0.33
51.15	2.28	0.33
51.30	2.28	0.33
51.45	2.28	0.33
51.60	2.28	0.33
51.75	2.28	0.33
51.90	2.28	0.33
52.05	2.28	0.33
52.20	2.28	0.33
52.35	2.28	0.33
52.50	2.28	0.33
52.65	2.28	0.33
52.80	2.28	0.33
52.95	2.28	0.33
53.10	2.28	0.33
53.25	2.28	0.33
53.40	2.28	0.33
53.55	2.28	0.33
53.70	2.28	0.33
53.85	2.28	0.33
54.00	2.28	0.33
54.15	2.28	0.33
54.30	2.28	0.33
54.45	2.28	0.33
54.60	2.28	0.33
54.75	2.28	0.33
54.90	2.28	0.33
55.05	2.28	0.33

55.20	2.29	0.34
55.35	2.29	0.34
55.50	2.29	0.34
55.65	2.29	0.34
55.80	2.29	0.34
55.95	2.29	0.34
56.10	2.29	0.34
56.25	2.29	0.34
56.40	2.29	0.34
56.55	2.29	0.34
56.70	2.29	0.34
56.85	2.29	0.34
57.00	2.29	0.34
57.15	2.29	0.34
57.30	2.29	0.34
57.45	2.29	0.34
57.60	2.29	0.34
57.75	2.29	0.34
57.90	2.29	0.34
58.05	2.29	0.34
58.20	2.29	0.34
58.35	2.29	0.34
58.50	2.29	0.34
58.65	2.29	0.34
58.80	2.29	0.34
58.95	2.29	0.34
59.10	2.29	0.34
59.25	2.29	0.34
59.40	2.29	0.34
59.55	2.29	0.34
59.70	2.29	0.34
59.85	2.29	0.34
60.00	2.29	0.34

55.20	2.28	0.33
55.35	2.28	0.33
55.50	2.28	0.33
55.65	2.28	0.33
55.80	2.28	0.33
55.95	2.28	0.33
56.10	2.28	0.33
56.25	2.28	0.33
56.40	2.28	0.33
56.55	2.28	0.33
56.70	2.28	0.33
56.85	2.28	0.33
57.00	2.28	0.33
57.15	2.28	0.33
57.30	2.28	0.33
57.45	2.28	0.33
57.60	2.28	0.33
57.75	2.28	0.33
57.90	2.28	0.33
58.05	2.28	0.33
58.20	2.28	0.33
58.35	2.28	0.33
58.50	2.28	0.33
58.65	2.28	0.33
58.80	2.28	0.33
58.95	2.28	0.33
59.10	2.28	0.33
59.25	2.28	0.33
59.40	2.28	0.33
59.55	2.28	0.33
59.70	2.28	0.33
59.85	2.28	0.33
60.00	2.28	0.33

Table C5 Tabulated time series data for  $\alpha = 16^\circ$ ;  $\theta = 10^\circ$  arced labyrinth weir at H/P = 0.5

FLOW-3D (coarse mesh)			FLOW-3D (medium mesh)			FLOW-3D (fine mesh)			FLOW-3D (fine mesh, 2nd order)		
Cell count:	346,668		Cell count:	680,064		Cell count:	3,306,877		Cell count:	3,306,877	
<b>P</b>	8.00	in	<b>P</b>	8.00	in	<b>P</b>	8.00	in	<b>P</b>	8.00	in
<b><math>\alpha</math></b>	16.00	deg	<b><math>\alpha</math></b>	16.00	deg	<b><math>\alpha</math></b>	16.00	deg	<b><math>\alpha</math></b>	16.00	deg
<b><math>\theta</math></b>	10.00	deg	<b><math>\theta</math></b>	10.00	deg	<b><math>\theta</math></b>	10.00	deg	<b><math>\theta</math></b>	10.00	deg
<b>L</b>	122.95	in	<b>L</b>	122.95	in	<b>L</b>	122.95	in	<b>L</b>	122.95	in
<b>L</b>	10.25	ft	<b>L</b>	10.25	ft	<b>L</b>	10.25	ft	<b>L</b>	10.25	ft
<b>tw</b>	1.00	in	<b>tw</b>	1.00	in	<b>tw</b>	1.00	in	<b>tw</b>	1.00	in
<b>g</b>	32.19	ft/s <sup>2</sup>	<b>g</b>	32.19	ft/s <sup>2</sup>	<b>g</b>	32.19	ft/s <sup>2</sup>	<b>g</b>	32.19	ft/s <sup>2</sup>
<b>Q</b>	5.92	cfs	<b>Q</b>	5.74	cfs	<b>Q</b>	5.67	cfs	<b>Q</b>	5.62	cfs
<b>h</b>	1.11		<b>h</b>	1.28		<b>h</b>	1.29		<b>h</b>	1.30	
<b>H</b>	0.16	ft	<b>H</b>	0.33	ft	<b>H</b>	0.33	ft	<b>H</b>	0.35	ft
<b>H/P</b>	0.24	-	<b>H/P</b>	0.49	-	<b>H/P</b>	0.49	-	<b>H/P</b>	0.52	-
<b>Cd</b>	1.726	-	<b>Cd</b>	0.559	-	<b>Cd</b>	0.547	-	<b>Cd</b>	0.500	-
<b>Cd<sub>emp</sub></b>	0.695	-	<b>Cd<sub>emp</sub></b>	0.549	-	<b>Cd<sub>emp</sub></b>	0.548	-	<b>Cd<sub>emp</sub></b>	0.533	-
<b><math>\varepsilon_{Cd-emp}</math></b>	148.43%	-	<b><math>\varepsilon_{Cd-emp}</math></b>	1.82%	-	<b><math>\varepsilon_{Cd-emp}</math></b>	-0.06%	-	<b><math>\varepsilon_{Cd-emp}</math></b>	-6.25%	-
time	h	H	time	h	H	time	h	H	time	h	H
0.00	1.29	0.33	0.00	1.29	0.33	0.00	1.29	0.33	0.00	1.29	0.33
0.60	1.30	0.34	0.60	1.29	0.34	0.60	1.29	0.34	0.60	1.29	0.34
1.20	1.36	0.40	1.20	1.33	0.37	1.20	1.33	0.37	1.20	1.33	0.37
1.80	1.38	0.42	1.80	1.36	0.40	1.80	1.36	0.40	1.80	1.36	0.40
2.40	1.37	0.42	2.40	1.37	0.41	2.40	1.37	0.41	2.40	1.37	0.41
3.00	1.34	0.39	3.00	1.32	0.36	3.00	1.32	0.36	3.00	1.32	0.36
3.60	1.20	0.24	3.60	1.31	0.35	3.60	1.31	0.35	3.60	1.31	0.35
4.20	1.37	0.41	4.20	1.31	0.35	4.20	1.31	0.35	4.20	1.31	0.35
4.80	1.18	0.23	4.80	1.27	0.31	4.80	1.27	0.32	4.80	1.28	0.32
5.40	1.21	0.26	5.40	1.30	0.34	5.40	1.30	0.34	5.40	1.30	0.34
6.00	1.12	0.16	6.00	1.29	0.33	6.00	1.27	0.31	6.00	1.24	0.29
6.60	1.29	0.33	6.60	1.29	0.33	6.60	1.31	0.35	6.60	1.33	0.37
7.20	1.30	0.34	7.20	1.29	0.33	7.20	1.29	0.33	7.20	1.28	0.32
7.80	1.16	0.20	7.80	1.31	0.35	7.80	1.32	0.37	7.80	1.32	0.37
8.40	1.25	0.29	8.40	1.32	0.36	8.40	1.33	0.37	8.40	1.35	0.39
9.00	1.35	0.39	9.00	1.32	0.37	9.00	1.29	0.34	9.00	1.27	0.32
9.60	1.11	0.16	9.60	1.30	0.34	9.60	1.33	0.38	9.60	1.34	0.39
10.20	1.25	0.30	10.20	1.29	0.33	10.20	1.28	0.33	10.20	1.25	0.29
10.80	1.14	0.18	10.80	1.27	0.32	10.80	1.29	0.34	10.80	1.31	0.36
11.40	1.11	0.15	11.40	1.29	0.34	11.40	1.29	0.34	11.40	1.29	0.33
12.00	1.37	0.41	12.00	1.33	0.37	12.00	1.30	0.35	12.00	1.33	0.37
12.60	1.14	0.18	12.60	1.26	0.30	12.60	1.25	0.30	12.60	1.26	0.31
13.20	1.10	0.15	13.20	1.30	0.34	13.20	1.31	0.35	13.20	1.35	0.39
13.80	1.18	0.22	13.80	1.30	0.34	13.80	1.29	0.33	13.80	1.31	0.36
14.40	1.16	0.21	14.40	1.29	0.34	14.40	1.32	0.36	14.40	1.32	0.37
15.00	1.16	0.21	15.00	1.33	0.37	15.00	1.31	0.35	15.00	1.29	0.33
15.60	1.27	0.31	15.60	1.31	0.35	15.60	1.30	0.34	15.60	1.28	0.33
16.20	1.14	0.18	16.20	1.27	0.31	16.20	1.29	0.33	16.20	1.36	0.40
16.80	1.10	0.14	16.80	1.30	0.34	16.80	1.30	0.34	16.80	1.29	0.33
17.40	1.20	0.24	17.40	1.30	0.34	17.40	1.28	0.33	17.40	1.33	0.37
18.00	1.10	0.15	18.00	1.29	0.34	18.00	1.29	0.34	18.00	1.31	0.36
18.60	1.15	0.20	18.60	1.28	0.33	18.60	1.27	0.32	18.60	1.26	0.31
19.20	1.14	0.18	19.20	1.27	0.32	19.20	1.29	0.33	19.20	1.27	0.32
19.80	1.08	0.12	19.80	1.29	0.33	19.80	1.29	0.33	19.80	1.40	0.44
20.40	1.13	0.18	20.40	1.31	0.35	20.40	1.30	0.35	20.40	1.23	0.28
21.00	1.18	0.22	21.00	1.30	0.34	21.00	1.31	0.35	21.00	1.34	0.38
21.60	1.15	0.19	21.60	1.30	0.34	21.60	1.30	0.34	21.60	1.29	0.34
22.20	1.13	0.17	22.20	1.28	0.33	22.20	1.28	0.33	22.20	1.26	0.30
22.80	1.14	0.18	22.80	1.30	0.34	22.80	1.31	0.35	22.80	1.27	0.31
23.40	1.10	0.15	23.40	1.29	0.33	23.40	1.29	0.34	23.40	1.34	0.38
24.00	1.14	0.19	24.00	1.29	0.33	24.00	1.29	0.34	24.00	1.33	0.38
24.60	1.13	0.17	24.60	1.28	0.33	24.60	1.28	0.33	24.60	1.30	0.34
25.20	1.11	0.16	25.20	1.28	0.33	25.20	1.29	0.33	25.20	1.33	0.37
25.80	1.12	0.16	25.80	1.27	0.32	25.80	1.28	0.33	25.80	1.24	0.28
26.40	1.11	0.15	26.40	1.31	0.35	26.40	1.30	0.34	26.40	1.30	0.34

27.00	1.10	0.14
27.60	1.14	0.18
28.20	1.13	0.17
28.80	1.11	0.15
29.40	1.12	0.16
30.00	1.11	0.15
30.60	1.11	0.15
31.20	1.13	0.17
31.80	1.11	0.16
32.40	1.10	0.15
33.00	1.12	0.16
33.60	1.10	0.14
34.20	1.12	0.16
34.80	1.11	0.15
35.40	1.11	0.16
36.00	1.10	0.15
36.60	1.11	0.16
37.20	1.11	0.16
37.80	1.11	0.15
38.40	1.12	0.16
39.00	1.10	0.15
39.60	1.11	0.15
40.20	1.11	0.15
40.80	1.11	0.16
41.40	1.11	0.15
42.00	1.11	0.15
42.60	1.10	0.14
43.20	1.11	0.15
43.80	1.12	0.16
44.40	1.10	0.14
45.00	1.11	0.15
45.60	1.10	0.15
46.20	1.11	0.15
46.80	1.12	0.17
47.40	1.11	0.15
48.00	1.09	0.14
48.60	1.11	0.15
49.20	1.10	0.15
49.80	1.11	0.15
50.40	1.11	0.15
51.00	1.11	0.15
51.60	1.11	0.15
52.20	1.10	0.14
52.80	1.11	0.15
53.40	1.11	0.15
54.00	1.11	0.16
54.60	1.12	0.16
55.20	1.13	0.18
55.80	1.12	0.16
56.40	1.12	0.16
57.00	1.13	0.17
57.60	1.13	0.17
58.20	1.13	0.17
58.80	1.12	0.16
59.40	1.13	0.17
60.00	1.13	0.17

27.00	1.29	0.33
27.60	1.29	0.33
28.20	1.28	0.32
28.80	1.30	0.34
29.40	1.29	0.33
30.00	1.29	0.34
30.60	1.28	0.33
31.20	1.28	0.32
31.80	1.28	0.33
32.40	1.29	0.33
33.00	1.29	0.33
33.60	1.29	0.33
34.20	1.28	0.32
34.80	1.29	0.33
35.40	1.29	0.33
36.00	1.29	0.33
36.60	1.28	0.33
37.20	1.28	0.32
37.80	1.28	0.33
38.40	1.29	0.33
39.00	1.28	0.33
39.60	1.28	0.33
40.20	1.28	0.33
40.80	1.28	0.33
41.40	1.29	0.33
42.00	1.29	0.33
42.60	1.28	0.33
43.20	1.28	0.33
43.80	1.29	0.33
44.40	1.28	0.33
45.00	1.28	0.33
45.60	1.28	0.33
46.20	1.28	0.33
46.80	1.28	0.33
47.40	1.28	0.33
48.00	1.28	0.33
48.60	1.28	0.33
49.20	1.28	0.33
49.80	1.29	0.33
50.40	1.28	0.33
51.00	1.28	0.33
51.60	1.28	0.33
52.20	1.28	0.33
52.80	1.28	0.33
53.40	1.28	0.33
54.00	1.28	0.33
54.60	1.28	0.33
55.20	1.28	0.33
55.80	1.28	0.33
56.40	1.28	0.33
57.00	1.29	0.33
57.60	1.28	0.33
58.20	1.28	0.33
58.80	1.28	0.33
59.40	1.28	0.33
60.00	1.28	0.33

27.00	1.29	0.33
27.60	1.29	0.34
28.20	1.29	0.33
28.80	1.29	0.33
29.40	1.29	0.33
30.00	1.29	0.34
30.60	1.28	0.33
31.20	1.28	0.33
31.80	1.29	0.33
32.40	1.29	0.33
33.00	1.29	0.33
33.60	1.29	0.33
34.20	1.28	0.33
34.80	1.29	0.34
35.40	1.29	0.33
36.00	1.28	0.33
36.60	1.29	0.33
37.20	1.29	0.33
37.80	1.29	0.33
38.40	1.29	0.33
39.00	1.29	0.33
39.60	1.29	0.33
40.20	1.29	0.33
40.80	1.28	0.33
41.40	1.29	0.33
42.00	1.28	0.33
42.60	1.29	0.33
43.20	1.28	0.33
43.80	1.29	0.33
44.40	1.29	0.33
45.00	1.29	0.33
45.60	1.28	0.33
46.20	1.29	0.33
46.80	1.29	0.33
47.40	1.29	0.33
48.00	1.29	0.33
48.60	1.29	0.33
49.20	1.28	0.33
49.80	1.29	0.33
50.40	1.28	0.33
51.00	1.29	0.33
51.60	1.29	0.33
52.20	1.29	0.33
52.80	1.29	0.33
53.40	1.29	0.33
54.00	1.28	0.33
54.60	1.29	0.33
55.20	1.28	0.33
55.80	1.29	0.33
56.40	1.29	0.33
57.00	1.29	0.33
57.60	1.28	0.33
58.20	1.29	0.33
58.80	1.29	0.33
59.40	1.29	0.33
60.00	1.29	0.33

27.00	1.32	0.37
27.60	1.36	0.40
28.20	1.20	0.24
28.80	1.39	0.44
29.40	1.28	0.32
30.00	1.33	0.37
30.60	1.35	0.40
31.20	1.22	0.26
31.80	1.29	0.33
32.40	1.26	0.31
33.00	1.37	0.41
33.60	1.30	0.34
34.20	1.26	0.30
34.80	1.30	0.34
35.40	1.22	0.26
36.00	1.42	0.46
36.60	1.24	0.29
37.20	1.37	0.41
37.80	1.26	0.31
38.40	1.24	0.28
39.00	1.36	0.40
39.60	1.30	0.35
40.20	1.32	0.37
40.80	1.33	0.37
41.40	1.25	0.29
42.00	1.35	0.40
42.60	1.21	0.25
43.20	1.19	0.23
43.80	1.39	0.44
44.40	1.22	0.27
45.00	1.28	0.33
45.60	1.24	0.29
46.20	1.29	0.33
46.80	1.37	0.41
47.40	1.28	0.32
48.00	1.34	0.38
48.60	1.25	0.29
49.20	1.35	0.39
49.80	1.29	0.33
50.40	1.35	0.39
51.00	1.27	0.31
51.60	1.22	0.27
52.20	1.26	0.31
52.80	1.40	0.45
53.40	1.20	0.24
54.00	1.36	0.40
54.60	1.30	0.34
55.20	1.28	0.32
55.80	1.30	0.34
56.40	1.42	0.46
57.00	1.27	0.31
57.60	1.30	0.35
58.20	1.24	0.28
58.80	1.35	0.40
59.40	1.32	0.36
60.00	1.36	0.40

Table C6 Tabulated time series data for  $\alpha = 16^\circ$ ;  $\theta = 10^\circ$  arced labyrinth weir at H/P = 0.5

FLOW -3D (fine mesh, 1 Eq.)		
Cell count:		3,306,877
P	8.00	in
$\alpha$	16.00	deg
$\theta$	10.00	deg
L	122.95	in
L	10.25	ft
tw	1.00	in
g	32.19	ft/s <sup>2</sup>
Q	5.61	cfs
h	1.31	
H	0.35	ft
H/P	0.53	-
Cd	0.494	-
Cd <sub>emp</sub>	0.532	-
$\epsilon_{Cd-emp}$	<b>-7.08%</b>	-

FLOW-3D (fine mesh, k- $\varepsilon$ )		
Cell count:		3,306,877
P	8.00	in
$\alpha$	16.00	deg
$\theta$	10.00	deg
L	122.95	in
L	10.25	ft
tw	1.00	in
g	32.19	ft/s <sup>2</sup>
Q	5.66	cfs
h	1.29	
H	0.33	ft
H/P	0.49	-
Cd	0.548	-
Cd <sub>emp</sub>	0.548	-
$\epsilon_{Cd-emp}$	<b>0.00%</b>	-

FLOW-3D (fine mesh, k- $\omega$ )		
Cell count:		3,306,877
P	8.00	in
$\alpha$	16.00	deg
$\theta$	10.00	deg
L	122.95	in
L	10.25	ft
tw	1.00	in
g	32.19	ft/s <sup>2</sup>
Q	5.62	cfs
h	1.28	
H	0.33	ft
H/P	0.49	-
Cd	0.547	-
Cd <sub>emp</sub>	0.549	-
$\epsilon_{Cd-emp}$	<b>-0.43%</b>	-

time	h	H
0.00	1.29	0.33
0.60	1.29	0.34
1.20	1.33	0.37
1.80	1.36	0.40
2.40	1.37	0.41
3.00	1.32	0.36
3.60	1.31	0.35
4.20	1.31	0.35
4.80	1.28	0.32
5.40	1.30	0.34
6.00	1.24	0.28
6.60	1.33	0.37
7.20	1.29	0.34
7.80	1.33	0.37
8.40	1.35	0.39
9.00	1.27	0.32
9.60	1.33	0.37
10.20	1.28	0.32
10.80	1.32	0.37
11.40	1.29	0.33
12.00	1.32	0.36
12.60	1.30	0.34
13.20	1.31	0.35
13.80	1.30	0.35
14.40	1.29	0.33

time	h	H
0.00	1.29	0.33
0.60	1.30	0.34
1.20	1.35	0.40
1.80	1.34	0.38
2.40	1.35	0.40
3.00	1.34	0.38
3.60	1.30	0.34
4.20	1.32	0.36
4.80	1.28	0.33
5.40	1.25	0.30
6.00	1.30	0.35
6.60	1.28	0.32
7.20	1.32	0.36
7.80	1.31	0.35
8.40	1.31	0.36
9.00	1.32	0.36
9.60	1.32	0.37
10.20	1.30	0.35
10.80	1.28	0.32
11.40	1.30	0.34
12.00	1.28	0.32
12.60	1.28	0.32
13.20	1.30	0.34
13.80	1.30	0.34
14.40	1.30	0.34

time	h	H
0.00	1.29	0.33
0.60	1.30	0.34
1.20	1.35	0.40
1.80	1.34	0.38
2.40	1.35	0.40
3.00	1.34	0.38
3.60	1.30	0.34
4.20	1.32	0.37
4.80	1.29	0.33
5.40	1.25	0.30
6.00	1.30	0.35
6.60	1.28	0.33
7.20	1.32	0.36
7.80	1.30	0.35
8.40	1.31	0.35
9.00	1.32	0.37
9.60	1.31	0.35
10.20	1.32	0.37
10.80	1.27	0.32
11.40	1.30	0.35
12.00	1.28	0.33
12.60	1.27	0.32
13.20	1.30	0.34
13.80	1.30	0.35
14.40	1.30	0.34

15.00	1.33	0.37
15.60	1.28	0.32
16.20	1.34	0.38
16.80	1.28	0.33
17.40	1.29	0.33
18.00	1.31	0.36
18.60	1.30	0.34
19.20	1.33	0.37
19.80	1.26	0.30
20.40	1.31	0.36
21.00	1.40	0.44
21.60	1.25	0.29
22.20	1.28	0.33
22.80	1.27	0.32
23.40	1.39	0.43
24.00	1.25	0.30
24.60	1.39	0.43
25.20	1.27	0.31
25.80	1.29	0.33
26.40	1.31	0.36
27.00	1.28	0.32
27.60	1.23	0.27
28.20	1.27	0.31
28.80	1.40	0.44
29.40	1.14	0.18
30.00	1.45	0.49
30.60	1.34	0.38
31.20	1.26	0.31
31.80	1.37	0.42
32.40	1.27	0.31
33.00	1.34	0.39
33.60	1.31	0.36
34.20	1.22	0.26
34.80	1.35	0.40
35.40	1.30	0.35
36.00	1.26	0.30
36.60	1.32	0.36
37.20	1.25	0.29
37.80	1.40	0.45
38.40	1.24	0.28
39.00	1.27	0.32
39.60	1.42	0.46
40.20	1.24	0.28
40.80	1.40	0.44
41.40	1.24	0.28

15.00	1.31	0.35
15.60	1.30	0.34
16.20	1.31	0.35
16.80	1.29	0.33
17.40	1.29	0.33
18.00	1.28	0.33
18.60	1.28	0.33
19.20	1.29	0.34
19.80	1.28	0.33
20.40	1.29	0.34
21.00	1.30	0.35
21.60	1.29	0.33
22.20	1.31	0.35
22.80	1.29	0.33
23.40	1.29	0.34
24.00	1.29	0.33
24.60	1.28	0.33
25.20	1.29	0.33
25.80	1.29	0.33
26.40	1.28	0.33
27.00	1.29	0.33
27.60	1.30	0.34
28.20	1.29	0.34
28.80	1.29	0.33
29.40	1.29	0.33
30.00	1.29	0.33
30.60	1.29	0.33
31.20	1.28	0.33
31.80	1.28	0.33
32.40	1.29	0.33
33.00	1.29	0.33
33.60	1.29	0.33
34.20	1.29	0.33
34.80	1.29	0.33
35.40	1.29	0.33
36.00	1.28	0.33
36.60	1.28	0.33
37.20	1.29	0.33
37.80	1.28	0.32
38.40	1.28	0.33
39.00	1.28	0.33
39.60	1.28	0.33
40.20	1.29	0.33
40.80	1.29	0.33
41.40	1.28	0.33

15.00	1.30	0.34
15.60	1.31	0.35
16.20	1.31	0.35
16.80	1.29	0.33
17.40	1.29	0.33
18.00	1.29	0.33
18.60	1.28	0.32
19.20	1.29	0.33
19.80	1.29	0.33
20.40	1.29	0.34
21.00	1.30	0.34
21.60	1.29	0.33
22.20	1.31	0.35
22.80	1.28	0.33
23.40	1.30	0.34
24.00	1.28	0.33
24.60	1.29	0.33
25.20	1.29	0.34
25.80	1.29	0.33
26.40	1.29	0.33
27.00	1.29	0.34
27.60	1.30	0.34
28.20	1.29	0.34
28.80	1.29	0.33
29.40	1.29	0.33
30.00	1.29	0.33
30.60	1.29	0.33
31.20	1.28	0.33
31.80	1.28	0.33
32.40	1.29	0.33
33.00	1.29	0.33
33.60	1.29	0.33
34.20	1.29	0.33
34.80	1.29	0.33
35.40	1.29	0.33
36.00	1.28	0.32
36.60	1.29	0.33
37.20	1.29	0.33
37.80	1.28	0.33
38.40	1.29	0.33
39.00	1.28	0.33
39.60	1.29	0.33
40.20	1.29	0.33
40.80	1.28	0.33
41.40	1.28	0.33

42.00	1.34	0.39
42.60	1.31	0.35
43.20	1.19	0.23
43.80	1.43	0.48
44.40	1.31	0.36
45.00	1.22	0.26
45.60	1.36	0.41
46.20	1.33	0.38
46.80	1.23	0.27
47.40	1.29	0.33
48.00	1.35	0.39
48.60	1.20	0.24
49.20	1.36	0.40
49.80	1.23	0.27
50.40	1.27	0.31
51.00	1.30	0.34
51.60	1.33	0.38
52.20	1.33	0.38
52.80	1.43	0.47
53.40	1.28	0.33
54.00	1.29	0.33
54.60	1.27	0.32
55.20	1.39	0.44
55.80	1.24	0.29
56.40	1.36	0.40
57.00	1.23	0.27
57.60	1.35	0.40
58.20	1.29	0.33
58.80	1.31	0.36
59.40	1.37	0.42
60.00	1.28	0.33

42.00	1.29	0.33
42.60	1.28	0.33
43.20	1.28	0.33
43.80	1.29	0.33
44.40	1.29	0.33
45.00	1.28	0.33
45.60	1.29	0.33
46.20	1.28	0.33
46.80	1.29	0.33
47.40	1.29	0.33
48.00	1.28	0.33
48.60	1.29	0.33
49.20	1.29	0.33
49.80	1.29	0.33
50.40	1.29	0.33
51.00	1.28	0.33
51.60	1.29	0.33
52.20	1.29	0.33
52.80	1.28	0.33
53.40	1.29	0.33
54.00	1.29	0.33
54.60	1.28	0.33
55.20	1.29	0.33
55.80	1.29	0.33
56.40	1.28	0.33
57.00	1.29	0.33
57.60	1.28	0.33
58.20	1.28	0.33
58.80	1.29	0.33
59.40	1.28	0.33
60.00	1.28	0.33

42.00	1.29	0.33
42.60	1.28	0.33
43.20	1.28	0.33
43.80	1.28	0.33
44.40	1.28	0.33
45.00	1.28	0.33
45.60	1.28	0.33
46.20	1.28	0.33
46.80	1.29	0.33
47.40	1.28	0.33
48.00	1.28	0.33
48.60	1.29	0.33
49.20	1.28	0.33
49.80	1.28	0.33
50.40	1.28	0.33
51.00	1.28	0.33
51.60	1.29	0.33
52.20	1.28	0.33
52.80	1.28	0.33
53.40	1.28	0.33
54.00	1.29	0.33
54.60	1.28	0.33
55.20	1.28	0.33
55.80	1.28	0.33
56.40	1.28	0.33
57.00	1.28	0.33
57.60	1.28	0.33
58.20	1.28	0.33
58.80	1.29	0.33
59.40	1.28	0.33
60.00	1.28	0.33

Table C7 Tabulated time series data for  $\alpha = 16^\circ$ ;  $\theta = 10^\circ$  arced labyrinth weir at H/P = 0.7

STAR CCM+ (coarse mesh)		
Cell count:	440,955	
<b>P</b>	8.00	in
<b><math>\alpha</math></b>	16.00	deg
<b><math>\theta</math></b>	10.00	deg
<b>L</b>	122.95	in
<b>L</b>	10.25	ft
<b>tw</b>	1.00	in
<b>g</b>	32.19	ft/s <sup>2</sup>
<b>Q</b>	8.24	cfs
<b>h</b>	2.43	
<b>H</b>	0.47	ft
<b>H/P</b>	0.70	-
<b>Cd</b>	0.468	-
<b>Cd<sub>emp</sub></b>	0.459	-
<b><math>\epsilon_{Cd-emp}</math></b>	<b>1.88%</b>	-

STAR CCM+ (medium mesh)		
Cell count:	1,027,961	
<b>P</b>	8.00	in
<b><math>\alpha</math></b>	16.00	deg
<b><math>\theta</math></b>	10.00	deg
<b>L</b>	122.95	in
<b>L</b>	10.25	ft
<b>tw</b>	1.00	in
<b>g</b>	32.19	ft/s <sup>2</sup>
<b>Q</b>	8.06	cfs
<b>h</b>	2.40	
<b>H</b>	0.44	ft
<b>H/P</b>	0.66	-
<b>Cd</b>	0.501	-
<b>Cd<sub>emp</sub></b>	0.473	-
<b><math>\epsilon_{Cd-emp}</math></b>	<b>5.90%</b>	-

STAR CCM+ (fine mesh)		
Cell count:	2,754,245	
<b>P</b>	8.00	in
<b><math>\alpha</math></b>	16.00	deg
<b><math>\theta</math></b>	10.00	deg
<b>L</b>	122.95	in
<b>L</b>	10.25	ft
<b>tw</b>	1.00	in
<b>g</b>	32.19	ft/s <sup>2</sup>
<b>Q</b>	8.39	cfs
<b>h</b>	2.38	
<b>H</b>	0.43	ft
<b>H/P</b>	0.64	-
<b>Cd</b>	0.549	-
<b>Cd<sub>emp</sub></b>	0.481	-
<b><math>\epsilon_{Cd-emp}</math></b>	<b>14.12%</b>	-

time	h	H
45.00	2.43	0.48
45.15	2.44	0.48
45.30	2.44	0.48
45.45	2.44	0.48
45.60	2.44	0.48
45.75	2.44	0.48
45.90	2.44	0.48
46.05	2.44	0.48
46.20	2.43	0.48
46.35	2.43	0.48
46.50	2.43	0.48
46.65	2.43	0.48
46.80	2.43	0.48
46.95	2.43	0.47
47.10	2.43	0.47
47.25	2.43	0.47
47.40	2.43	0.48
47.55	2.43	0.48
47.70	2.43	0.48
47.85	2.43	0.48
48.00	2.43	0.48
48.15	2.44	0.48
48.30	2.44	0.48
48.45	2.44	0.48
48.60	2.44	0.48
48.75	2.44	0.48
48.90	2.44	0.48
49.05	2.44	0.48

time	h	H
45.00	2.41	0.45
45.15	2.41	0.45
45.30	2.41	0.45
45.45	2.41	0.45
45.60	2.41	0.45
45.75	2.41	0.45
45.90	2.41	0.45
46.05	2.41	0.45
46.20	2.41	0.45
46.35	2.41	0.45
46.50	2.41	0.45
46.65	2.41	0.45
46.80	2.41	0.45
46.95	2.40	0.45
47.10	2.40	0.45
47.25	2.40	0.45
47.40	2.40	0.45
47.55	2.40	0.45
47.70	2.40	0.45
47.85	2.40	0.45
48.00	2.40	0.45
48.15	2.40	0.45
48.30	2.40	0.45
48.45	2.40	0.45
48.60	2.40	0.45
48.75	2.40	0.45
48.90	2.40	0.45
49.05	2.40	0.45

time	h	H
45.00	2.38	0.43
45.15	2.38	0.43
45.30	2.38	0.43
45.45	2.38	0.43
45.60	2.38	0.43
45.75	2.38	0.43
45.90	2.38	0.43
46.05	2.38	0.43
46.20	2.38	0.43
46.35	2.38	0.43
46.50	2.38	0.43
46.65	2.38	0.43
46.80	2.38	0.43
46.95	2.38	0.43
47.10	2.38	0.43
47.25	2.38	0.43
47.40	2.38	0.43
47.55	2.38	0.43
47.70	2.38	0.43
47.85	2.38	0.43
48.00	2.38	0.43
48.15	2.38	0.43
48.30	2.38	0.43
48.45	2.38	0.43
48.60	2.38	0.43
48.75	2.38	0.43
48.90	2.38	0.43
49.05	2.38	0.43

49.20	2.44	0.48
49.35	2.44	0.48
49.50	2.44	0.48
49.65	2.44	0.48
49.80	2.44	0.48
49.95	2.44	0.48
50.10	2.44	0.48
50.25	2.44	0.48
50.40	2.44	0.48
50.55	2.44	0.48
50.70	2.44	0.48
50.85	2.44	0.48
51.00	2.44	0.48
51.15	2.44	0.48
51.30	2.43	0.48
51.45	2.43	0.48
51.60	2.43	0.48
51.75	2.43	0.47
51.90	2.43	0.47
52.05	2.43	0.47
52.20	2.43	0.47
52.35	2.43	0.47
52.50	2.42	0.47
52.65	2.42	0.47
52.80	2.42	0.47
52.95	2.42	0.46
53.10	2.42	0.46
53.25	2.42	0.46
53.40	2.42	0.46
53.55	2.42	0.46
53.70	2.42	0.46
53.85	2.42	0.46
54.00	2.41	0.46
54.15	2.41	0.46
54.30	2.41	0.46
54.45	2.41	0.46
54.60	2.41	0.46
54.75	2.41	0.45
54.90	2.41	0.45
55.05	2.41	0.45
55.20	2.41	0.45
55.35	2.41	0.45
55.50	2.41	0.45
55.65	2.41	0.45
55.80	2.41	0.45
55.95	2.41	0.45
56.10	2.41	0.45
56.25	2.41	0.45
56.40	2.41	0.45

49.20	2.40	0.44
49.35	2.40	0.44
49.50	2.40	0.44
49.65	2.40	0.44
49.80	2.40	0.44
49.95	2.40	0.44
50.10	2.40	0.44
50.25	2.40	0.44
50.40	2.40	0.44
50.55	2.40	0.44
50.70	2.40	0.44
50.85	2.40	0.44
51.00	2.40	0.44
51.15	2.40	0.44
51.30	2.40	0.44
51.45	2.40	0.44
51.60	2.40	0.44
51.75	2.40	0.44
51.90	2.40	0.44
52.05	2.40	0.44
52.20	2.40	0.44
52.35	2.40	0.44
52.50	2.40	0.44
52.65	2.40	0.44
52.80	2.40	0.44
52.95	2.40	0.44
53.10	2.40	0.44
53.25	2.40	0.44
53.40	2.40	0.44
53.55	2.40	0.44
53.70	2.40	0.44
53.85	2.40	0.44
54.00	2.40	0.44
54.15	2.40	0.44
54.30	2.39	0.44
54.45	2.39	0.44
54.60	2.39	0.44
54.75	2.39	0.44
54.90	2.39	0.44
55.05	2.39	0.44
55.20	2.39	0.44
55.35	2.39	0.44
55.50	2.39	0.44
55.65	2.39	0.44
55.80	2.39	0.44
55.95	2.39	0.44
56.10	2.39	0.44
56.25	2.39	0.44
56.40	2.39	0.44

49.20	2.38	0.43
49.35	2.38	0.43
49.50	2.38	0.43
49.65	2.38	0.43
49.80	2.38	0.43
49.95	2.38	0.43
50.10	2.38	0.43
50.25	2.38	0.43
50.40	2.38	0.43
50.55	2.38	0.43
50.70	2.38	0.43
50.85	2.38	0.43
51.00	2.38	0.43
51.15	2.38	0.43
51.30	2.38	0.43
51.45	2.38	0.43
51.60	2.38	0.43
51.75	2.38	0.43
51.90	2.38	0.43
52.05	2.38	0.43
52.20	2.38	0.43
52.35	2.38	0.43
52.50	2.38	0.43
52.65	2.38	0.43
52.80	2.38	0.43
52.95	2.38	0.43
53.10	2.38	0.43
53.25	2.38	0.43
53.40	2.38	0.43
53.55	2.38	0.43
53.70	2.38	0.43
53.85	2.38	0.43
54.00	2.38	0.43
54.15	2.38	0.43
54.30	2.38	0.43
54.45	2.38	0.43
54.60	2.38	0.43
54.75	2.38	0.43
54.90	2.38	0.43
55.05	2.38	0.43
55.20	2.38	0.43
55.35	2.38	0.43
55.50	2.38	0.43
55.65	2.38	0.43
55.80	2.38	0.43
55.95	2.38	0.43
56.10	2.38	0.43
56.25	2.38	0.43
56.40	2.38	0.43

56.55	2.41	0.45
56.70	2.41	0.45
56.85	2.41	0.45
57.00	2.41	0.46
57.15	2.41	0.46
57.30	2.41	0.46
57.45	2.41	0.46
57.60	2.42	0.46
57.75	2.42	0.46
57.90	2.42	0.46
58.05	2.42	0.46
58.20	2.42	0.46
58.35	2.42	0.46
58.50	2.42	0.46
58.65	2.42	0.46
58.80	2.42	0.47
58.95	2.42	0.47
59.10	2.42	0.47
59.25	2.42	0.47
59.40	2.42	0.47
59.55	2.42	0.47
59.70	2.42	0.47
59.85	2.42	0.47
60.00	2.42	0.47

56.55	2.39	0.44
56.70	2.39	0.44
56.85	2.39	0.44
57.00	2.39	0.44
57.15	2.39	0.44
57.30	2.39	0.44
57.45	2.39	0.44
57.60	2.39	0.44
57.75	2.39	0.44
57.90	2.39	0.44
58.05	2.39	0.44
58.20	2.39	0.44
58.35	2.39	0.44
58.50	2.39	0.44
58.65	2.39	0.44
58.80	2.39	0.44
58.95	2.39	0.44
59.10	2.39	0.44
59.25	2.39	0.44
59.40	2.39	0.44
59.55	2.40	0.44
59.70	2.40	0.44
59.85	2.40	0.44
60.00	2.40	0.44

56.55	2.38	0.43
56.70	2.38	0.43
56.85	2.38	0.43
57.00	2.38	0.43
57.15	2.38	0.43
57.30	2.38	0.43
57.45	2.38	0.43
57.60	2.38	0.43
57.75	2.38	0.43
57.90	2.38	0.43
58.05	2.38	0.43
58.20	2.38	0.43
58.35	2.38	0.43
58.50	2.38	0.43
58.65	2.38	0.43
58.80	2.38	0.43
58.95	2.38	0.43
59.10	2.38	0.43
59.25	2.38	0.43
59.40	2.38	0.43
59.55	2.38	0.43
59.70	2.38	0.43
59.85	2.38	0.43
60.00	2.38	0.43

Table C8 Tabulated time series data for  $\alpha = 16^\circ$ ;  $\theta = 10^\circ$  arced labyrinth weir at H/P = 0.7

FLOW-3D (coarse mesh)		
Cell count:	346,668	
<b>P</b>	8.00	in
<b><math>\alpha</math></b>	16.00	deg
<b><math>\theta</math></b>	10.00	deg
<b>L</b>	122.95	in
<b>L</b>	10.25	ft
<b>tw</b>	1.00	in
<b>g</b>	32.19	ft/s <sup>2</sup>
<b>Q</b>	8.02	cfs
<b>h</b>	1.23	
<b>H</b>	0.27	ft
<b>H/P</b>	0.40	-
<b>Cd</b>	1.045	-
<b>Cd<sub>emp</sub></b>	0.599	-
<b><math>\epsilon_{Cd-emp}</math></b>	<b>74.53%</b>	-

FLOW-3D (medium mesh)		
Cell count:	680,064	
<b>P</b>	8.00	in
<b><math>\alpha</math></b>	16.00	deg
<b><math>\theta</math></b>	10.00	deg
<b>L</b>	122.95	in
<b>L</b>	10.25	ft
<b>tw</b>	1.00	in
<b>g</b>	32.19	ft/s <sup>2</sup>
<b>Q</b>	7.94	cfs
<b>h</b>	1.40	
<b>H</b>	0.45	ft
<b>H/P</b>	0.67	-
<b>Cd</b>	0.488	-
<b>Cd<sub>emp</sub></b>	0.471	-
<b><math>\epsilon_{Cd-emp}</math></b>	<b>3.53%</b>	-

FLOW-3D (fine mesh)		
Cell count:	3,306,877	
<b>P</b>	8.00	in
<b><math>\alpha</math></b>	16.00	deg
<b><math>\theta</math></b>	10.00	deg
<b>L</b>	122.95	in
<b>L</b>	10.25	ft
<b>tw</b>	1.00	in
<b>g</b>	32.19	ft/s <sup>2</sup>
<b>Q</b>	7.87	cfs
<b>h</b>	1.40	
<b>H</b>	0.45	ft
<b>H/P</b>	0.67	-
<b>Cd</b>	0.484	-
<b>Cd<sub>emp</sub></b>	0.471	-
<b><math>\epsilon_{Cd-emp}</math></b>	<b>2.62%</b>	-

time	h	H
0.00	1.42	0.47
0.60	1.43	0.47
1.20	1.48	0.52
1.80	1.50	0.54
2.40	1.48	0.53
3.00	1.42	0.46
3.60	1.40	0.44
4.20	1.38	0.42
4.80	1.32	0.36
5.40	1.33	0.37
6.00	1.37	0.41
6.60	1.39	0.44
7.20	1.29	0.33
7.80	1.37	0.41
8.40	1.34	0.38
9.00	1.37	0.41
9.60	1.46	0.51
10.20	1.27	0.32
10.80	1.31	0.35
11.40	1.29	0.33
12.00	1.27	0.32
12.60	1.35	0.40
13.20	1.30	0.34
13.80	1.29	0.33
14.40	1.30	0.34
15.00	1.32	0.36

time	h	H
0.00	1.42	0.47
0.60	1.43	0.47
1.20	1.48	0.52
1.80	1.50	0.54
2.40	1.50	0.54
3.00	1.44	0.48
3.60	1.45	0.49
4.20	1.43	0.48
4.80	1.38	0.42
5.40	1.41	0.46
6.00	1.42	0.46
6.60	1.42	0.47
7.20	1.42	0.46
7.80	1.43	0.48
8.40	1.46	0.50
9.00	1.44	0.48
9.60	1.43	0.47
10.20	1.40	0.44
10.80	1.40	0.44
11.40	1.43	0.48
12.00	1.41	0.45
12.60	1.40	0.44
13.20	1.42	0.47
13.80	1.43	0.47
14.40	1.43	0.48
15.00	1.43	0.47

time	h	H
0.00	1.43	0.47
0.60	1.43	0.47
1.20	1.48	0.52
1.80	1.50	0.54
2.40	1.50	0.54
3.00	1.44	0.48
3.60	1.45	0.49
4.20	1.43	0.48
4.80	1.38	0.42
5.40	1.41	0.46
6.00	1.42	0.46
6.60	1.43	0.47
7.20	1.42	0.46
7.80	1.44	0.48
8.40	1.46	0.50
9.00	1.43	0.47
9.60	1.43	0.48
10.20	1.41	0.46
10.80	1.38	0.42
11.40	1.43	0.47
12.00	1.41	0.45
12.60	1.40	0.45
13.20	1.43	0.48
13.80	1.44	0.48
14.40	1.43	0.47
15.00	1.43	0.48

15.60	1.34	0.39
16.20	1.24	0.28
16.80	1.32	0.37
17.40	1.21	0.25
18.00	1.27	0.31
18.60	1.35	0.40
19.20	1.18	0.22
19.80	1.32	0.36
20.40	1.21	0.26
21.00	1.27	0.31
21.60	1.33	0.37
22.20	1.30	0.34
22.80	1.18	0.22
23.40	1.26	0.31
24.00	1.26	0.31
24.60	1.30	0.34
25.20	1.14	0.18
25.80	1.32	0.36
26.40	1.15	0.19
27.00	1.29	0.33
27.60	1.39	0.44
28.20	1.14	0.19
28.80	1.23	0.27
29.40	1.26	0.30
30.00	1.24	0.29
30.60	1.30	0.35
31.20	1.18	0.22
31.80	1.17	0.21
32.40	1.27	0.31
33.00	1.26	0.30
33.60	1.23	0.27
34.20	1.29	0.33
34.80	1.19	0.24
35.40	1.18	0.22
36.00	1.35	0.40
36.60	1.20	0.24
37.20	1.19	0.23
37.80	1.30	0.34
38.40	1.09	0.14
39.00	1.29	0.33
39.60	1.34	0.38
40.20	1.10	0.14
40.80	1.25	0.29
41.40	1.25	0.29
42.00	1.21	0.25
42.60	1.28	0.33
43.20	1.22	0.26

15.60	1.41	0.45
16.20	1.41	0.46
16.80	1.41	0.46
17.40	1.42	0.46
18.00	1.40	0.44
18.60	1.41	0.45
19.20	1.41	0.45
19.80	1.41	0.46
20.40	1.43	0.47
21.00	1.41	0.46
21.60	1.41	0.45
22.20	1.40	0.44
22.80	1.43	0.47
23.40	1.39	0.44
24.00	1.40	0.45
24.60	1.40	0.45
25.20	1.40	0.45
25.80	1.42	0.46
26.40	1.41	0.45
27.00	1.40	0.44
27.60	1.41	0.45
28.20	1.41	0.45
28.80	1.41	0.45
29.40	1.41	0.45
30.00	1.40	0.44
30.60	1.40	0.44
31.20	1.41	0.45
31.80	1.41	0.45
32.40	1.41	0.45
33.00	1.40	0.44
33.60	1.41	0.45
34.20	1.41	0.45
34.80	1.41	0.45
35.40	1.40	0.44
36.00	1.40	0.44
36.60	1.40	0.44
37.20	1.41	0.45
37.80	1.40	0.44
38.40	1.41	0.45
39.00	1.40	0.44
39.60	1.40	0.45
40.20	1.40	0.45
40.80	1.41	0.45
41.40	1.40	0.44
42.00	1.40	0.45
42.60	1.40	0.44
43.20	1.41	0.45

15.60	1.40	0.44
16.20	1.43	0.47
16.80	1.40	0.44
17.40	1.42	0.47
18.00	1.40	0.44
18.60	1.40	0.45
19.20	1.41	0.45
19.80	1.42	0.46
20.40	1.42	0.46
21.00	1.42	0.46
21.60	1.40	0.45
22.20	1.41	0.45
22.80	1.43	0.47
23.40	1.39	0.44
24.00	1.41	0.45
24.60	1.40	0.44
25.20	1.41	0.45
25.80	1.41	0.46
26.40	1.41	0.45
27.00	1.41	0.45
27.60	1.41	0.45
28.20	1.41	0.45
28.80	1.41	0.45
29.40	1.41	0.45
30.00	1.40	0.44
30.60	1.40	0.44
31.20	1.40	0.45
31.80	1.41	0.45
32.40	1.40	0.45
33.00	1.40	0.44
33.60	1.41	0.45
34.20	1.41	0.45
34.80	1.41	0.45
35.40	1.40	0.44
36.00	1.40	0.44
36.60	1.40	0.44
37.20	1.41	0.45
37.80	1.40	0.44
38.40	1.41	0.45
39.00	1.40	0.44
39.60	1.41	0.45
40.20	1.40	0.45
40.80	1.40	0.45
41.40	1.40	0.44
42.00	1.40	0.44
42.60	1.40	0.44
43.20	1.41	0.45

43.80	1.13	0.17
44.40	1.31	0.36
45.00	1.20	0.24
45.60	1.22	0.26
46.20	1.29	0.33
46.80	1.11	0.16
47.40	1.25	0.30
48.00	1.31	0.35
48.60	1.11	0.16
49.20	1.38	0.42
49.80	1.16	0.20
50.40	1.08	0.13
51.00	1.40	0.44
51.60	1.22	0.26
52.20	1.13	0.18
52.80	1.33	0.37
53.40	1.13	0.18
54.00	1.24	0.28
54.60	1.33	0.37
55.20	1.13	0.17
55.80	1.23	0.27
56.40	1.26	0.30
57.00	1.18	0.22
57.60	1.29	0.33
58.20	1.22	0.26
58.80	1.14	0.18
59.40	1.30	0.35
60.00	1.24	0.28

43.80	1.40	0.44
44.40	1.40	0.44
45.00	1.40	0.44
45.60	1.41	0.45
46.20	1.40	0.44
46.80	1.40	0.45
47.40	1.40	0.44
48.00	1.40	0.45
48.60	1.40	0.44
49.20	1.40	0.45
49.80	1.40	0.44
50.40	1.40	0.45
51.00	1.40	0.44
51.60	1.40	0.45
52.20	1.40	0.45
52.80	1.40	0.45
53.40	1.40	0.44
54.00	1.40	0.44
54.60	1.40	0.45
55.20	1.40	0.45
55.80	1.40	0.44
56.40	1.40	0.44
57.00	1.40	0.44
57.60	1.40	0.45
58.20	1.40	0.45
58.80	1.40	0.44
59.40	1.40	0.45
60.00	1.40	0.45

43.80	1.40	0.44
44.40	1.40	0.44
45.00	1.40	0.44
45.60	1.41	0.45
46.20	1.40	0.44
46.80	1.40	0.45
47.40	1.40	0.44
48.00	1.40	0.45
48.60	1.40	0.45
49.20	1.40	0.44
49.80	1.40	0.44
50.40	1.40	0.45
51.00	1.40	0.44
51.60	1.40	0.45
52.20	1.40	0.44
52.80	1.40	0.45
53.40	1.40	0.44
54.00	1.40	0.45
54.60	1.40	0.45
55.20	1.40	0.45
55.80	1.40	0.44
56.40	1.40	0.44
57.00	1.40	0.44
57.60	1.40	0.45
58.20	1.40	0.45
58.80	1.40	0.44
59.40	1.40	0.44
60.00	1.40	0.45

Table C9 Tabulated time series data for  $\alpha = 16^\circ$ ;  $\theta = 10^\circ$  arced labyrinth weir at H/P = 0.8

STAR CCM+ (fine mesh)		
Cell count:	2,754,245	
<b>P</b>	8.00	in
<b><math>\alpha</math></b>	16.00	deg
<b><math>\theta</math></b>	10.00	deg
<b>L</b>	122.95	in
<b>L</b>	10.25	ft
<b>tw</b>	1.00	in
<b>g</b>	32.19	ft/s <sup>2</sup>
<b>Q</b>	9.42	cfs
<b>h</b>	2.45	
<b>H</b>	0.49	ft
<b>H/P</b>	0.74	-
<b>Cd</b>	0.498	-
<b>Cd<sub>emp</sub></b>	0.449	-
<b><math>\epsilon_{Cd-emp}</math></b>	<b>10.97%</b>	-

FLOW-3D (fine mesh)		
Cell count:	3,306,877	
<b>P</b>	8.00	in
<b><math>\alpha</math></b>	16.00	deg
<b><math>\theta</math></b>	10.00	deg
<b>L</b>	122.95	in
<b>L</b>	10.25	ft
<b>tw</b>	1.00	in
<b>g</b>	32.19	ft/s <sup>2</sup>
<b>Q</b>	8.79	cfs
<b>h</b>	1.46	
<b>H</b>	0.50	ft
<b>H/P</b>	0.75	-
<b>Cd</b>	0.451	-
<b>Cd<sub>emp</sub></b>	0.445	-
<b><math>\epsilon_{Cd-emp}</math></b>	<b>1.34%</b>	-

time	h	H
45.00	2.45	0.45
45.15	2.45	0.45
45.30	2.45	0.45
45.45	2.45	0.45
45.60	2.45	0.45
45.75	2.45	0.45
45.90	2.45	0.45
46.05	2.45	0.45
46.20	2.45	0.45
46.35	2.45	0.45
46.50	2.45	0.45
46.65	2.45	0.45
46.80	2.45	0.45
46.95	2.45	0.45
47.10	2.45	0.45
47.25	2.45	0.45
47.40	2.45	0.45
47.55	2.45	0.45
47.70	2.45	0.45
47.85	2.45	0.45
48.00	2.45	0.45
48.15	2.45	0.45
48.30	2.45	0.45
48.45	2.45	0.45

time	h	H
0.00	1.41	0.45
0.60	1.41	0.45
1.20	1.42	0.47
1.80	1.42	0.46
2.40	1.42	0.46
3.00	1.42	0.47
3.60	1.42	0.46
4.20	1.42	0.47
4.80	1.42	0.46
5.40	1.42	0.47
6.00	1.43	0.47
6.60	1.44	0.48
7.20	1.44	0.48
7.80	1.43	0.48
8.40	1.44	0.48
9.00	1.44	0.48
9.60	1.44	0.48
10.20	1.44	0.48
10.80	1.44	0.48
11.40	1.44	0.48
12.00	1.44	0.49
12.60	1.45	0.49
13.20	1.44	0.49
13.80	1.45	0.49

48.60	2.45	0.45
48.75	2.45	0.45
48.90	2.45	0.45
49.05	2.45	0.45
49.20	2.45	0.45
49.35	2.45	0.45
49.50	2.45	0.45
49.65	2.45	0.45
49.80	2.45	0.45
49.95	2.45	0.45
50.10	2.45	0.45
50.25	2.45	0.45
50.40	2.45	0.45
50.55	2.45	0.45
50.70	2.45	0.45
50.85	2.45	0.45
51.00	2.45	0.45
51.15	2.45	0.45
51.30	2.45	0.45
51.45	2.45	0.45
51.60	2.44	0.44
51.75	2.45	0.45
51.90	2.45	0.45
52.05	2.45	0.45
52.20	2.45	0.45
52.35	2.45	0.45
52.50	2.45	0.45
52.65	2.45	0.45
52.80	2.45	0.45
52.95	2.45	0.45
53.10	2.45	0.45
53.25	2.45	0.45
53.40	2.45	0.45
53.55	2.45	0.45
53.70	2.45	0.45
53.85	2.45	0.45
54.00	2.45	0.45
54.15	2.44	0.44
54.30	2.45	0.45
54.45	2.45	0.45
54.60	2.45	0.45
54.75	2.45	0.45
54.90	2.45	0.45
55.05	2.45	0.45

14.40	1.45	0.49
15.00	1.45	0.49
15.60	1.45	0.49
16.20	1.44	0.49
16.80	1.44	0.49
17.40	1.45	0.49
18.00	1.45	0.49
18.60	1.45	0.49
19.20	1.45	0.49
19.80	1.45	0.49
20.40	1.45	0.50
21.00	1.45	0.50
21.60	1.45	0.50
22.20	1.45	0.50
22.80	1.45	0.50
23.40	1.45	0.50
24.00	1.45	0.50
24.60	1.45	0.50
25.20	1.45	0.50
25.80	1.45	0.50
26.40	1.46	0.50
27.00	1.46	0.50
27.60	1.45	0.50
28.20	1.46	0.50
28.80	1.46	0.50
29.40	1.46	0.50
30.00	1.46	0.50
30.60	1.45	0.50
31.20	1.46	0.50
31.80	1.46	0.50
32.40	1.46	0.50
33.00	1.46	0.50
33.60	1.46	0.50
34.20	1.46	0.50
34.80	1.46	0.50
35.40	1.46	0.50
36.00	1.46	0.50
36.60	1.46	0.50
37.20	1.46	0.50
37.80	1.46	0.50
38.40	1.46	0.50
39.00	1.46	0.50
39.60	1.46	0.50
40.20	1.46	0.50

55.20	2.45	0.45
55.35	2.44	0.44
55.50	2.45	0.45
55.65	2.44	0.44
55.80	2.45	0.45
55.95	2.45	0.45
56.10	2.45	0.45
56.25	2.45	0.45
56.40	2.45	0.45
56.55	2.45	0.45
56.70	2.45	0.45
56.85	2.45	0.45
57.00	2.45	0.45
57.15	2.45	0.45
57.30	2.46	0.46
57.45	2.46	0.46
57.60	2.45	0.45
57.75	2.46	0.46
57.90	2.45	0.45
58.05	2.46	0.46
58.20	2.45	0.45
58.35	2.45	0.45
58.50	2.46	0.46
58.65	2.46	0.46
58.80	2.46	0.46
58.95	2.45	0.45
59.10	2.45	0.45
59.25	2.46	0.46
59.40	2.45	0.45
59.55	2.46	0.46
59.70	2.45	0.45
59.85	2.46	0.46
60.00	2.45	0.45

40.80	1.46	0.50
41.40	1.46	0.50
42.00	1.46	0.50
42.60	1.46	0.50
43.20	1.46	0.50
43.80	1.46	0.50
44.40	1.46	0.50
45.00	1.46	0.50
45.60	1.46	0.50
46.20	1.46	0.50
46.80	1.46	0.50
47.40	1.46	0.50
48.00	1.46	0.50
48.60	1.46	0.50
49.20	1.46	0.50
49.80	1.46	0.50
50.40	1.46	0.50
51.00	1.46	0.50
51.60	1.46	0.50
52.20	1.46	0.50
52.80	1.46	0.50
53.40	1.46	0.50
54.00	1.46	0.50
54.60	1.46	0.50
55.20	1.46	0.50
55.80	1.46	0.50
56.40	1.46	0.50
57.00	1.46	0.50
57.60	1.46	0.50
58.20	1.46	0.50
58.80	1.46	0.50
59.40	1.46	0.50
60.00	1.46	0.50

Table C10 Tabulated time series data for  $\alpha = 20^\circ$ ;  $\theta = 30^\circ$  arced labyrinth weir at H/P = 0.3

STAR CCM+ (coarse mesh)		
Cell count:	250,089	
P	8.00	in
$\alpha$	20.00	deg
$\theta$	30.00	deg
L	202.71	in
L	16.89	ft
tw	1.00	in
g	32.19	ft/s <sup>2</sup>
Q	7.18	cfs
h	0.90	
H	0.23	ft
H/P	0.35	-
Cd	0.715	-
Cd <sub>emp</sub>	0.671	-
$\varepsilon_{Cd-emp}$	<b>6.46%</b>	-

STAR CCM+ (medium mesh)		
Cell count:	720,239	
P	8.00	in
$\alpha$	20.00	deg
$\theta$	30.00	deg
L	202.71	in
L	16.89	ft
tw	1.00	in
g	32.19	ft/s <sup>2</sup>
Q	7.18	cfs
h	0.90	
H	0.23	ft
H/P	0.35	-
Cd	0.720	-
Cd <sub>emp</sub>	0.672	-
$\varepsilon_{Cd-emp}$	<b>7.09%</b>	-

STAR CCM+ (fine mesh)		
Cell count:	3,290,304	
P	8.00	in
$\alpha$	20.00	deg
$\theta$	30.00	deg
L	202.71	in
L	16.89	ft
tw	1.00	in
g	32.19	ft/s <sup>2</sup>
Q	7.18	cfs
h	0.90	
H	0.23	ft
H/P	0.34	-
Cd	0.725	-
Cd <sub>emp</sub>	0.673	-
$\varepsilon_{Cd-emp}$	<b>7.75%</b>	-

STAR CCM+ (fine mesh, 1 Eq.)		
Cell count:	3,290,304	
P	8.00	in
$\alpha$	20.00	deg
$\theta$	30.00	deg
L	202.71	in
L	16.89	ft
tw	1.00	in
g	32.19	ft/s <sup>2</sup>
Q	7.18	cfs
h	0.89	
H	0.23	ft
H/P	0.34	-
Cd	0.731	-
Cd <sub>emp</sub>	0.674	-
$\varepsilon_{Cd-emp}$	<b>8.43%</b>	-

time	h	H
45.00	10.78	2.78
45.15	10.78	2.78
45.30	10.78	2.78
45.45	10.78	2.78
45.60	10.78	2.78
45.75	10.77	2.77
45.90	10.77	2.77
46.05	10.77	2.77
46.20	10.77	2.77
46.35	10.77	2.77
46.50	10.77	2.77
46.65	10.77	2.77
46.80	10.77	2.77
46.95	10.77	2.77
47.10	10.77	2.77
47.25	10.77	2.77
47.40	10.78	2.78
47.55	10.78	2.78
47.70	10.78	2.78
47.85	10.78	2.78
48.00	10.78	2.78
48.15	10.77	2.77
48.30	10.77	2.77
48.45	10.77	2.77
48.60	10.77	2.77
48.75	10.77	2.77
48.90	10.77	2.77
49.05	10.77	2.77
49.20	10.77	2.77
49.35	10.77	2.77
49.50	10.77	2.77
49.65	10.78	2.78
49.80	10.78	2.78
49.95	10.78	2.78
50.10	10.78	2.78
50.25	10.78	2.78
50.40	10.78	2.78
50.55	10.78	2.78
50.70	10.78	2.78
50.85	10.77	2.77
51.00	10.77	2.77
51.15	10.77	2.77
51.30	10.77	2.77
51.45	10.77	2.77
51.60	10.77	2.77
51.75	10.77	2.77
51.90	10.77	2.77

time	h	H
45.00	10.76	2.76
45.15	10.76	2.76
45.30	10.76	2.76
45.45	10.76	2.76
45.60	10.76	2.76
45.75	10.76	2.76
45.90	10.76	2.76
46.05	10.76	2.76
46.20	10.76	2.76
46.35	10.76	2.76
46.50	10.76	2.76
46.65	10.76	2.76
46.80	10.76	2.76
46.95	10.76	2.76
47.10	10.76	2.76
47.25	10.76	2.76
47.40	10.76	2.76
47.55	10.76	2.76
47.70	10.76	2.76
47.85	10.76	2.76
48.00	10.76	2.76
48.15	10.76	2.76
48.30	10.76	2.76
48.45	10.76	2.76
48.60	10.76	2.76
48.75	10.76	2.76
48.90	10.76	2.76
49.05	10.76	2.76
49.20	10.76	2.76
49.35	10.76	2.76
49.50	10.76	2.76
49.65	10.76	2.76
49.80	10.76	2.76
49.95	10.76	2.76
50.10	10.76	2.76
50.25	10.76	2.76
50.40	10.76	2.76
50.55	10.76	2.76
50.70	10.76	2.76
50.85	10.76	2.76
51.00	10.76	2.76
51.15	10.76	2.76
51.30	10.76	2.76
51.45	10.76	2.76
51.60	10.76	2.76
51.75	10.76	2.76
51.90	10.76	2.76

time	h	H
45.00	10.74	2.74
45.15	10.73	2.73
45.30	10.73	2.73
45.45	10.73	2.73
45.60	10.73	2.73
45.75	10.73	2.73
45.90	10.73	2.73
46.05	10.73	2.73
46.20	10.73	2.73
46.35	10.73	2.73
46.50	10.73	2.73
46.65	10.73	2.73
46.80	10.73	2.73
46.95	10.73	2.73
47.10	10.73	2.73
47.25	10.73	2.73
47.40	10.73	2.73
47.55	10.73	2.73
47.70	10.73	2.73
47.85	10.73	2.73
48.00	10.73	2.73
48.15	10.73	2.73
48.30	10.73	2.73
48.45	10.73	2.73
48.60	10.73	2.73
48.75	10.73	2.73
48.90	10.73	2.73
49.05	10.73	2.73
49.20	10.73	2.73
49.35	10.73	2.73
49.50	10.73	2.73
49.65	10.73	2.73
49.80	10.73	2.73
49.95	10.73	2.73
50.10	10.73	2.73
50.25	10.73	2.73
50.40	10.73	2.73
50.55	10.73	2.73
50.70	10.73	2.73
50.85	10.73	2.73
51.00	10.73	2.73
51.15	10.73	2.73
51.30	10.73	2.73
51.45	10.73	2.73
51.60	10.73	2.73
51.75	10.73	2.73
51.90	10.73	2.73



Table C11 Tabulated time series data for  $\alpha = 20^\circ$ ;  $\theta = 30^\circ$  arced labyrinth weir at H/P = 0.3

STAR CCM+ (fine mesh, $k-\varepsilon$ )		
Cell count:	3,290,304	
<b>P</b>	8.00	in
<b><math>\alpha</math></b>	20.00	deg
<b><math>\theta</math></b>	30.00	deg
<b>L</b>	202.71	in
<b>L</b>	16.89	ft
<b>tw</b>	1.00	in
<b>g</b>	32.19	ft/s <sup>2</sup>
<b>Q</b>	7.18	cfs
<b>h</b>	0.90	
<b>H</b>	0.23	ft
<b>H/P</b>	0.35	-
<b>Cd</b>	0.715	-
<b>Cd<sub>emp</sub></b>	0.671	-
<b><math>\varepsilon_{Cd-emp}</math></b>	<b>6.50%</b>	-

STAR CCM+ (fine mesh, $k-\omega$ )		
Cell count:	3,290,304	
<b>P</b>	8.00	in
<b><math>\alpha</math></b>	20.00	deg
<b><math>\theta</math></b>	30.00	deg
<b>L</b>	202.71	in
<b>L</b>	16.89	ft
<b>tw</b>	1.00	in
<b>g</b>	32.19	ft/s <sup>2</sup>
<b>Q</b>	7.18	cfs
<b>h</b>	0.90	
<b>H</b>	0.23	ft
<b>H/P</b>	0.34	-
<b>Cd</b>	0.723	-
<b>Cd<sub>emp</sub></b>	0.673	-
<b><math>\varepsilon_{Cd-emp}</math></b>	<b>7.44%</b>	-

time	h	H
45.00	10.77	2.77
45.15	10.77	2.77
45.30	10.77	2.77
45.45	10.77	2.77
45.60	10.77	2.77
45.75	10.77	2.77
45.90	10.77	2.77
46.05	10.77	2.77
46.20	10.77	2.77
46.35	10.77	2.77
46.50	10.77	2.77
46.65	10.77	2.77
46.80	10.77	2.77
46.95	10.77	2.77
47.10	10.77	2.77
47.25	10.77	2.77
47.40	10.77	2.77
47.55	10.77	2.77
47.70	10.77	2.77
47.85	10.77	2.77
48.00	10.77	2.77
48.15	10.77	2.77
48.30	10.77	2.77
48.45	10.77	2.77

time	h	H
45.00	10.76	2.76
45.19	10.76	2.76
45.39	10.75	2.75
45.58	10.75	2.75
45.78	10.76	2.76
45.97	10.76	2.76
46.17	10.75	2.75
46.36	10.75	2.75
46.56	10.76	2.76
46.75	10.75	2.75
46.95	10.75	2.75
47.14	10.76	2.76
47.34	10.76	2.76
47.53	10.75	2.75
47.73	10.75	2.75
47.92	10.75	2.75
48.12	10.75	2.75
48.31	10.75	2.75
48.51	10.75	2.75
48.70	10.75	2.75
48.90	10.75	2.75
49.09	10.75	2.75
49.29	10.75	2.75
49.48	10.75	2.75

48.60	10.77	2.77
48.75	10.77	2.77
48.90	10.77	2.77
49.05	10.77	2.77
49.20	10.77	2.77
49.35	10.77	2.77
49.50	10.77	2.77
49.65	10.77	2.77
49.80	10.77	2.77
49.95	10.77	2.77
50.10	10.77	2.77
50.25	10.77	2.77
50.40	10.77	2.77
50.55	10.77	2.77
50.70	10.77	2.77
50.85	10.77	2.77
51.00	10.77	2.77
51.15	10.77	2.77
51.30	10.77	2.77
51.45	10.77	2.77
51.60	10.77	2.77
51.75	10.77	2.77
51.90	10.77	2.77
52.05	10.77	2.77
52.20	10.77	2.77
52.35	10.77	2.77
52.50	10.77	2.77
52.65	10.77	2.77
52.80	10.77	2.77
52.95	10.77	2.77
53.10	10.77	2.77
53.25	10.77	2.77
53.40	10.77	2.77
53.55	10.77	2.77
53.70	10.77	2.77
53.85	10.77	2.77
54.00	10.77	2.77
54.15	10.77	2.77
54.30	10.77	2.77
54.45	10.77	2.77
54.60	10.77	2.77
54.75	10.77	2.77
54.90	10.77	2.77
55.05	10.77	2.77

49.68	10.75	2.75
49.87	10.75	2.75
50.06	10.75	2.75
50.26	10.75	2.75
50.45	10.75	2.75
50.65	10.75	2.75
50.84	10.75	2.75
51.04	10.76	2.76
51.23	10.75	2.75
51.43	10.75	2.75
51.62	10.75	2.75
51.82	10.76	2.76
52.01	10.75	2.75
52.21	10.75	2.75
52.40	10.75	2.75
52.60	10.75	2.75
52.79	10.75	2.75
52.99	10.75	2.75
53.18	10.75	2.75
53.38	10.76	2.76
53.57	10.75	2.75
53.77	10.75	2.75
53.96	10.75	2.75
54.16	10.76	2.76
54.35	10.75	2.75
54.55	10.75	2.75
54.74	10.75	2.75
54.94	10.75	2.75
55.13	10.75	2.75
55.32	10.75	2.75
55.52	10.75	2.75
55.71	10.75	2.75
55.91	10.75	2.75
56.10	10.75	2.75
56.30	10.75	2.75
56.49	10.75	2.75
56.69	10.75	2.75
56.88	10.75	2.75
57.08	10.75	2.75
57.27	10.75	2.75
57.47	10.75	2.75
57.66	10.75	2.75
57.86	10.75	2.75
58.05	10.75	2.75

55.20	10.77	2.77
55.35	10.77	2.77
55.50	10.77	2.77
55.65	10.77	2.77
55.80	10.77	2.77
55.95	10.77	2.77
56.10	10.77	2.77
56.25	10.77	2.77
56.40	10.77	2.77
56.55	10.77	2.77
56.70	10.77	2.77
56.85	10.77	2.77
57.00	10.77	2.77
57.15	10.77	2.77
57.30	10.77	2.77
57.45	10.77	2.77
57.60	10.77	2.77
57.75	10.77	2.77
57.90	10.77	2.77
58.05	10.77	2.77
58.20	10.77	2.77
58.35	10.77	2.77
58.50	10.77	2.77
58.65	10.77	2.77
58.80	10.77	2.77
58.95	10.77	2.77
59.10	10.77	2.77
59.25	10.77	2.77
59.40	10.77	2.77
59.55	10.77	2.77
59.70	10.77	2.77
59.85	10.77	2.77
60.00	10.77	2.77

58.25	10.75	2.75
58.44	10.75	2.75
58.64	10.75	2.75
58.83	10.75	2.75
59.03	10.75	2.75
59.22	10.75	2.75
59.42	10.75	2.75
59.61	10.75	2.75
59.81	10.75	2.75
60.00	10.75	2.75

Table C12 Tabulated time series data for  $\alpha = 20^\circ$ ;  $\theta = 30^\circ$  arced labyrinth weir at H/P = 0.3

FLOW-3D (coarse mesh)		
Cell count:	293,940	
P	8.00	in
$\alpha$	16.00	deg
$\theta$	10.00	deg
L	101.36	in
L	8.45	ft
tw	1.00	in
g	32.19	ft/s <sup>2</sup>
Q	2.84	cfs
h	0.74	
H	0.07	ft
H/P	0.10	-
Cd	3.513	-
Cd <sub>emp</sub>	0.657	-
$\epsilon_{Cd-emp}$	<b>434.80%</b>	-

FLOW-3D (medium mesh)		
Cell count:	576,684	
P	8.00	in
$\alpha$	16.00	deg
$\theta$	10.00	deg
L	101.36	in
L	8.45	ft
tw	1.00	in
g	32.19	ft/s <sup>2</sup>
Q	2.84	cfs
h	1.15	
H	0.19	ft
H/P	0.29	-
Cd	0.737	-
Cd <sub>emp</sub>	0.702	-
$\epsilon_{Cd-emp}$	<b>4.99%</b>	-

FLOW-3D (fine mesh)		
Cell count:	2,841,660	
P	8.00	in
$\alpha$	16.00	deg
$\theta$	10.00	deg
L	101.36	in
L	8.45	ft
tw	1.00	in
g	32.19	ft/s <sup>2</sup>
Q	2.84	cfs
h	1.15	
H	0.20	ft
H/P	0.30	-
Cd	0.718	-
Cd <sub>emp</sub>	0.700	-
$\epsilon_{Cd-emp}$	<b>2.65%</b>	-

time	h	H
0.00	1.16	0.20
0.60	1.17	0.22
1.20	1.19	0.23
1.80	1.09	0.13
2.40	1.03	0.07
3.00	0.95	-0.01
3.60	0.93	-0.03
4.20	0.92	-0.03
4.80	0.95	-0.01
5.40	0.92	-0.03
6.00	0.82	-0.14
6.60	0.82	-0.13
7.20	0.73	-0.23
7.80	0.90	-0.06
8.40	0.87	-0.09
9.00	0.85	-0.11
9.60	0.80	-0.15
10.20	0.80	-0.15
10.80	0.74	-0.21
11.40	0.80	-0.16
12.00	0.79	-0.16
12.60	0.77	-0.18
13.20	0.78	-0.18
13.80	0.80	-0.15
14.40	0.75	-0.21
15.00	0.74	-0.22
15.60	0.77	-0.19
16.20	0.74	-0.22
16.80	0.76	-0.20
17.40	0.77	-0.19

time	h	H
0.00	1.16	0.20
0.60	1.16	0.20
1.20	1.17	0.22
1.80	1.20	0.24
2.40	1.20	0.24
3.00	1.17	0.22
3.60	1.17	0.21
4.20	1.16	0.20
4.80	1.13	0.18
5.40	1.16	0.20
6.00	1.15	0.19
6.60	1.15	0.19
7.20	1.17	0.21
7.80	1.15	0.19
8.40	1.17	0.21
9.00	1.18	0.23
9.60	1.17	0.22
10.20	1.16	0.20
10.80	1.15	0.19
11.40	1.15	0.19
12.00	1.17	0.21
12.60	1.15	0.19
13.20	1.15	0.19
13.80	1.15	0.19
14.40	1.15	0.20
15.00	1.17	0.21
15.60	1.18	0.22
16.20	1.15	0.19
16.80	1.15	0.20
17.40	1.15	0.20

time	h	H
0.00	1.16	0.20
0.60	1.16	0.20
1.20	1.18	0.22
1.80	1.20	0.24
2.40	1.20	0.24
3.00	1.17	0.22
3.60	1.17	0.21
4.20	1.16	0.20
4.80	1.14	0.18
5.40	1.16	0.20
6.00	1.15	0.19
6.60	1.15	0.19
7.20	1.17	0.21
7.80	1.15	0.19
8.40	1.17	0.21
9.00	1.19	0.23
9.60	1.18	0.22
10.20	1.16	0.20
10.80	1.15	0.19
11.40	1.15	0.19
12.00	1.17	0.21
12.60	1.15	0.19
13.20	1.15	0.19
13.80	1.15	0.19
14.40	1.15	0.20
15.00	1.17	0.21
15.60	1.18	0.22
16.20	1.15	0.19
16.80	1.16	0.20
17.40	1.16	0.20

18.00	0.74	-0.22
18.60	0.73	-0.22
19.20	0.74	-0.21
19.80	0.74	-0.22
20.40	0.75	-0.21
21.00	0.74	-0.22
21.60	0.75	-0.21
22.20	0.75	-0.21
22.80	0.74	-0.21
23.40	0.74	-0.22
24.00	0.74	-0.21
24.60	0.74	-0.22
25.20	0.74	-0.22
25.80	0.74	-0.22
26.40	0.74	-0.22
27.00	0.74	-0.22
27.60	0.74	-0.22
28.20	0.74	-0.22
28.80	0.74	-0.22
29.40	0.74	-0.22
30.00	0.74	-0.21
30.60	0.73	-0.23
31.20	0.74	-0.22
31.80	0.74	-0.22
32.40	0.74	-0.22
33.00	0.74	-0.22
33.60	0.73	-0.22
34.20	0.74	-0.22
34.80	0.73	-0.23
35.40	0.74	-0.22
36.00	0.73	-0.22
36.60	0.75	-0.21
37.20	0.73	-0.23
37.80	0.74	-0.21
38.40	0.75	-0.21
39.00	0.73	-0.22
39.60	0.73	-0.23
40.20	0.74	-0.22
40.80	0.74	-0.22
41.40	0.74	-0.22
42.00	0.74	-0.22
42.60	0.74	-0.22
43.20	0.72	-0.23
43.80	0.74	-0.22
44.40	0.73	-0.22
45.00	0.73	-0.22
45.60	0.74	-0.21
46.20	0.73	-0.22
46.80	0.74	-0.22
47.40	0.74	-0.22

18.00	1.16	0.20
18.60	1.16	0.20
19.20	1.15	0.19
19.80	1.14	0.18
20.40	1.16	0.20
21.00	1.16	0.20
21.60	1.16	0.21
22.20	1.15	0.20
22.80	1.15	0.19
23.40	1.15	0.20
24.00	1.16	0.20
24.60	1.16	0.20
25.20	1.16	0.20
25.80	1.14	0.18
26.40	1.14	0.19
27.00	1.16	0.20
27.60	1.16	0.20
28.20	1.15	0.20
28.80	1.15	0.20
29.40	1.15	0.19
30.00	1.15	0.20
30.60	1.16	0.20
31.20	1.16	0.20
31.80	1.14	0.19
32.40	1.15	0.19
33.00	1.15	0.19
33.60	1.15	0.20
34.20	1.16	0.20
34.80	1.15	0.19
35.40	1.15	0.19
36.00	1.15	0.20
36.60	1.15	0.20
37.20	1.15	0.20
37.80	1.15	0.19
38.40	1.15	0.19
39.00	1.15	0.20
39.60	1.15	0.19
40.20	1.15	0.20
40.80	1.15	0.20
41.40	1.15	0.19
42.00	1.15	0.19
42.60	1.15	0.20
43.20	1.15	0.19
43.80	1.15	0.20
44.40	1.15	0.19
45.00	1.15	0.19
45.60	1.15	0.19
46.20	1.15	0.20
46.80	1.15	0.19
47.40	1.15	0.19

18.00	1.16	0.20
18.60	1.16	0.20
19.20	1.15	0.20
19.80	1.14	0.18
20.40	1.16	0.20
21.00	1.16	0.20
21.60	1.17	0.21
22.20	1.16	0.20
22.80	1.15	0.20
23.40	1.16	0.20
24.00	1.16	0.21
24.60	1.16	0.20
25.20	1.16	0.20
25.80	1.14	0.19
26.40	1.15	0.19
27.00	1.16	0.20
27.60	1.16	0.20
28.20	1.16	0.20
28.80	1.16	0.20
29.40	1.15	0.19
30.00	1.16	0.20
30.60	1.16	0.20
31.20	1.16	0.21
31.80	1.15	0.19
32.40	1.15	0.19
33.00	1.15	0.20
33.60	1.16	0.20
34.20	1.16	0.20
34.80	1.15	0.19
35.40	1.15	0.20
36.00	1.16	0.20
36.60	1.16	0.20
37.20	1.16	0.20
37.80	1.15	0.20
38.40	1.15	0.19
39.00	1.16	0.20
39.60	1.15	0.20
40.20	1.15	0.20
40.80	1.15	0.20
41.40	1.15	0.19
42.00	1.15	0.20
42.60	1.16	0.20
43.20	1.15	0.20
43.80	1.16	0.20
44.40	1.15	0.19
45.00	1.15	0.19
45.60	1.15	0.20
46.20	1.16	0.20
46.80	1.15	0.20
47.40	1.15	0.20

48.00	0.73	-0.23
48.60	0.74	-0.21
49.20	0.74	-0.22
49.80	0.73	-0.22
50.40	0.73	-0.22
51.00	0.73	-0.22
51.60	0.74	-0.22
52.20	0.73	-0.23
52.80	0.73	-0.22
53.40	0.73	-0.23
54.00	0.74	-0.22
54.60	0.73	-0.23
55.20	0.74	-0.22
55.80	0.74	-0.22
56.40	0.73	-0.23
57.00	0.74	-0.21
57.60	0.74	-0.22
58.20	0.73	-0.22
58.80	0.73	-0.22
59.40	0.73	-0.22
60.00	0.74	-0.22

48.00	1.15	0.19
48.60	1.15	0.19
49.20	1.16	0.20
49.80	1.15	0.19
50.40	1.15	0.19
51.00	1.15	0.20
51.60	1.15	0.19
52.20	1.15	0.20
52.80	1.15	0.19
53.40	1.15	0.19
54.00	1.15	0.19
54.60	1.15	0.19
55.20	1.15	0.19
55.80	1.15	0.20
56.40	1.15	0.19
57.00	1.15	0.19
57.60	1.15	0.19
58.20	1.15	0.19
58.80	1.15	0.20
59.40	1.15	0.20
60.00	1.15	0.19

48.00	1.15	0.19
48.60	1.15	0.20
49.20	1.16	0.20
49.80	1.16	0.20
50.40	1.15	0.20
51.00	1.15	0.20
51.60	1.15	0.19
52.20	1.16	0.20
52.80	1.15	0.20
53.40	1.15	0.20
54.00	1.15	0.20
54.60	1.15	0.20
55.20	1.15	0.19
55.80	1.16	0.20
56.40	1.15	0.19
57.00	1.15	0.20
57.60	1.15	0.20
58.20	1.15	0.20
58.80	1.16	0.20
59.40	1.16	0.20
60.00	1.15	0.19

Table C13 Tabulated time series data for  $\alpha = 20^\circ$ ;  $\theta = 30^\circ$  arced labyrinth weir at H/P = 0.4

STAR CCM+ (fine mesh)		
Cell count:	1,876,868	
<b>P</b>	8.000	in
<b><math>\alpha</math></b>	20.000	deg
<b><math>\theta</math></b>	30.000	deg
<b>L</b>	202.711	in
<b>L</b>	16.893	ft
<b>tw</b>	1.000	in
<b>g</b>	32.185	ft/s <sup>2</sup>
<b>Q</b>	7.969	cfs
<b>h</b>	0.912	
<b>H</b>	0.246	ft
<b>H/P</b>	0.368	-
<b>Cd</b>	0.738	-
<b>Cd<sub>emp</sub></b>	0.658	-
<b><math>\epsilon_{Cd-emp}</math></b>	<b>12.18%</b>	-

FLOW-3D (fine mesh)		
Cell count:	2,841,660	
<b>P</b>	8.000	in
<b><math>\alpha</math></b>	20.000	deg
<b><math>\theta</math></b>	30.000	deg
<b>L</b>	101.355	in
<b>L</b>	8.446	ft
<b>tw</b>	1.000	in
<b>g</b>	32.185	ft/s <sup>2</sup>
<b>Q</b>	3.985	cfs
<b>h</b>	1.219	
<b>H</b>	0.262	ft
<b>H/P</b>	0.393	-
<b>Cd</b>	0.657	-
<b>Cd<sub>emp</sub></b>	0.642	-
<b><math>\epsilon_{Cd-emp}</math></b>	<b>2.39%</b>	-

time	h	H
45.00	10.913	9.956
45.15	10.916	9.959
45.30	10.919	9.962
45.45	10.921	9.965
45.60	10.924	9.967
45.75	10.927	9.970
45.90	10.929	9.973
46.05	10.932	9.975
46.20	10.934	9.977
46.35	10.937	9.980
46.50	10.939	9.982
46.65	10.941	9.985
46.80	10.943	9.987
46.95	10.945	9.989
47.10	10.947	9.991
47.25	10.949	9.993
47.40	10.951	9.994
47.55	10.953	9.996
47.70	10.954	9.998
47.85	10.956	9.999
48.00	10.957	10.000
48.15	10.958	10.002
48.30	10.959	10.003
48.45	10.960	10.004

time	h	H
0.002	1.225	0.268
0.600	1.227	0.270
1.200	1.249	0.292
1.800	1.275	0.318
2.400	1.280	0.324
3.000	1.246	0.289
3.600	1.243	0.286
4.200	1.227	0.270
4.800	1.200	0.243
5.400	1.229	0.272
6.000	1.213	0.257
6.600	1.217	0.260
7.200	1.246	0.289
7.800	1.215	0.258
8.400	1.256	0.299
9.000	1.271	0.314
9.600	1.235	0.278
10.200	1.217	0.261
10.800	1.215	0.258
11.400	1.223	0.266
12.000	1.236	0.280
12.600	1.215	0.258
13.200	1.206	0.249
13.800	1.233	0.276

48.60	10.961	10.005
48.75	10.962	10.005
48.90	10.963	10.006
49.05	10.964	10.007
49.20	10.964	10.007
49.35	10.965	10.008
49.50	10.965	10.008
49.65	10.965	10.008
49.80	10.965	10.009
49.95	10.966	10.009
50.10	10.966	10.009
50.25	10.966	10.009
50.40	10.965	10.009
50.55	10.965	10.009
50.70	10.965	10.008
50.85	10.965	10.008
51.00	10.964	10.008
51.15	10.964	10.007
51.30	10.964	10.007
51.45	10.963	10.007
51.60	10.963	10.006
51.75	10.962	10.006
51.90	10.962	10.005
52.05	10.961	10.005
52.20	10.961	10.004
52.35	10.960	10.003
52.50	10.960	10.003
52.65	10.959	10.002
52.80	10.958	10.002
52.95	10.958	10.001
53.10	10.957	10.000
53.25	10.956	10.000
53.40	10.956	9.999
53.55	10.955	9.999
53.70	10.955	9.998
53.85	10.954	9.997
54.00	10.953	9.997
54.15	10.953	9.996
54.30	10.952	9.995
54.45	10.951	9.995
54.60	10.951	9.994
54.75	10.950	9.993
54.90	10.949	9.993
55.05	10.949	9.992

14.400	1.228	0.271
15.000	1.247	0.290
15.600	1.248	0.292
16.200	1.200	0.243
16.800	1.237	0.280
17.400	1.224	0.268
18.000	1.222	0.265
18.600	1.224	0.267
19.200	1.209	0.252
19.800	1.208	0.252
20.400	1.242	0.285
21.000	1.228	0.271
21.600	1.232	0.276
22.200	1.219	0.263
22.800	1.220	0.264
23.400	1.238	0.282
24.000	1.224	0.268
24.600	1.222	0.265
25.200	1.215	0.259
25.800	1.208	0.251
26.400	1.226	0.269
27.000	1.234	0.277
27.600	1.221	0.264
28.200	1.222	0.265
28.800	1.225	0.269
29.400	1.220	0.263
30.000	1.228	0.272
30.600	1.227	0.270
31.200	1.211	0.254
31.800	1.220	0.263
32.400	1.219	0.262
33.000	1.225	0.268
33.600	1.225	0.268
34.200	1.221	0.264
34.800	1.215	0.258
35.400	1.228	0.271
36.000	1.223	0.266
36.600	1.226	0.269
37.200	1.217	0.260
37.800	1.214	0.257
38.400	1.220	0.264
39.000	1.223	0.266
39.600	1.219	0.262
40.200	1.222	0.265

55.20	10.948	9.991
55.35	10.947	9.991
55.50	10.947	9.990
55.65	10.946	9.989
55.80	10.945	9.988
55.95	10.944	9.988
56.10	10.943	9.987
56.25	10.943	9.986
56.40	10.942	9.985
56.55	10.941	9.984
56.70	10.940	9.983
56.85	10.939	9.982
57.00	10.938	9.981
57.15	10.937	9.980
57.30	10.936	9.979
57.45	10.935	9.978
57.60	10.934	9.977
57.75	10.933	9.976
57.90	10.932	9.975
58.05	10.931	9.974
58.20	10.929	9.973
58.35	10.928	9.972
58.50	10.927	9.970
58.65	10.926	9.969
58.80	10.925	9.968
58.95	10.923	9.967
59.10	10.922	9.966
59.25	10.921	9.964
59.40	10.920	9.963
59.55	10.919	9.962
59.70	10.917	9.961
59.85	10.916	9.960
60.00	10.915	9.958

40.800	1.215	0.259
41.400	1.217	0.260
42.000	1.227	0.270
42.600	1.223	0.267
43.200	1.213	0.257
43.800	1.222	0.265
44.400	1.214	0.257
45.000	1.221	0.264
45.600	1.223	0.266
46.200	1.217	0.260
46.800	1.215	0.258
47.400	1.220	0.263
48.000	1.221	0.264
48.600	1.224	0.267
49.200	1.218	0.261
49.800	1.216	0.260
50.400	1.220	0.263
51.000	1.219	0.262
51.600	1.222	0.265
52.200	1.219	0.262
52.800	1.213	0.256
53.400	1.219	0.262
54.000	1.221	0.265
54.600	1.215	0.259
55.200	1.223	0.266
55.800	1.215	0.258
56.400	1.218	0.261
57.000	1.221	0.264
57.600	1.220	0.263
58.200	1.217	0.260
58.800	1.220	0.263
59.400	1.214	0.257
60.000	1.220	0.263

Table C14. Tabulated time series data for  $\alpha = 20^\circ$ ;  $\theta = 30^\circ$  arced labyrinth weir at H/P = 0.5

STAR CCM+ (fine mesh)		
Cell count:	1,886,083	
P	8.00	in
$\alpha$	20.00	deg
$\theta$	30.00	deg
L	202.71	in
L	16.89	ft
tw	1.00	in
g	32.19	ft/s <sup>2</sup>
Q	9.34	cfs
h	0.95	
H	0.28	ft
H/P	0.43	-
Cd	0.69	-
Cd <sub>emp</sub>	0.62	-
$\varepsilon_{Cd-emp}$	<b>10.33%</b>	-

FLOW-3D (fine mesh)		
Cell count:	3,306,877	
P	8.00	in
$\alpha$	20.00	deg
$\theta$	30.00	deg
L	101.36	in
L	8.45	ft
tw	1.00	in
g	32.19	ft/s <sup>2</sup>
Q	4.745	cfs
h	1.257	
H	0.300	ft
H/P	0.451	-
Cd	0.638	-
Cd <sub>emp</sub>	0.604	-
$\varepsilon_{Cd-emp}$	<b>5.52%</b>	-

FLOW -3D (fine mesh, 1st order)		
Cell count:	3,306,877	
P	8.00	in
$\alpha$	20.00	deg
$\theta$	30.00	deg
L	101.36	in
L	8.45	ft
tw	1.00	in
g	32.19	ft/s <sup>2</sup>
Q	4.745	cfs
h	1.269	
H	0.312	ft
H/P	0.468	-
Cd	0.602	-
Cd <sub>emp</sub>	0.593	-
$\varepsilon_{Cd-emp}$	<b>1.58%</b>	-

FLOW -3D (fine mesh, 1 Eq.)		
Cell count:	3,306,877	
P	8.00	in
$\alpha$	20.00	deg
$\theta$	30.00	deg
L	101.36	in
L	8.45	ft
tw	1.00	in
g	32.19	ft/s <sup>2</sup>
Q	4.745	cfs
h	1.271	
H	0.315	ft
H/P	0.472	-
Cd	0.595	-
Cd <sub>emp</sub>	0.590	-
$\varepsilon_{Cd-emp}$	<b>0.72%</b>	-

time	h	H
45.00	11.399	3.399
45.15	11.399	3.399
45.3	11.399	3.399
45.45	11.399	3.399
45.6	11.399	3.399
45.75	11.399	3.399
45.9	11.399	3.399
46.05	11.399	3.399
46.2	11.399	3.399
46.35	11.399	3.399
46.5	11.399	3.399
46.65	11.399	3.399
46.8	11.399	3.399
46.95	11.399	3.399
47.1	11.399	3.399
47.25	11.399	3.399
47.4	11.399	3.399
47.55	11.399	3.399
47.7	11.400	3.400
47.85	11.400	3.400
48	11.400	3.400
48.15	11.400	3.400
48.3	11.400	3.400
48.45	11.400	3.400
48.6	11.400	3.400
48.75	11.400	3.400
48.9	11.400	3.400
49.05	11.400	3.400
49.2	11.400	3.400
49.35	11.400	3.400
49.5	11.400	3.400
49.65	11.400	3.400
49.8	11.401	3.401
49.95	11.401	3.401
50.1	11.401	3.401
50.25	11.401	3.401
50.4	11.401	3.401
50.55	11.401	3.401
50.7	11.401	3.401
50.85	11.401	3.401
51	11.401	3.401
51.15	11.401	3.401
51.3	11.401	3.401

time	h	H
0.002	1.292	0.335
0.600	1.294	0.337
1.200	1.320	0.364
1.800	1.352	0.395
2.400	1.350	0.394
3.000	1.310	0.353
3.600	1.308	0.351
4.200	1.281	0.325
4.800	1.250	0.294
5.400	1.292	0.336
6.000	1.263	0.306
6.600	1.289	0.332
7.200	1.298	0.342
7.800	1.276	0.320
8.400	1.324	0.367
9.000	1.323	0.366
9.600	1.278	0.322
10.200	1.269	0.312
10.800	1.257	0.300
11.400	1.279	0.323
12.000	1.286	0.330
12.600	1.245	0.289
13.200	1.275	0.318
13.800	1.266	0.310
14.400	1.289	0.333
15.000	1.310	0.353
15.600	1.257	0.300
16.200	1.277	0.320
16.800	1.274	0.318
17.400	1.265	0.308
18.000	1.276	0.319
18.600	1.254	0.297
19.200	1.243	0.286
19.800	1.279	0.322
20.400	1.277	0.321
21.000	1.278	0.321
21.600	1.268	0.312
22.200	1.255	0.299
22.800	1.282	0.325
23.400	1.266	0.309
24.000	1.273	0.310
24.600	1.256	0.299
25.200	1.243	0.287

time	h	H
0.002	1.292	0.335
0.600	1.294	0.337
1.200	1.322	0.365
1.800	1.352	0.395
2.400	1.350	0.393
3.000	1.312	0.355
3.600	1.305	0.349
4.200	1.281	0.324
4.800	1.254	0.297
5.400	1.297	0.341
6.000	1.271	0.314
6.600	1.292	0.336
7.200	1.294	0.337
7.800	1.281	0.325
8.400	1.328	0.371
9.000	1.322	0.365
9.600	1.284	0.327
10.200	1.274	0.318
10.800	1.268	0.311
11.400	1.288	0.331
12.000	1.291	0.334
12.600	1.252	0.295
13.200	1.285	0.329
13.800	1.274	0.318
14.400	1.297	0.341
15.000	1.317	0.360
15.600	1.260	0.303
16.200	1.285	0.329
16.800	1.283	0.326
17.400	1.276	0.320
18.000	1.286	0.329
18.600	1.266	0.309
19.200	1.256	0.299
19.800	1.289	0.333
20.400	1.286	0.329
21.000	1.289	0.333
21.600	1.275	0.319
22.200	1.268	0.312
22.800	1.290	0.334
23.400	1.279	0.322
24.000	1.276	0.319
24.600	1.270	0.314
25.200	1.259	0.302

51.45	11.401	3.401
51.6	11.401	3.401
51.75	11.401	3.401
51.9	11.401	3.401
52.05	11.401	3.401
52.2	11.401	3.401
52.35	11.401	3.401
52.5	11.402	3.402
52.65	11.402	3.402
52.8	11.402	3.402
52.95	11.402	3.402
53.1	11.402	3.402
53.25	11.402	3.402
53.4	11.402	3.402
53.55	11.402	3.402
53.7	11.402	3.402
53.85	11.402	3.402
54	11.402	3.402
54.15	11.402	3.402
54.3	11.402	3.402
54.45	11.402	3.402
54.6	11.402	3.402
54.75	11.402	3.402
54.9	11.402	3.402
55.05	11.402	3.402
55.2	11.402	3.402
55.35	11.402	3.402
55.5	11.402	3.402
55.65	11.402	3.402
55.8	11.402	3.402
55.95	11.402	3.402
56.1	11.402	3.402
56.25	11.402	3.402
56.4	11.402	3.402
56.55	11.402	3.402
56.7	11.401	3.401
56.85	11.401	3.401
57	11.401	3.401
57.15	11.401	3.401
57.3	11.401	3.401
57.45	11.401	3.401
57.6	11.401	3.401
57.75	11.401	3.401
57.9	11.401	3.401
58.05	11.401	3.401
58.2	11.401	3.401
58.35	11.401	3.401
58.5	11.401	3.401
58.65	11.401	3.401
58.8	11.400	3.400
58.95	11.400	3.400
59.1	11.400	3.400
59.25	11.400	3.400
59.4	11.400	3.400
59.55	11.400	3.400
59.7	11.400	3.400
59.85	11.400	3.400
60	11.400	3.400

25.800	1.265	0.308
26.400	1.274	0.317
27.000	1.260	0.303
27.600	1.264	0.308
28.200	1.265	0.308
28.800	1.260	0.303
29.400	1.270	0.313
30.000	1.268	0.311
30.600	1.249	0.292
31.200	1.255	0.298
31.800	1.259	0.303
32.400	1.263	0.306
33.000	1.266	0.309
33.600	1.256	0.300
34.200	1.256	0.299
34.800	1.263	0.307
35.400	1.262	0.306
36.000	1.266	0.310
36.600	1.251	0.294
37.200	1.252	0.296
37.800	1.264	0.307
38.400	1.257	0.301
39.000	1.258	0.301
39.600	1.264	0.308
40.200	1.249	0.292
40.800	1.262	0.306
41.400	1.264	0.307
42.000	1.257	0.301
42.600	1.257	0.300
43.200	1.257	0.300
43.800	1.255	0.298
44.400	1.261	0.305
45.000	1.257	0.301
45.600	1.256	0.299
46.200	1.255	0.298
46.800	1.257	0.300
47.400	1.263	0.306
48.000	1.260	0.303
48.600	1.253	0.296
49.200	1.257	0.300
49.800	1.258	0.301
50.400	1.257	0.300
51.000	1.262	0.306
51.600	1.251	0.295
52.200	1.254	0.297
52.800	1.264	0.307
53.400	1.254	0.297
54.000	1.262	0.306
54.600	1.256	0.299
55.200	1.252	0.295
55.800	1.261	0.304
56.400	1.257	0.300
57.000	1.257	0.300
57.600	1.259	0.302
58.200	1.252	0.295
58.800	1.263	0.306
59.400	1.257	0.300
60.000	1.256	0.300

25.800	1.277	0.320
26.400	1.283	0.326
27.000	1.268	0.312
27.600	1.272	0.315
28.200	1.274	0.317
28.800	1.271	0.314
29.400	1.282	0.325
30.000	1.273	0.317
30.600	1.263	0.306
31.200	1.266	0.309
31.800	1.272	0.315
32.400	1.272	0.315
33.000	1.275	0.318
33.600	1.265	0.309
34.200	1.271	0.314
34.800	1.274	0.317
35.400	1.274	0.317
36.000	1.274	0.318
36.600	1.265	0.309
37.200	1.264	0.307
37.800	1.274	0.317
38.400	1.269	0.313
39.000	1.269	0.312
39.600	1.269	0.313
40.200	1.265	0.308
40.800	1.274	0.317
41.400	1.275	0.319
42.000	1.266	0.309
42.600	1.272	0.316
43.200	1.262	0.305
43.800	1.272	0.316
44.400	1.274	0.317
45.000	1.265	0.308
45.600	1.267	0.310
46.200	1.270	0.314
46.800	1.268	0.311
47.400	1.276	0.319
48.000	1.266	0.309
48.600	1.268	0.312
49.200	1.269	0.312
49.800	1.268	0.311
50.400	1.271	0.314
51.000	1.270	0.313
51.600	1.264	0.307
52.200	1.271	0.314
52.800	1.268	0.311
53.400	1.271	0.314
54.000	1.271	0.314
54.600	1.267	0.310
55.200	1.265	0.308
55.800	1.274	0.317
56.400	1.267	0.310
57.000	1.270	0.313
57.600	1.267	0.311
58.200	1.266	0.310
58.800	1.270	0.313
59.400	1.271	0.315
60.000	1.266	0.309

25.800	1.280	0.323
26.400	1.285	0.328
27.000	1.271	0.315
27.600	1.274	0.317
28.200	1.276	0.319
28.800	1.274	0.317
29.400	1.283	0.326
30.000	1.275	0.319
30.600	1.265	0.309
31.200	1.268	0.311
31.800	1.275	0.318
32.400	1.274	0.318
33.000	1.277	0.320
33.600	1.268	0.311
34.200	1.273	0.317
34.800	1.277	0.320
35.400	1.276	0.320
36.000	1.276	0.319
36.600	1.269	0.312
37.200	1.268	0.311
37.800	1.275	0.318
38.400	1.273	0.316
39.000	1.273	0.316
39.600	1.271	0.314
40.200	1.268	0.312
40.800	1.276	0.319
41.400	1.278	0.321
42.000	1.268	0.311
42.600	1.276	0.319
43.200	1.264	0.307
43.800	1.275	0.318
44.400	1.277	0.320
45.000	1.268	0.311
45.600	1.269	0.312
46.200	1.273	0.316
46.800	1.271	0.314
47.400	1.279	0.322
48.000	1.267	0.311
48.600	1.271	0.315
49.200	1.272	0.315
49.800	1.271	0.314
50.400	1.274	0.318
51.000	1.272	0.315
51.600	1.266	0.310
52.200	1.275	0.318
52.800	1.269	0.313
53.400	1.274	0.317
54.000	1.273	0.317
54.600	1.270	0.313
55.200	1.268	0.311
55.800	1.275	0.318
56.400	1.269	0.313
57.000	1.273	0.316
57.600	1.269	0.313
58.200	1.271	0.314
58.800	1.271	0.315
59.400	1.274	0.317
60.000	1.270	0.313

Table C15. Tabulated time series data for  $\alpha = 20^\circ$ ;  $\theta = 30^\circ$  arced labyrinth weir at H/P = 0.5

FLOW-3D (fine mesh, $k-\varepsilon$ )			FLOW-3D (fine mesh, $k-\omega$ )		
Cell count:	3,306,877		Cell count:	3,306,877	
<b>P</b>	8.00	in	<b>P</b>	8.00	in
<b><math>\alpha</math></b>	20.00	deg	<b><math>\alpha</math></b>	20.00	deg
<b><math>\theta</math></b>	30.00	deg	<b><math>\theta</math></b>	30.00	deg
<b>L</b>	101.36	in	<b>L</b>	101.36	in
<b>L</b>	8.45	ft	<b>L</b>	8.45	ft
<b>tw</b>	1.00	in	<b>tw</b>	1.00	in
<b>g</b>	32.19	ft/s <sup>2</sup>	<b>g</b>	32.19	ft/s <sup>2</sup>
<b>Q</b>	4.745	cfs	<b>Q</b>	4.745	cfs
<b>h</b>	1.263		<b>h</b>	1.260	
<b>H</b>	0.306	ft	<b>H</b>	0.304	ft
<b>H/P</b>	0.459	-	<b>H/P</b>	0.455	-
<b>Cd</b>	0.620	-	<b>Cd</b>	0.628	-
<b>Cd<sub>emp</sub></b>	0.599	-	<b>Cd<sub>emp</sub></b>	0.601	-
<b><math>\epsilon_{Cd-emp}</math></b>	<b>3.55%</b>	-	<b><math>\epsilon_{Cd-emp}</math></b>	<b>4.42%</b>	-

time	h	H	time	h	H
0.002	1.292	0.335	0.002	1.292	0.335
0.600	1.294	0.337	0.600	1.294	0.337
1.200	1.320	0.364	1.200	1.322	0.365
1.800	1.352	0.395	1.800	1.352	0.395
2.400	1.350	0.394	2.400	1.350	0.393
3.000	1.310	0.353	3.000	1.311	0.354
3.600	1.308	0.351	3.600	1.304	0.348
4.200	1.281	0.324	4.200	1.280	0.323
4.800	1.250	0.293	4.800	1.250	0.293
5.400	1.291	0.334	5.400	1.293	0.336
6.000	1.262	0.305	6.000	1.267	0.311
6.600	1.288	0.331	6.600	1.290	0.334
7.200	1.296	0.339	7.200	1.294	0.337
7.800	1.275	0.318	7.800	1.277	0.321
8.400	1.324	0.367	8.400	1.328	0.371
9.000	1.322	0.365	9.000	1.322	0.365
9.600	1.279	0.323	9.600	1.284	0.327
10.200	1.268	0.312	10.200	1.269	0.312
10.800	1.257	0.300	10.800	1.261	0.304
11.400	1.280	0.323	11.400	1.284	0.327
12.000	1.287	0.330	12.000	1.287	0.331
12.600	1.246	0.289	12.600	1.245	0.288
13.200	1.276	0.319	13.200	1.276	0.319
13.800	1.268	0.312	13.800	1.265	0.309
14.400	1.289	0.333	14.400	1.293	0.336

15.000	1.318	0.362
15.600	1.257	0.300
16.200	1.277	0.321
16.800	1.275	0.318
17.400	1.266	0.309
18.000	1.278	0.322
18.600	1.253	0.296
19.200	1.245	0.289
19.800	1.280	0.324
20.400	1.280	0.323
21.000	1.281	0.324
21.600	1.269	0.312
22.200	1.257	0.300
22.800	1.284	0.327
23.400	1.269	0.312
24.000	1.269	0.312
24.600	1.258	0.302
25.200	1.246	0.290
25.800	1.269	0.312
26.400	1.278	0.322
27.000	1.262	0.306
27.600	1.266	0.309
28.200	1.267	0.310
28.800	1.264	0.307
29.400	1.275	0.319
30.000	1.270	0.314
30.600	1.253	0.296
31.200	1.260	0.303
31.800	1.264	0.307
32.400	1.267	0.310
33.000	1.271	0.314
33.600	1.260	0.303
34.200	1.262	0.305
34.800	1.269	0.312
35.400	1.267	0.310
36.000	1.270	0.313
36.600	1.255	0.299
37.200	1.257	0.300
37.800	1.268	0.311
38.400	1.263	0.307
39.000	1.261	0.304
39.600	1.269	0.312
40.200	1.255	0.298
40.800	1.268	0.311
41.400	1.268	0.312
42.000	1.260	0.304

15.000	1.315	0.358
15.600	1.257	0.300
16.200	1.280	0.323
16.800	1.277	0.320
17.400	1.267	0.311
18.000	1.280	0.323
18.600	1.255	0.298
19.200	1.245	0.288
19.800	1.281	0.325
20.400	1.279	0.322
21.000	1.283	0.327
21.600	1.270	0.313
22.200	1.258	0.302
22.800	1.286	0.330
23.400	1.271	0.314
24.000	1.269	0.312
24.600	1.260	0.303
25.200	1.246	0.289
25.800	1.268	0.311
26.400	1.277	0.320
27.000	1.258	0.301
27.600	1.267	0.310
28.200	1.266	0.309
28.800	1.264	0.307
29.400	1.274	0.317
30.000	1.270	0.313
30.600	1.254	0.298
31.200	1.259	0.303
31.800	1.262	0.305
32.400	1.265	0.308
33.000	1.269	0.313
33.600	1.259	0.303
34.200	1.260	0.304
34.800	1.267	0.310
35.400	1.268	0.312
36.000	1.268	0.312
36.600	1.254	0.297
37.200	1.257	0.300
37.800	1.267	0.311
38.400	1.261	0.305
39.000	1.258	0.302
39.600	1.265	0.309
40.200	1.254	0.297
40.800	1.267	0.310
41.400	1.267	0.310
42.000	1.258	0.302

42.600	1.263	0.306
43.200	1.258	0.302
43.800	1.264	0.307
44.400	1.266	0.309
45.000	1.259	0.302
45.600	1.263	0.306
46.200	1.261	0.304
46.800	1.262	0.305
47.400	1.270	0.313
48.000	1.263	0.307
48.600	1.260	0.303
49.200	1.263	0.306
49.800	1.262	0.305
50.400	1.265	0.308
51.000	1.266	0.309
51.600	1.259	0.302
52.200	1.260	0.303
52.800	1.267	0.310
53.400	1.261	0.305
54.000	1.267	0.310
54.600	1.263	0.307
55.200	1.259	0.302
55.800	1.267	0.310
56.400	1.262	0.305
57.000	1.261	0.305
57.600	1.264	0.308
58.200	1.257	0.300
58.800	1.267	0.310
59.400	1.263	0.307
60.000	1.260	0.303
42.600	1.262	0.305
43.200	1.259	0.302
43.800	1.261	0.305
44.400	1.264	0.307
45.000	1.258	0.301
45.600	1.258	0.301
46.200	1.258	0.301
46.800	1.260	0.304
47.400	1.264	0.307
48.000	1.261	0.305
48.600	1.258	0.301
49.200	1.261	0.305
49.800	1.261	0.304
50.400	1.262	0.305
51.000	1.264	0.307
51.600	1.257	0.300
52.200	1.257	0.301
52.800	1.264	0.308
53.400	1.258	0.302
54.000	1.265	0.308
54.600	1.260	0.304
55.200	1.255	0.298
55.800	1.265	0.308
56.400	1.260	0.304
57.000	1.260	0.303
57.600	1.261	0.305
58.200	1.254	0.297
58.800	1.265	0.309
59.400	1.261	0.304
60.000	1.259	0.302

Table C16. Tabulated time series data for  $\alpha = 20^\circ$ ;  $\theta = 30^\circ$  arced labyrinth weir at H/P = 0.7

STAR CCM+ (fine mesh)			FLOW-3D (coarse mesh)			FLOW-3D (medium mesh)			FLOW-3D (fine mesh)		
Cell count:	1,885,423 <th data-kind="ghost"></th> <th>Cell count:</th> <td data-cs="2" data-kind="parent">293,940<th data-kind="ghost"></th><th>Cell count:</th><td data-cs="2" data-kind="parent">576,684<th data-kind="ghost"></th><th>Cell count:</th><td data-cs="2" data-kind="parent">2,841,660</td><th data-kind="ghost"></th></td></td>		Cell count:	293,940 <th data-kind="ghost"></th> <th>Cell count:</th> <td data-cs="2" data-kind="parent">576,684<th data-kind="ghost"></th><th>Cell count:</th><td data-cs="2" data-kind="parent">2,841,660</td><th data-kind="ghost"></th></td>		Cell count:	576,684 <th data-kind="ghost"></th> <th>Cell count:</th> <td data-cs="2" data-kind="parent">2,841,660</td> <th data-kind="ghost"></th>		Cell count:	2,841,660	
P	8.00	in	P	8.00	in	P	8.00	in	P	8.00	in
$\alpha$	20.00	deg	$\alpha$	20.00	deg	$\alpha$	20.00	deg	$\alpha$	20.00	deg
$\theta$	30.00	deg	$\theta$	30.00	deg	$\theta$	30.00	deg	$\theta$	30.00	deg
L	202.71	in	L	101.36	in	L	101.36	in	L	101.36	in
L	16.89	ft	L	8.45	ft	L	8.45	ft	L	8.45	ft
tw	1.00	in	tw	1.00	in	tw	1.00	in	tw	1.00	in
g	32.19	ft/s <sup>2</sup>	g	32.19	ft/s <sup>2</sup>	g	32.19	ft/s <sup>2</sup>	g	32.19	ft/s <sup>2</sup>
Q	9.487	cfs	Q	6.555	cfs	Q	6.555	cfs	Q	6.555	cfs
h	0.949		h	0.967		h	1.376		h	1.382	
H	0.283	ft	H	0.300	ft	H	0.420	ft	H	0.425	ft
H/P	0.424	-	H/P	0.450	-	H/P	0.630	-	H/P	0.638	-
Cd	0.699	-	Cd	0.882	-	Cd	0.534	-	Cd	0.524	-
Cd <sub>emp</sub>	0.622	-	Cd <sub>emp</sub>	0.605	-	Cd <sub>emp</sub>	0.498	-	Cd <sub>emp</sub>	0.494	-
$\varepsilon_{Cd-emp}$	12.40%	-	$\varepsilon_{Cd-emp}$	45.92%	-	$\varepsilon_{Cd-emp}$	7.12%	-	$\varepsilon_{Cd-emp}$	5.97%	-
time	h	H	time	h	H	time	h	H	time	h	H
45.00	11.399	3.399	0.002	1.425	0.468	0.002	1.425	0.468	0.002	1.425	0.468
45.15	11.399	3.399	0.600	1.428	0.471	0.600	1.426	0.469	0.600	1.428	0.472
45.3	11.399	3.399	1.200	1.438	0.482	1.200	1.430	0.473	1.200	1.438	0.482
45.45	11.399	3.399	1.800	1.438	0.481	1.800	1.438	0.481	1.800	1.438	0.482
45.6	11.399	3.399	2.400	1.394	0.437	2.400	1.422	0.465	2.400	1.416	0.459
45.75	11.399	3.399	3.000	1.341	0.384	3.000	1.396	0.439	3.000	1.391	0.434
45.9	11.399	3.399	3.600	1.319	0.362	3.600	1.394	0.437	3.600	1.410	0.453
46.05	11.399	3.399	4.200	1.260	0.303	4.200	1.373	0.416	4.200	1.370	0.413
46.2	11.399	3.399	4.800	1.245	0.289	4.800	1.335	0.378	4.800	1.341	0.385
46.35	11.399	3.399	5.400	1.172	0.216	5.400	1.373	0.416	5.400	1.400	0.444
46.5	11.399	3.399	6.000	1.280	0.324	6.000	1.356	0.399	6.000	1.369	0.413
46.65	11.399	3.399	6.600	1.175	0.218	6.600	1.351	0.394	6.600	1.389	0.432
46.8	11.399	3.399	7.200	1.136	0.179	7.200	1.368	0.412	7.200	1.377	0.420
46.95	11.399	3.399	7.800	1.146	0.190	7.800	1.353	0.396	7.800	1.373	0.416
47.1	11.399	3.399	8.400	1.121	0.165	8.400	1.376	0.419	8.400	1.420	0.463
47.25	11.399	3.399	9.000	1.244	0.287	9.000	1.384	0.427	9.000	1.413	0.456
47.4	11.399	3.399	9.600	1.132	0.175	9.600	1.387	0.430	9.600	1.381	0.424
47.55	11.399	3.399	10.200	1.142	0.186	10.200	1.364	0.407	10.200	1.359	0.403
47.7	11.400	3.400	10.800	1.035	0.078	10.800	1.344	0.387	10.800	1.379	0.423
47.85	11.400	3.400	11.400	1.114	0.157	11.400	1.379	0.422	11.400	1.400	0.444
48	11.400	3.400	12.000	1.066	0.109	12.000	1.362	0.406	12.000	1.373	0.416
48.15	11.400	3.400	12.600	1.152	0.195	12.600	1.363	0.406	12.600	1.360	0.403
48.3	11.400	3.400	13.200	1.015	0.058	13.200	1.349	0.392	13.200	1.385	0.428
48.45	11.400	3.400	13.800	1.078	0.122	13.800	1.364	0.408	13.800	1.366	0.409
48.6	11.400	3.400	14.400	1.006	0.049	14.400	1.358	0.401	14.400	1.420	0.463
48.75	11.400	3.400	15.000	1.096	0.139	15.000	1.384	0.428	15.000	1.396	0.440
48.9	11.400	3.400	15.600	1.096	0.139	15.600	1.375	0.418	15.600	1.357	0.400
49.05	11.400	3.400	16.200	1.052	0.096	16.200	1.358	0.401	16.200	1.397	0.440
49.2	11.400	3.400	16.800	1.004	0.047	16.800	1.364	0.407	16.800	1.377	0.421
49.35	11.400	3.400	17.400	1.043	0.087	17.400	1.374	0.417	17.400	1.391	0.434
49.5	11.400	3.400	18.000	1.032	0.075	18.000	1.365	0.408	18.000	1.376	0.420
49.65	11.400	3.400	18.600	1.061	0.104	18.600	1.367	0.411	18.600	1.362	0.405
49.8	11.401	3.401	19.200	1.013	0.056	19.200	1.359	0.402	19.200	1.373	0.416
49.95	11.401	3.401	19.800	1.008	0.052	19.800	1.356	0.399	19.800	1.394	0.437
50.1	11.401	3.401	20.400	0.994	0.038	20.400	1.368	0.411	20.400	1.389	0.433
50.25	11.401	3.401	21.000	1.037	0.080	21.000	1.370	0.413	21.000	1.384	0.427
50.4	11.401	3.401	21.600	1.010	0.053	21.600	1.374	0.418	21.600	1.370	0.413
50.55	11.401	3.401	22.200	1.036	0.079	22.200	1.365	0.408	22.200	1.396	0.440
50.7	11.401	3.401	22.800	0.999	0.042	22.800	1.366	0.410	22.800	1.387	0.430
50.85	11.401	3.401	23.400	0.993	0.036	23.400	1.368	0.412	23.400	1.378	0.421
51	11.401	3.401	24.000	1.005	0.049	24.000	1.372	0.415	24.000	1.382	0.426
51.15	11.401	3.401	24.600	1.014	0.058	24.600	1.369	0.413	24.600	1.360	0.403
51.3	11.401	3.401	25.200	1.002	0.045	25.200	1.366	0.409	25.200	1.380	0.423
51.45	11.401	3.401	25.800	0.997	0.040	25.800	1.360	0.403	25.800	1.394	0.437
51.6	11.401	3.401	26.400	0.992	0.035	26.400	1.368	0.411	26.400	1.377	0.420
51.75	11.401	3.401	27.000	0.978	0.021	27.000	1.372	0.415	27.000	1.378	0.421

51.9	11.401	3.401
52.05	11.401	3.401
52.2	11.401	3.401
52.35	11.401	3.401
52.5	11.402	3.402
52.65	11.402	3.402
52.8	11.402	3.402
52.95	11.402	3.402
53.1	11.402	3.402
53.25	11.402	3.402
53.4	11.402	3.402
53.55	11.402	3.402
53.7	11.402	3.402
53.85	11.402	3.402
54	11.402	3.402
54.15	11.402	3.402
54.3	11.402	3.402
54.45	11.402	3.402
54.6	11.402	3.402
54.75	11.402	3.402
54.9	11.402	3.402
55.05	11.402	3.402
55.2	11.402	3.402
55.35	11.402	3.402
55.5	11.402	3.402
55.65	11.402	3.402
55.8	11.402	3.402
55.95	11.402	3.402
56.1	11.402	3.402
56.25	11.402	3.402
56.4	11.402	3.402
56.55	11.402	3.402
56.7	11.401	3.401
56.85	11.401	3.401
57	11.401	3.401
57.15	11.401	3.401
57.3	11.401	3.401
57.45	11.401	3.401
57.6	11.401	3.401
57.75	11.401	3.401
57.9	11.401	3.401
58.05	11.401	3.401
58.2	11.401	3.401
58.35	11.401	3.401
58.5	11.401	3.401
58.65	11.401	3.401
58.8	11.400	3.400
58.95	11.400	3.400
59.1	11.400	3.400
59.25	11.400	3.400
59.4	11.400	3.400
59.55	11.400	3.400
59.7	11.400	3.400
59.85	11.400	3.400
60	11.400	3.400

27.600	1.006	0.050
28.200	0.976	0.020
28.800	1.013	0.056
29.400	0.980	0.024
30.000	0.971	0.014
30.600	0.981	0.024
31.200	0.993	0.037
31.800	0.985	0.028
32.400	0.985	0.029
33.000	0.978	0.022
33.600	0.972	0.015
34.200	1.007	0.051
34.800	0.971	0.015
35.400	0.985	0.029
36.000	0.959	0.003
36.600	0.987	0.031
37.200	0.971	0.014
37.800	0.975	0.019
38.400	0.961	0.005
39.000	0.989	0.032
39.600	0.959	0.003
40.200	0.978	0.022
40.800	0.985	0.028
41.400	0.972	0.015
42.000	0.980	0.023
42.600	0.964	0.007
43.200	0.963	0.007
43.800	0.958	0.002
44.400	0.982	0.026
45.000	0.959	0.002
45.600	0.970	0.014
46.200	0.962	0.005
46.800	0.965	0.008
47.400	0.988	0.032
48.000	0.969	0.012
48.600	0.985	0.029
49.200	0.948	-0.009
49.800	0.977	0.020
50.400	0.959	0.002
51.000	0.949	-0.008
51.600	0.983	0.026
52.200	0.950	-0.007
52.800	0.967	0.011
53.400	0.974	0.017
54.000	0.935	-0.022
54.600	1.002	0.046
55.200	0.964	0.007
55.800	0.960	0.003
56.400	0.976	0.019
57.000	0.941	-0.015
57.600	0.971	0.014
58.200	0.965	0.008
58.800	0.982	0.026
59.400	0.941	-0.016
60.000	0.987	0.030

27.600	1.370	0.413
28.200	1.367	0.410
28.800	1.371	0.414
29.400	1.369	0.412
30.000	1.372	0.415
30.600	1.373	0.416
31.200	1.370	0.413
31.800	1.365	0.409
32.400	1.370	0.413
33.000	1.371	0.415
33.600	1.371	0.415
34.200	1.372	0.416
34.800	1.370	0.413
35.400	1.371	0.414
36.000	1.374	0.417
36.600	1.375	0.419
37.200	1.372	0.416
37.800	1.369	0.413
38.400	1.371	0.415
39.000	1.374	0.417
39.600	1.374	0.417
40.200	1.374	0.417
40.800	1.373	0.416
41.400	1.373	0.416
42.000	1.374	0.417
42.600	1.377	0.420
43.200	1.375	0.419
43.800	1.374	0.417
44.400	1.373	0.417
45.000	1.373	0.416
45.600	1.376	0.419
46.200	1.377	0.420
46.800	1.375	0.418
47.400	1.373	0.417
48.000	1.375	0.419
48.600	1.377	0.420
49.200	1.377	0.420
49.800	1.376	0.419
50.400	1.375	0.418
51.000	1.376	0.419
51.600	1.376	0.420
52.200	1.377	0.420
52.800	1.376	0.419
53.400	1.377	0.420
54.000	1.375	0.419
54.600	1.377	0.420
55.200	1.377	0.421
55.800	1.378	0.421
56.400	1.377	0.420
57.000	1.376	0.420
57.600	1.377	0.420
58.200	1.378	0.422
58.800	1.378	0.421
59.400	1.377	0.420
60.000	1.377	0.420

27.600	1.382	0.425
28.200	1.385	0.428
28.800	1.391	0.434
29.400	1.381	0.425
30.000	1.370	0.413
30.600	1.376	0.420
31.200	1.385	0.428
31.800	1.384	0.427
32.400	1.378	0.421
33.000	1.380	0.423
33.600	1.379	0.422
34.200	1.387	0.430
34.800	1.387	0.431
35.400	1.379	0.423
36.000	1.370	0.414
36.600	1.387	0.430
37.200	1.381	0.424
37.800	1.380	0.423
38.400	1.380	0.423
39.000	1.377	0.420
39.600	1.383	0.426
40.200	1.387	0.431
40.800	1.381	0.424
41.400	1.380	0.423
42.000	1.382	0.425
42.600	1.382	0.425
43.200	1.384	0.427
43.800	1.382	0.425
44.400	1.376	0.419
45.000	1.382	0.425
45.600	1.381	0.424
46.200	1.386	0.429
46.800	1.379	0.422
47.400	1.382	0.425
48.000	1.381	0.425
48.600	1.383	0.426
49.200	1.384	0.427
49.800	1.382	0.425
50.400	1.376	0.419
51.000	1.384	0.427
51.600	1.383	0.426
52.200	1.380	0.424
52.800	1.382	0.425
53.400	1.380	0.423
54.000	1.383	0.426
54.600	1.385	0.428
55.200	1.381	0.425
55.800	1.382	0.425
56.400	1.380	0.423
57.000	1.383	0.426
57.600	1.384	0.427
58.200	1.378	0.421
58.800	1.382	0.425
59.400	1.381	0.425
60.000	1.382	0.425

Table C17. Tabulated time series data for  $\alpha = 20^\circ$ ;  $\theta = 30^\circ$  arced labyrinth weir at H/P = 0.8

STAR CCM+ (fine mesh)		
Cell count:		
P	8.000	in
$\alpha$	20.000	deg
$\theta$	30.000	deg
L	202.711	in
L	16.893	ft
tw	1.000	in
g	32.185	ft/s <sup>2</sup>
Q	15.297	cfs
h	1.187	
H	0.520	ft
H/P	0.780	-
Cd	0.452	-
Cd <sub>emp</sub>	0.432	-
$\epsilon_{Cd-emp}$	<b>4.45%</b>	-

FLOW-3D (fine mesh)		
Cell count:		
P	8.000	in
$\alpha$	16.000	deg
$\theta$	10.000	deg
L	101.355	in
L	8.446	ft
tw	1.000	in
g	32.185	ft/s <sup>2</sup>
Q	7.650	cfs
h	1.431	
H	0.475	ft
H/P	0.712	-
Cd	0.518	-
Cd <sub>emp</sub>	0.459	-
$\epsilon_{Cd-emp}$	<b>12.71%</b>	-

time	h	H
45.00	14.240	6.240
45.15	14.241	6.241
45.3	14.237	6.237
45.45	14.246	6.246
45.6	14.440	6.440
45.75	14.240	6.240
45.9	14.240	6.240
46.05	14.240	6.240
46.2	14.241	6.241
46.35	14.237	6.237
46.5	14.246	6.246
46.65	14.440	6.440
46.8	14.240	6.240
46.95	14.240	6.240
47.1	14.240	6.240
47.25	14.241	6.241
47.4	14.237	6.237
47.55	14.246	6.246
47.7	14.440	6.440
47.85	14.240	6.240
48	14.240	6.240
48.15	14.240	6.240
48.3	14.241	6.241
48.45	14.237	6.237
48.6	14.246	6.246
48.75	14.440	6.440

time	h	H
0.002	1.438	0.482
0.600	1.438	0.482
1.200	1.438	0.481
1.800	1.432	0.475
2.400	1.405	0.449
3.000	1.388	0.431
3.600	1.404	0.448
4.200	1.401	0.444
4.800	1.338	0.381
5.400	1.384	0.427
6.000	1.377	0.420
6.600	1.381	0.424
7.200	1.394	0.438
7.800	1.376	0.419
8.400	1.382	0.425
9.000	1.404	0.448
9.600	1.409	0.452
10.200	1.401	0.444
10.800	1.372	0.416
11.400	1.378	0.422
12.000	1.393	0.436
12.600	1.397	0.440
13.200	1.387	0.430
13.800	1.389	0.432
14.400	1.388	0.431
15.000	1.392	0.436

48.9	14.240	6.240
49.05	14.240	6.240
49.2	14.240	6.240
49.35	14.241	6.241
49.5	14.240	6.240
49.65	14.241	6.241
49.8	14.237	6.237
49.95	14.240	6.240
50.1	14.241	6.241
50.25	14.237	6.237
50.4	14.246	6.246
50.55	14.440	6.440
50.7	14.240	6.240
50.85	14.240	6.240
51	14.240	6.240
51.15	14.240	6.240
51.3	20.240	#####
51.45	14.240	6.240
51.6	14.241	6.241
51.75	14.237	6.237
51.9	14.240	6.240
52.05	14.241	6.241
52.2	14.237	6.237
52.35	14.240	6.240
52.5	14.241	6.241
52.65	14.237	6.237
52.8	14.246	6.246
52.95	14.440	6.440
53.1	14.240	6.240
53.25	14.240	6.240
53.4	14.440	6.440
53.55	14.240	6.240
53.7	14.240	6.240
53.85	14.240	6.240
54	14.241	6.241
54.15	14.237	6.237
54.3	14.246	6.246
54.45	14.440	6.440
54.6	14.240	6.240
54.75	14.240	6.240
54.9	14.240	6.240
55.05	14.240	6.240
55.2	14.240	6.240
55.35	14.240	6.240
55.5	14.240	6.240
55.65	14.240	6.240
55.8	14.240	6.240

15.600	1.406	0.449
16.200	1.420	0.463
16.800	1.392	0.435
17.400	1.393	0.436
18.000	1.405	0.448
18.600	1.398	0.441
19.200	1.405	0.448
19.800	1.408	0.452
20.400	1.392	0.436
21.000	1.397	0.441
21.600	1.410	0.453
22.200	1.413	0.456
22.800	1.413	0.457
23.400	1.408	0.451
24.000	1.408	0.451
24.600	1.408	0.451
25.200	1.410	0.454
25.800	1.413	0.457
26.400	1.416	0.459
27.000	1.408	0.452
27.600	1.407	0.450
28.200	1.411	0.454
28.800	1.414	0.457
29.400	1.417	0.461
30.000	1.414	0.457
30.600	1.414	0.458
31.200	1.410	0.453
31.800	1.412	0.455
32.400	1.420	0.463
33.000	1.419	0.462
33.600	1.414	0.458
34.200	1.412	0.455
34.800	1.416	0.460
35.400	1.419	0.462
36.000	1.418	0.462
36.600	1.420	0.464
37.200	1.423	0.466
37.800	1.415	0.459
38.400	1.420	0.463
39.000	1.423	0.466
39.600	1.423	0.466
40.200	1.426	0.470
40.800	1.420	0.463
41.400	1.423	0.467
42.000	1.422	0.465
42.600	1.424	0.467
43.200	1.428	0.471

55.95	14.240	6.240
56.1	14.240	6.240
56.25	14.240	6.240
56.4	14.240	6.240
56.55	14.240	6.240
56.7	14.240	6.240
56.85	14.240	6.240
57	14.240	6.240
57.15	14.240	6.240
57.3	14.240	6.240
57.45	14.240	6.240
57.6	14.240	6.240
57.75	14.240	6.240
57.9	14.240	6.240
58.05	14.240	6.240
58.2	14.240	6.240
58.35	14.240	6.240
58.5	14.240	6.240
58.65	14.240	6.240
58.8	14.240	6.240
58.95	14.240	6.240
59.1	14.240	6.240
59.25	14.240	6.240
59.4	14.240	6.240
59.55	14.240	6.240
59.7	14.240	6.240
59.85	14.240	6.240
60	14.240	6.240

43.800	1.427	0.470
44.400	1.427	0.470
45.000	1.423	0.467
45.600	1.426	0.470
46.200	1.428	0.472
46.800	1.429	0.473
47.400	1.430	0.474
48.000	1.429	0.472
48.600	1.429	0.472
49.200	1.429	0.472
49.800	1.428	0.471
50.400	1.429	0.473
51.000	1.432	0.476
51.600	1.433	0.477
52.200	1.429	0.472
52.800	1.431	0.474
53.400	1.432	0.476
54.000	1.433	0.476
54.600	1.434	0.477
55.200	1.435	0.479
55.800	1.434	0.477
56.400	1.432	0.475
57.000	1.433	0.476
57.600	1.436	0.479
58.200	1.437	0.480
58.800	1.435	0.478
59.400	1.434	0.478
60.000	1.436	0.479